

Protograph Bit-Interleaved Coded Modulation: A Bandwidth-Efficient Design Paradigm for 6G Wireless Communications

Yi Fang, *Senior Member, IEEE*, Pingping Chen, *Member, IEEE*, Yong Liang Guan, *Senior Member, IEEE*, Francis C. M. Lau, *Fellow, IEEE*, Yonghui Li, *Fellow, IEEE*, and Guanrong Chen, *Life Fellow, IEEE*

Abstract—Bit-interleaved coded modulation (BICM) has attracted considerable attention from the research community in the past three decades, because it can achieve desirable error performance with relatively low implementation complexity for a large number of communication and storage systems. By exploiting the iterative demapping and decoding (ID), the BICM is able to approach capacity limits of coded modulation over various channels. In recent years, protograph low-density parity-check (LDPC) codes and their spatially-coupled (SC) variants have emerged to be a pragmatic forward-error-correction (FEC) solution for BICM systems due to their tremendous error-correction capability and simple structures, and found widespread applications such as deep-space communication, satellite communication, wireless communication, optical communication, and data storage. This article offers a comprehensive survey on the state-of-the-art development of LDPC-BICM and its innovative SC variants over a variety of channel models, e.g., additive white Gaussian noise (AWGN) channels, fading channels, Poisson pulse position modulation (PPM) channels, and flash-memory channels. Of particular interest is code construction, constellation shaping, as well as bit-mapper design, where the receiver is formulated as a serially-concatenated decoding framework consisting of a soft-decision demapper and a belief-propagation decoder. Finally, several promising research directions are discussed, which have not been adequately addressed in the current literature.

Index terms— Bandwidth efficiency, bit-interleaved coded modulation, low-density parity-check code, protograph code.

I. INTRODUCTION

A. Overview of LDPC-BICM

To provide high-reliability and high-throughput transmission and storage is an extremely challenging task in modern bandwidth-limited communication and storage systems [1], [2]. In 1948, Shannon published a piece of milestone work, which revealed and proved that information (data) can be reliably transmitted over a noisy channel by using forward-error-correction

(FEC) codes with an arbitrarily high rate below the *channel capacity* (also called the *maximum achievable rate*) [3]. Since then, the research field of channel coding has been created, and a great deal of effort has been devoted to finding coding mechanisms that can strongly resist channel impairments and closely approach the channel capacity [4], [5]. In fact, FEC codes have stood out as a more promising choice to implement reliable communication systems compared with other error-correction techniques (e.g., data retransmission techniques), especially for low-latency and low-power applications [6]–[8].

Aiming to improve the spectral efficiency, there has been increasing demand for incorporating high-order modulation into FEC code design because it can transform several binary bits to a non-binary symbol through a high-order constellation [9]. As a pioneering work on the coded modulation (CM), the channel code and high-order modulation were properly combined into a single entity to improve the spectral efficiency of communication systems [10]. In this direction, great research efforts have been made to promote the development of the joint coding-and-modulation design. Specifically, trellis-coded modulation (TCM), which combines the trellis codes with phase-shift-keying/quadratic-amplitude modulations (PSK/QAM), was conceived in [11] to improve the transmission efficiency over additive white Gaussian noise (AWGN) channels. Later on, a symbol-level interleaver was added between the encoder and the modulator to improve the performance of TCM over fading channels [12]. As an alternative to TCM, multi-level CM (MLCM) was developed, which exploits different convolutional/turbo codes to protect a modulated symbol [13]–[15]. In particular, an individual binary code in the MLCM scheme was utilized to enhance the transmission reliability of each labeling bit within a modulated symbol. However, both TCM and MLCM schemes cannot maximize the minimum Hamming distance of an FEC code, which results in a non-trivial gap to the channel capacity in fading scenarios.

To overcome the aforementioned weakness, a great deal of research effort has been devoted to developing more robust combinational solutions that can adequately exploit the potential advantages of coding and modulation. In 1993, a breakthrough in coding theory was marked by the inception of turbo codes [16]. The turbo code, which concatenates two individual convolutional codes through a bit-level interleaver in parallel, is capable of accomplishing performance very close to the channel capacity with iterative decoding [17]. Inspired by the fundamental work in [16], it was re-discovered [18] that the low-density parity-check (LDPC) codes can also approach the channel capacity under iterative decoding. More importantly, the notable success of “turbo

Y. Fang is with the School of Information Engineering, Guangdong University of Technology, Guangzhou 510006, China, and also with the State Key Laboratory of Integrated Services Networks, Xidian University, Xi’an 710126, China (email: fangyi@gdut.edu.cn).

P. Chen is with the Department of Electronic Information, Fuzhou University, Fuzhou 350116, China (e-mail: ppchen.xm@gmail.com). *Corresponding author: Pingping Chen.*

Y. L. Guan is with the School of Electrical and Electronic Engineering, Nanyang Technological University, Singapore 639798 (e-mail: eyl-guan@ntu.edu.sg).

F. C. M. Lau is with the Department of Electronic and Information Engineering, Hong Kong Polytechnic University, Hong Kong (e-mail: encmlau@polyu.edu.hk).

Y. Li Li is with the School of Electrical and Information Engineering, The University of Sydney, Sydney, NSW 2006, Australia (e-mail: yonghui.li@sydney.edu.au).

G. Chen is with the Department of Electronic Engineering, City University of Hong Kong, Hong Kong (e-mail: eegchen@cityu.edu.hk).

principle” opened up an important direction to design near-capacity bandwidth-efficient CM systems. In 1992, a novel CM scheme was proposed in [19], referred to as *bit-interleaved coded modulation (BICM)*, which is a serial concatenation of a channel code, a bit-level interleaver, and a high-order modulation. It can achieve higher diversity order and better performance than the conventional TCM over fading channels. Then, a thorough information-theoretic study on BICM was carried out in [20] in terms of channel-capacity and asymptotic-performance analysis. It was also demonstrated in [20] that using soft-decision demodulation (i.e., demapping) could help reasonably compensate the performance loss incurred by separating coding and modulation in BICM. In fact, the intrinsic serial concatenated structure of BICM resembles a turbo code, so using iterative demapping and decoding (ID) may yield an additional performance gain. Motivated by this feature, effective ID algorithms with hard-decision and soft-decision feedbacks for convolutional-based BICM, were developed in [21] and [22] respectively, leading to BICM-ID frameworks, which reduce the performance loss caused by independent demapping. In general, the soft-decision-aided BICM-ID performs better than the hard-decision-aided BICM-ID because soft information carries more reliable message of the transmitted symbols compared with hard information. More precisely, it is possible to achieve capacity-approaching performance for BICM-ID with the aid of a powerful channel code, an optimized bit interleaver (i.e., bit mapper), and a carefully chosen constellation [23]–[25].

However, the convolutional-based BICM is unable to have good near-capacity performance even with a sophisticated design [26]. As a remedy, more powerful FEC codes (e.g., turbo codes and LDPC codes [27]–[29]) were developed for BICM systems, showing that they can operate very close to the channel capacity under some specific constellations [30]–[37].¹ In fact, LDPC codes possess better error performance and lower decoding complexity than turbo codes, and thus were recognized as one of the most powerful FEC codes that enable error-free transmissions with rates up to the channel capacity for communication and storage systems since the late 1990s [38]–[44]. Due to its flexible design and excellent performance, BICM has been further deployed in a wide range of practical applications and industry standards, e.g., wireless local area networks, digital video broadcasting-satellite-second generation (DVB-S2), and the fourth/fifth-generation (i.e., 4G/5G) mobile networks, thereby marking a paradigmatic shift in the CM field [45]–[48].

With the continuous development of analysis tools and construction methodologies [49], LDPC codes have become a prospective type of FEC codes to formulate pragmatic BICM systems, which not only can achieve high throughput but also enable satisfactory performance over different types of channels, including AWGN channels, fading channels, Poisson pulse position modulation (PPM) channels, multi-level-cell (MLC) flash memory channels, and underwater acoustic channels [50]–[61]. According to the salient feature of BICM, a large number of theoretic analysis methodologies were developed, such as density evolution (DE) [35], [38], [62], extrinsic information trans-

fer (EXIT) function [63], [64], asymptotic weight enumerator (AWE) [23], [65]–[67], and harmonic mean of minimum squared Euclidean distance (HMMSED) [20], [46], [68], [69], to characterize the asymptotic performance and to facilitate optimization of the system. Based on these theoretical advancements, great endeavor has been dedicated to improving the performance and reducing the complexity of the LDPC-BICM from the perspectives of code construction [54], [55], [70]–[75], constellation shaping [63], [76]–[80], bit-mapper optimization [51], [81]–[90], as well as receiver design [24], [60], [91]–[97]. Although several capacity-approaching LDPC-BICM systems have been devised in recent years, the irregular structures of the designed codes suffer from difficult implementation, which becomes a major obstacle in practical applications. Besides, the capacity-approaching LDPC codes and its BICM relatives always have undesirable high-SNR performance, making them unfavorable for the applications with extremely low bit-error-rate (BER) requirement, such as data storage and optical communication.

To circumvent the above-mentioned limitations, structured LDPC codes, such as protograph LDPC (PLDPC) codes and quasi-cyclic (QC) LDPC codes, have emerged as a competitive component in BICM systems, which can achieve outstanding performance with simple design and easy hardware implementation [98]–[106]. Particularly, these two types of LDPC codes possess linear encoding and decoding complexity, and hence attracted increasing interest from both academic and industrial communities [107]–[113]. In fact, the QC-LDPC codes can be considered as a special version of the PLDPC codes, for which the macroscopic structure can be described by a small-size graph, called *protograph* [114], [115]. An advantage of the PLDPC codes is that they are able to achieve desirable performance in both low- and high-SNR regions after proper designs [43]. Thereby, two rate-compatible PLDPC codes has been already selected as the channel coding schemes for 5G new-radio standard [110], [112]. Nowadays, the research work on PLDPC-BICM and its variants has grown rapidly to improve the performance of modern communication and storage systems [57], [71], [73]. For example, PLDPC codes and bit mappers have been considerably advanced for *MPSK/MQAM*-aided BICM systems over different types of channels [71], [83], [116]–[120] during the past fifteen years.

To extend BICM for other emerging scenarios, PLDPC codes have been combined with other types of modulations, such as code-phase-shift keying (CPSK) modulation [121], on-off-keying (OOK) modulation [122] and PPM [54], [123]–[125], to support more diverse transmission and storage services. Moreover, exploiting the differential chaos-shift keying (DCSK) modulation [126], [127], several novel PLDPC-BICM schemes were devised for block-fading channels, which are of particular interest for low-power and low-complexity short-range wireless communication applications [64], [92], [128]–[130]. In addition, in the non-orthogonal multiple access (NOMA) scenarios [131]–[133], the optimization of PLDPC-BICM schemes has been investigated to achieve desirable performance in 5G systems [134]. Inspired by the appealing advantages of PLDPC-BICM, research efforts have been devoted to the joint design of this technique and physical-layer network coding (PNC) in order to realize higher-throughput wireless communications [135], [136].

¹“BICM” will be used to collectively represent both “BICM-ID” and “BICM with non-iterative decoding (BICM-NI)” in this article, although it was initially utilized to represent “BICM-NI” only.

More recently, spatially-coupled (SC) PLDPC codes, which are generated by serially coupling a sequence of PLDPC codes into a single coupled chain, have emerged as a powerful FEC scheme [137]. As a type of convolutional-like codes, the SC-PLDPC codes not only can obtain additional “*convolutional gains*” over the conventional PLDPC codes, but also can keep a better balance between the decoding threshold and minimum free or Hamming distance [67], [138], [139]. Accordingly, research interest turned to optimization and analysis of different types of SC-PLDPC codes, such as terminated (TE) and tail-biting (TB) SC-PLDPC codes under different transmission environments [61], [140]–[147]. Based on carefully designed SC-PLDPC codes, several spectral-efficiency BICM systems were proposed for satellite broadcasting communication, wireless communication, and optical communication [102], [148]–[156]. Moreover, SC-PLDPC codes have been employed to improve the performance of modern dense flash-memory devices, including MLC, triple-level-cell (TLC), and quadruple-level-cell (QLC) flash memory, which can be regarded as high-order pulse-amplitude modulation (PAM)-aided discrete memoryless channels [56], [157]–[161]. In parallel with the transmitter design progress, the low-complexity message passing decoding algorithms were designed for the SC-PLDPC-BICM systems, so as to ease the hardware implementation [162], [163]. Today, research on PLDPC-BICM and its SC variant has opened up a promising direction in the CM field, which has gained tremendous attention from industry.

During the first decade of this century, there have been several tutorial and survey-type of articles regarding the BICM [23]–[25]. On the one hand, comprehensive overviews of the convolutional- and turbo-BICM-ID were presented in [23] and [24], which also analyzed the feasibility of LDPC-BICM-ID. On the other hand, a general review on the attainable LDPC coded modulations, including both non-binary CM and binary BICM techniques, was presented in [25]. These articles summarized the research progress before 2009, more than a decade ago. Moreover, they did not discuss the research progress regarding PLDPC-BICM. Since 2010, the study of BICM has moved into a new stage and experienced a rapid development, in which the PLDPC-BICM plays an important role as an alternative in addressing new challenges from modern communication and storage applications. In fact, a systematic design guideline for the PLDPC-BICM is still lacking in the literature today. Therefore, it is timely needed to put forward a thorough overview of the up-to-date research advancements in PLDPC-BICM systems to meet the stringent reliability-and-throughput demand of modern communication and storage equipment [164]–[173]. For ease of understanding this article, Table I provides a brief glimpse at the the major contributions in the historical evolution of PLDPC-BICM paradigm during the past two decades, with a special highlight on the encoder, constellation and interleaver design.

B. Organization and Structure of This Survey

This article provides a survey of PLDPC-BICM on the most recent works investigating joint design of binary PLDPC codes and high-order modulations to support high-reliability and high-rate digital communications and data storage. Specifically, it will start by introducing the fundamental configuration, transmission

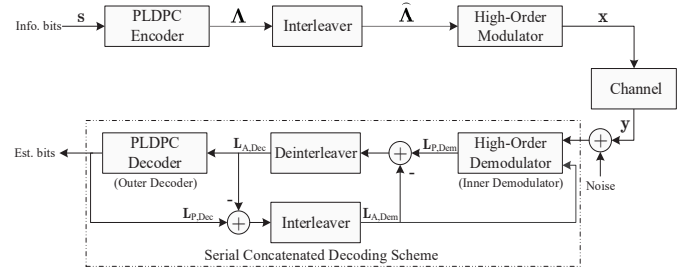


Fig. 1. Block diagram of a general PLDPC-BICM-ID system.

mechanism, and the information-theoretic limit of the PLDPC-BICM. Then, some preliminary basis of PLDPC codes will be discussed, which can be seamlessly combined with high-order modulations to construct bandwidth-efficient BICM systems. Further, some typical theoretical-analysis tools will be reviewed, which have been extensively adopted for designing PLDPC-BICM. On the basis of the above preliminaries, the enabling design methodologies will be classified for PLDPC-BICM systems over different transmission channels, such as AWGN channels, fading channels, Poisson PPM channels, and NAND flash-memory channels. In particular, state-of-the-art technologies will be described, including code construction, constellation shaping and bit-mapper design, which are useful for enabling the relevant systems with capacity-approaching performance. Additionally, several promising research directions will be introduced, which may further enhance the robustness of the PLDPC-BICM and expand its application domain. Since the aim is to present a focal review on PLDPC-BICM techniques rather than presenting an extensive coverage of all BICM techniques, some irrelevant topics are excluded. This is the first attempt to systematically provide design guidelines for a concatenated framework comprising PLDPC codes, bit mappers and high-order modulations. Although the references are not exhaustive, this survey could serve as a starting point for further studies on the topics of interest.

The structure of this article is organized as follows. Section II describes the system model and transmission mechanism of the PLDPC-BICM with emphasis on its transceiver architecture, channel model and channel capacity. Section III presents basic concepts of PLDPC codes and reviews some theoretical-analysis tools, which are always exploited to assess and optimize the performance of PLDPC-BICM. Sections IV~VII details the latest design paradigms of PLDPC-BICM over AWGN, fading, Poisson PPM and NAND flash-memory channels, respectively, which are used to characterize the statistic features of some classic transmission and storage environments. Sections VIII and X recommend some valuable future research directions and draw some conclusions, respectively. To facilitate reading, the acronyms used in the paper are listed in Table II.

II. SYSTEM MODEL AND TRANSMISSION MECHANISM OF PLDPC-BICM

We first describe the general PLDPC-BICM system architecture, and then present some preliminaries that will be useful throughout the article.

A. System Architecture

Fig. 1 depicts a general PLDPC-BICM system model. In this system, the source information bits $\mathbf{s} = (s_1, s_2, \dots, s_K)$ are first

TABLE I
MAJOR CONTRIBUTIONS IN PLDPC-BICM DESIGN

Year	Author(s)	Contribution
1992	Zehavi [19]	Conceived the concept of BICM to achieve bandwidth-efficient transmissions.
1997	Li <i>et al.</i> [21]	Introduced a hard-decision ID framework for BICM to establish a BICM-ID system.
1998	Brink [22]	Designed a soft-decision BICM-ID framework and illustrated that the anti-Gray labeling outperforms the Gray labeling in such a scenario.
1998	Caire <i>et al.</i> [20]	Provided a systematic information-theoretic study on BICM in terms of channel capacity and HMMSED.
2000	Knopp <i>et al.</i> [174]	Formulated a performance-analysis methodology for BICM-NI over non-ergodic block-fading channels.
2003	Thorpe [175]	Invented the PLDPC codes and introduced their representation methods.
2003	Brink <i>et al.</i> [176]	Constructed capacity-approaching repeat-accumulate (RA) codes, i.e., a special type of PLDPC codes, for QPSK-aided BICM-ID systems.
2005	Divsalar <i>et al.</i> [116]	Explored the applicability of PLDPC codes in BICM-NI systems and presented a novel bit-mapping scheme under the 16QAM.
2006	Liva <i>et al.</i> [40]	Discussed the spectral efficiency of RA-coded BICM systems with MPSK/MAPSK.
2009	Xie <i>et al.</i> [59]	Investigated the channel capacity and BER performance of the LDPC-BICM-ID systems with Gray-labeled and pseudo-Gray-labeled MAPSK.
2010	Jin <i>et al.</i> [118]	Proposed an optimal VDM scheme, which can obtain desirable threshold and WER enhancement over the water-filling VDM scheme in PLDPC-BICM-NI systems with 16QAM modulation.
2010	Barsoum <i>et al.</i> [177]	Formulated a protograph EXIT (PEXIT)-chart-aided PLDPC-code design method for BICM-ID systems over Poisson PPM channels.
2011	Nguyen <i>et al.</i> [83]	Developed a type of <i>enhanced AR4JA (EAR4JA) codes</i> and a two-stage-lifting-aided mapping (TSLM) to constitute a novel PLDPC-BICM system, which is suitable for a wide range of code rates and modulation orders.
2011	Kudekar <i>et al.</i> [138]	Conceived the concept of SC-PLDPC codes and revealed their inherent “threshold saturation” feature.
2013	Schmalen <i>et al.</i> [178]	Proposed a simple coding scheme that is universally suited for TE-SC-PLDPC-BICM systems with different constellation labelings.
2013	Zhou <i>et al.</i> [54]	Optimized PLDPC codes for BICM-ID systems over Poisson PPM channels by using a modified EXIT algorithm.
2014	Tang <i>et al.</i> [118]	Generalized the water-filling VDM scheme to combine any protograph with any modulation in BICM systems.
2014	Häger <i>et al.</i> [149]	Proposed an EXIT-aided bit-mapping optimization scheme for PLDPC-BICM systems with polarization-multiplexed (PM) QAM.
2014	Benaddi <i>et al.</i> [166]	Introduced a general design framework for PLDPC-BICM with continuous phase modulation (CPM).
2015	Tang <i>et al.</i> [122]	Optimized the PLDPC-BICM with OOK modulation in light-emitting diode (LED)-based visible light communication (VLC) systems.
2015	Lyu <i>et al.</i> [128]	Proposed a PLDPC-BICM-ID system with Walsh-code-based MDCSK modulation.
2015	Häger <i>et al.</i> [150]	Optimized the bit-mapping schemes for SC-PLDPC-BICM-NI to achieve high spectral-efficiency fiber-optical communications.
2016	Cammerer <i>et al.</i> [152]	Proposed a hybrid mapping scheme for TB-SC-PLDPC-BICM-ID systems with 16QAM modulation, which simultaneously adopts Gray- and SP-labeled constellations for a codeword to trigger the wave-like decoding.
2016	Steiner <i>et al.</i> [171]	Presented a PLDPC-code design method for ASK-aided BICM systems under shaped bit-metric decoding.
2017	Zhan <i>et al.</i> [92]	Proposed an ARJA BICM system with constellation-based MDCSK modulation, which benefits from higher spectral efficiency compared with the Walsh-code-based counterpart.
2017	Chen <i>et al.</i> [135]	Estimated the performance of AR3A-coded PNC BICM-ID systems over block-fading channels.
2017	Fang <i>et al.</i> [179]	Designed a family of multi-layer root-PLDPC codes for multi-relay coded-cooperative systems and extended their application to the QPSK-aided BICM scenario over block-fading channels.
2018	Chen <i>et al.</i> [57]	Constructed a family of RC-PLDPC codes and a novel bit-mapping scheme for MLC BICM-NI flash-memory systems.
2019	Fang <i>et al.</i> [71]	Presented an outage-limit-approaching PLDPC-BICM system over block-fading channels.
2019	Bu <i>et al.</i> [73]	Designed a family of high-rate PLDPC codes, called <i>optimized ARA (OARA) codes</i> , for BICM-ID flash-memory systems.
2020	Zhang <i>et al.</i> [102]	Developed a QC-SC-PLDPC-BICM scheme, which is able to achieve near-capacity performance with low implementation complexity.
2020	Yang <i>et al.</i> [154]	Presented novel constellation and bit-mapping schemes for TB-SC-PLDPC-BICM-ID systems.
2021	Yang <i>et al.</i> [180]	Constructed a type of structural quadrant (SQ) constellations for TB-SC-PLDPC-hierarchical modulated (HM)-BICM-ID systems.
2021	Dai <i>et al.</i> [181]	Designed a novel irregular-mapped (IM) PLDPC-BICM framework for VLC systems.

encoded into a rate- r binary PLDPC code $\Lambda = (v_1, v_2, \dots, v_N)$, where K is the information length, N is the codeword length, $r = \frac{K}{N-N_E} = \frac{K}{N_T}$ is the code rate, and N_E and N_T are the punctured and transmitted codeword lengths, respectively. The coded sequence is permuted by a bit-level interleaver to yield an interleaved bit sequence $\hat{\Lambda} = (\hat{v}_1, \hat{v}_2, \dots, \hat{v}_N)$, which is subsequently modulated to an M -ary symbol sequence $\mathbf{x} = (x_1, x_2, \dots, x_{N'})$, where $M > 2$ is the modulation order, $w = \log_2 M$ is the number of bits carried by a modulated symbol, and $N' = \frac{N}{w}$ is the length of symbol sequence. It is usually assumed that N is a multiple of w . In particular, every w interleaved coded bits are mapped to an M -ary symbol through a specific signal constellation. The modulated symbol sequence is then transmitted through a noisy channel.

At the receiver terminal, the “impaired” signal output from the channel is decoded by a serially concatenated decoding scheme, which contains a soft-input soft-output (SISO) inner demodulator (or *demapper*) and an SISO outer decoder [23]. To compensate the performance loss arising from separated demapping and decoding, the soft information, such as probabilistic and log-likelihood ratio (LLR) information, of the demodulator and decoder in the BICM system are updated in an iterative fashion, which is similar to the turbo decoding [24], [25]. Specifically, given the received signal \mathbf{y} and *a priori* LLR $\mathbf{L}_{A, \text{Dem}}$, the demodulator can compute its extrinsic LLR (i.e., $\mathbf{L}_{P, \text{Dem}} - \mathbf{L}_{A, \text{Dem}}$), which will be used as the *a priori* LLR $\mathbf{L}_{A, \text{Dec}}$ of the decoder. Subsequently, the decoder can calculate

its extrinsic LLR (i.e., $\mathbf{L}_{P, \text{Dec}} - \mathbf{L}_{A, \text{Dec}}$), which will be fed back to the demodulator as the updated *a priori* LLR for the next iteration. Some key components of this system are further elaborated as follows.

1) *PLDPC Encoder*: In the BICM-ID system, the PLDPC codes, are used as the channel coding scheme to enhance the reliability of the source information prior to the transmission over noisy channels. It has been demonstrated that the source information can be well protected when transmitting over a noisy and interference channel if the FEC codes are carefully designed [182], [183]. However, similarly to conventional FEC codes, the PLDPC code is constructed by appending some redundancy (i.e., parity-check bits) to the information bits, which leads to low throughput [184]. To partially overcome this weakness, puncturing techniques were developed to increase the code rate of such codes [67], [73]. In contrast to conventional LDPC codes, a well-designed puncturing scheme not only increases the transmission rate but also improves the error performance of PLDPC codes [43], [140]. For simplicity, the puncturing module is omitted in Fig. 1 as it can be embedded into the encoder.

2) *Interleaver (Bit Mapper)*: As PLDPC codes possess an intrinsic interleaving feature, there is no need to add an interleaver into a PLDPC-coded system with BPSK modulation. However, an individual bit interleaver (or *bit mapper*) is of great importance to guarantee the performance of the PLDPC-BICM system, especially over a fading channel, because it can optimize the mapping rule between the coded bits in a codeword and

TABLE II
LIST OF ACRONYMS USED IN THIS ARTICLE.

Acronym	Full Name	Acronym	Full Name
3D	three-dimensional	MSB/LSB	most/least significant bit
4G/5G	fourth/fifth-generation	MSEW	maximum squared Euclidean weight
ABSA	adaptive binary-switch algorithm	OOK	on-off-keying
AR3A/AR4A	accumulate-repeat-3/4-accumulate	OREC	octal rectangular
AR4JA/EAR4JA	accumulate-repeat-by-4-jagged-accumulate/enhanced AR4JA	PAM	pulse-amplitude modulation
ARA/IARA	accumulate-repeat-accumulate/improved ARA	PAS	probabilistic amplitude shaping
AWE	asymptotic weight enumerator	PDF	probability density function
AWGN	additive white Gaussian noise	PE/PEG	program-and-erase/progressive-edge-growth
BER/WER	bit/word error rate	PLDPC/DPLDPC	protograph LDPC/double-PLDPC
BICM	bit-interleaved coded modulation	PN/PM	pseudo-noise/polarization-multiplexed
BP/S-BP	belief propagation/shuffled BP	PNC	physical-layer network coding
HDD/SSD	hard disk drive/solid state drive	PPM	pulse position modulation
CM/MLCM	coded-modulation/multi-level CM	PSK/QAM	phase-shift-keying/quadratic-amplitude modulation
CPM	continuous phase modulation	QC	quasi-cyclic
CPSK	code-phase-shift keying	QRC	quaternary raised-cosine
CSI	channel state information	RA/RJA	repeat-accumulate/repeat-jagged-accumulate
DCSK	differential chaos-shift keying	RC	rate-compatible
DE	density evolution	RGB	red-green-blue
DT	direct-truncated	RP	root-protograph
DSSS	direct-sequence spread-spectrum	SC	spatially-coupled
DVB	digital video broadcasting	SISO	soft-input soft-output
EXIT/PEXIT	extrinsic information transfer/protograph EXIT	SLC/MLC	single/multi-level cell
FEC	forward error correction	SNR	signal-to-noise-ratio
GML	generalized-maximum-likelihood	SP	set-partitioning
GMSK	Gaussian minimum shift keying	SPMM	spatial-position matched mapping
HM	hierarchical modulated	SQ	structural quadrant
HMMSED	harmonic mean of the minimum squared Euclidean distance	TB/TE	tail-biting/terminated
ID/NI	iterative demapping and decoding/non-ID	TCM	trellis-coded modulation
i.i.d.	independent and identically distributed	TLC/QLC	triple/quadruple-level cell
IM	irregular mapping	TSLM	two-stage-lifting-aided mapping
LED	light-emitting diodes	TWR	two-way relay
LDPC/PLDPC	low-density parity-check/protograph-based LDPC	UEP	unequal-error-protection
LLR	log-likelihood ratio	VDMM	variable degree matched mapping
MAP/MDS	maximum a-posteriori/maximum-distance separable	VLC/VIS	visible light communication/voltage-sensing
MED	minimum Euclidean distance	VNDM	variable-node-degree-based mapping
MHDGR/MFDGR	minimum Hamming/free-distance growth rate	VNFAM	variable-node fractional-allocation mapping
MI/MMI	mutual information/maximum MI	VNMM	variable node matched mapping

labeling bits within a modulated symbol. A bit-level interleaver not only enables the PLDPC-BICM to achieve a larger diversity order over a fading channel, but also can better protect the high-priority coded bits [24]. To realize the unequal-error-protection (UEP) property and to acquire a desirable interleaving gain for a particular channel model, several bit-mapping schemes have been designed, such as water-filling-like mapping scheme [116], variable-degree matched mapping (VDMM) scheme [83], [118], [119], [122], variable-node matched mapping (VNMM) scheme [154], and UEP-based bit-mapping scheme [71], to optimize the interface between PLDPC-coded bits and modulated symbols.

3) *High-order Modulator*: To achieve high spectral efficiency, high-order modulations (i.e., with $M > 2$) instead of binary modulations are utilized in the PLDPC-BICM systems. In particular, the interleaved bit sequence is first uniformly divided into N' sub-sequences of length w , i.e.,

$$\hat{\mathbf{A}} = (\hat{v}_1, \hat{v}_2, \dots, \hat{v}_N) = (\hat{v}_{1,1}, \hat{v}_{1,2}, \dots, \hat{v}_{1,w}; \hat{v}_{2,1}, \hat{v}_{2,2}, \dots, \hat{v}_{2,w}; \dots; \hat{v}_{N',1}, \hat{v}_{N',2}, \dots, \hat{v}_{N',w}).$$

Then, the N' sub-sequences are mapped to N' transmitted symbols $\mathbf{x} = (x_1, x_2, \dots, x_{N'})$, where $x_k \triangleq (\hat{v}_{k,1}, \hat{v}_{k,2}, \dots, \hat{v}_{k,w})$ is chosen from an M -ary modulated signal constellation (i.e., signal set) \mathcal{X} with a labeling rule $\phi: \{0, 1\}^w \rightarrow \mathcal{X}$, $w = \log_2 M$, $|\mathcal{X}| = M$, and $k = 1, 2, \dots, N'$. Therefore, the transmitted symbol output from an M -ary modulator is associated with w binary coded bits (also called *labeling bits*). More precisely, the performance of a PLDPC-BICM is dependent not only on the modulation scheme but also on the labeling scheme. In this article, the system design approaches are outlined for

various modulation schemes tailored to different communication applications.

4) *Channel Models*: In the past two decades, BICM has been applied to various communication and storage systems, such as deep-space communication [116]–[119], wireless communication [128]–[130], [154], optical communication [122]–[124], [150], [181], and NAND-flash-based data storage [73], [97], [120]. To facilitate applications in such transmissions, AWGN channel, fast-fading channel, block-fading channel, Poisson PPM channel, and NAND flash-memory channel have been considered in developing design and analysis methodologies for the PLDPC-BICM systems. Among all the above-mentioned channels, AWGN channel is one of the simplest memoryless noisy channel models that can reasonably describe the fundamental characteristics of many realistic communication systems, including deep-space communication systems, visible light communication (VLC) systems, fiber-optical communication systems, as well as wireless communication systems. Despite its extreme simplicity, AWGN channel serves as an important model for designing capacity-approaching BICM schemes. As illustrated in [43], [185], the LDPC codes optimized for an AWGN channel can also exhibit excellent performance over other memoryless channel models, e.g., binary erasure channel and ergodic fast-fading channel. In this sense, the code-design criteria developed for PLDPC-BICM systems over AWGN channels are very promising for many practical applications and, therefore, have been intensively studied in recent years [59], [69], [76]–[78].

In addition to the AWGN, channel fading is another key factor

that degrades the transmission reliability of wireless communications. At the early stage of BICM studies, a transmitted signal was always assumed to suffer from Rayleigh fading over wireless channels. However, it has been demonstrated that Rayleigh distribution cannot accurately capture the underlying physical properties of several wireless communication systems, such as complex indoor environments, land mobile systems and ionospheric radio links, and thus is not a good model for such transmission [43]. As an improved and more general model, the Nakagami- m distribution was introduced to match the fading statistical behavior of many wireless communication channels. Specifically, the Nakagami- m distribution, which covers Rayleigh fading channel, Rician fading channel and AWGN channel as special cases, is able to offer the widest range of fading among all the existing distributions [186]–[188]. Due to the above-mentioned advantage, a great deal of research effort has been devoted to studying the PLDPC-code construction and their respective BICM-system design over Nakagami- m fading channels [99], [126], [179], [189], [190].

Besides, Poisson PPM channel [123], [124], [177] and flash-memory channel [157]–[160], [191]–[193], which are respectively utilized to characterize the free-space optical communication and non-volatile storage systems, may have quite different forms of transmitted signals (i.e., pulse position and read voltage), channel noises and gains. They will be further discussed in Sections VI and VII before getting into technical details.

As in the majority of existing works investigating the channel-coded BICM, the symbol-to-symbol interference is not considered here in the design and analysis for simplicity. Moreover, without loss of generality, for all the examples considered below, the scalar fading gains in a wireless fading channel are assumed to be subject to a Nakagami- m distribution, denoted by $|\alpha| \sim \mathcal{NAK}(m)$, where $m \geq \frac{1}{2}$ is the fading depth [186].

In general, the input-output relationship of an M -ary modulated PLDPC-BICM system over an AWGN/fading channel can be written as

$$y_k = \alpha_l x_k + n_k, \quad (1)$$

where $x_k \in \mathcal{X}$ is the M -ary complex-valued transmitted symbol, \mathcal{X} is the constellation set, y_k is the received signal, n_k is the complex Gaussian noise with zero mean and variance $\sigma_n^2 = \frac{N_0}{2}$ per dimension, N_0 is the noise power spectral density, $k = 1, 2, \dots, N'$; $\alpha_l = |\alpha_l| \exp(j\varphi_l)$ is the channel gain with $|\alpha_l|$ and φ_l being the scalar fading gain and phase shift, respectively, which satisfy the following properties: (i) $|\alpha_l| = \alpha$ (α controls the average power per symbol), $\varphi = 0$, and $l = k$ for an AWGN channel; (ii) $|\alpha_l| \sim \mathcal{NAK}(m)$, $\varphi \sim \mathcal{U}[-\pi, \pi]$ (i.e., a uniform distribution), and $l = k$ for a fast-fading channel, (iii) $|\alpha_l| \sim \mathcal{NAK}(m)$, $\varphi \sim \mathcal{U}[-\pi, \pi]$, and $l = 1 + \lfloor (k-1)/B' \rfloor$ (B' is the symbol block length and $\lfloor \cdot \rfloor$ is the floor operation) for a block-fading channel [71], [194]. Moreover, the spectral efficiency of a PLDPC-BICM system is defined as $R_{SE} = r \log_2 M = rw$. The average SNR per information bit is defined as $E_b/N_0 = (E_s/N_0)/R_{SE} = \gamma_s/R_{SE}$, where γ_s is the average symbol SNR and E_s is the average energy per transmitted symbol.

5) *Detector/Decoder*: At the receiver of the PLDPC-BICM-ID system, a turbo-like iterative decoding framework, which includes an inner demapper and an outer decoder, is employed to decode the ‘‘impaired’’ signal. In this iterative decoding

framework, the extrinsic information output from the decoder is fed back to the demodulator as its *a priori* information. Then, the *a posteriori* information of each labeling bit within an M -ary symbol output from the demodulator can be estimated by exploiting the *a priori* information of the remaining $w-1$ labeling bits, which will further help accelerate the convergence of the decoder. As such, the turbo-like decoding framework allows the BICM-ID system to extract more reliable soft information and to achieve better performance as compared with the BICM-NI system [71]. There are a variety of soft-information-oriented demodulation algorithms designed for BICM systems in the literature, such as maximum *a posteriori* (MAP) algorithm [91] and the max-sum approximation of its log-domain counterpart (i.e., Max-Log-MAP) [94]. Here, the MAP algorithm and log-domain belief-propagation (log-BP) algorithm [44], [195], [196] are adopted to implement the demodulator and decoder, respectively. The iteration between the inner demodulator and outer decoder is referred to as *global iteration*, while the iteration between the variable-node decoder and the check-node decoder in the PLDPC decoder is referred to as *local iteration* (or *BP iteration*). Especially, the BICM-ID is simplified to a BICM-NI if the number of global iterations is set to be one. The following discussions will focus on the transmitter design of the PLDPC-BICM, while treating the receiver architecture as a turbo-like decoder. It is assumed that the channel state information (CSI) can be perfectly captured by the receiver with the help of a well-designed channel estimator [179], [197], as assumed in most studies [35], [45], [59], [62]–[64], [71].

B. Channel Capacity

For an ergodic memoryless channel, the channel capacity C is defined as the maximum mutual information (MI) between the channel input X and output Y over all the channel input probability distributions $\{\Pr(x)\}$ [198]. As one of the most significant performance metrics for channel coding and BICM schemes over a given channel, the capacity C is used to quantify the information rate that the channel can reliably convey with the use of an FEC code. Nonetheless, the BICM system cannot continue to provide reliable transmission over the channel with any FEC code once the spectral efficiency exceeds the channel capacity (i.e., $R_{SE} > C$). The capacity of PLDPC-BICM over an AWGN channel is further analyzed below.

1) *Constellation-Unconstrained Capacity*: Suppose that the transmitted symbol x_k is randomly chosen from an infinite-size complex-Gaussian constellation \mathcal{X} . The capacity for an AWGN channel is given by [198]

$$C_{\text{Shannon}} = \log_2(1 + E_s/N_0) = \log_2(1 + \gamma_s), \quad (2)$$

where the power of transmitted symbol satisfies $\mathbb{E}[|x_k|^2] = E_s$ and the cardinality of the constellation satisfies $|\mathcal{X}| \rightarrow +\infty$. This equation is the well-known Shannon formula, which cannot be achieved by using a finite-size constellation.

2) *Constellation-Constrained Capacity*: From a practical point of view, it should be more realistic to map a PLDPC codeword to a symbol sequence chosen from a finite-size signal constellation χ , such as M PSK and M QAM, which has a uniform distribution for all the M component points $x_k \in \chi$. In this scenario, assuming that the M -ary transmitted symbol

sequence $(x_1, x_2, \dots, x_{N'})$ is directly mapped from a length- N' non-binary PLDPC codeword over $\mathbb{GF}(M)$, rather than from a length- N binary PLDPC codeword. The channel capacity can be specified by the average input-output MI [24], i.e.,

$$C_{\text{CM}} = I_{\text{CM}}(X; Y | \gamma_s) = w - \mathbb{E}_{x,y} \left[\log_2 \frac{\sum_{x' \in \mathcal{X}} f(y|x')}{f(y|x)} \right], \quad (3)$$

where $x \in \mathcal{X}$, $|\mathcal{X}| = M$, and $f(y|x')$ is the complex-Gaussian probability density function (PDF) [71]. The capacity defined in (3) is referred to as the *CM capacity*. As shown in [20], [24], [199], CM is able to achieve the maximum achievable rate of an M -ary modulated channel, and thus is viewed as an optimal transmission scheme.

For a BICM-NI scheme, the M -ary modulated channel can be considered as w independent parallel binary-input sub-channels. Thus, the *BICM capacity* is equal to the summation of the average MIs of the w sub-channels [20], i.e.,

$$\begin{aligned} C_{\text{BICM-NI}} &= \sum_{\mu=1}^w I_{\text{BICM-NI}}(\hat{v}_\mu; Y | \gamma_s) \\ &= w - \sum_{\mu=1}^w \mathbb{E}_{b,y} \left[\log_2 \frac{\sum_{x' \in \mathcal{X}} f(y|x')}{\sum_{x' \in \mathcal{X}_\mu^b} f(y|x')} \right], \quad (4) \end{aligned}$$

where \hat{v}_μ is the μ -th ($\mu = 1, 2, \dots, w$) labeling bits within a transmitted symbol $x \in \mathcal{X}$, and $\mathcal{X}_\mu^b \subset \mathcal{X}$ is the constellation subset of the signal points, in which the μ -th labeling bit has value $b \in \{0, 1\}$. In a BICM-NI scheme, the w labeling bits within the M -ary symbol are demapped independently, leading to some MI loss. As a result, BICM-NI is not able to maximize the achievable rate, and thus is a suboptimal transmission scheme. The suboptimality of the BICM-NI can be easily proved mathematically [20], [24], i.e., $C_{\text{BICM-NI}} \leq C_{\text{CM}}$.

To overcome the above drawback, in [21], [22], a serially concatenated iterative decoding framework was proposed for the BICM-NI system, wherein the extrinsic information can be iteratively updated between the inner demodulator and outer decoder (see Fig. 1), which establishes a BICM-ID system. In the BICM-ID system, the demodulation of one labeling bit within an M -ary symbol is dependent on the remaining $w-1$ bits such that their soft information can be substantially exploited. The serially concatenated iterative decoding framework is beneficial for compensating the mutual-information loss of the traditional BICM-NI, allowing the BICM-ID system to maximize the achievable rate [59], [68], [80], [91], [178], [200]. Due to the above superiority, the BICM-ID system is able to achieve excellent performance as the CM system, and thus can be viewed as an optimal transmission scheme. Accordingly, the CM capacity can be directly treated as the fundamental capacity limit of BICM-ID, as highlighted in [71], [201], [202].

Remark: The CM capacity is only relevant to the signal constellation but irrelevant to the labeling scheme, while the BICM capacity is relevant to both the signal constellation and labeling scheme. The CM and BICM capacities only indicate the fundamental performance limits of the BICM-ID and BICM-NI, respectively. In practice, the design of PLDPC codes, signal constellations, bit mappers and labeling schemes have significant influence on the system performance.

There exist numerous labeling rules for high-order constellations, most of which are feasible for BICM systems. However,

no labeling can achieve best performance over all scenarios [78]. Among all the existing labelings, Gray labeling [94], anti-Gray labeling [203], set-partitioning (SP) labeling [204], and maximum squared Euclidean weight (MSEW) labeling [78] have attracted particular interest in the CM community.

Example 1: Fig. 2 depicts the constellations of QPSK, 8PSK, and 16QAM, with Gray labeling, anti-Gray labeling, SP labeling, and MSEW labeling. Referring to this figure, the anti-Gray labeling, SP labeling, and MSEW labeling have identical constellation for QPSK modulation. Indeed, there are only two different possible labeling rules for QPSK constellation, since it consists of four different signal points. Thereby, anti-Gray labeling, SP labeling, and MSEW labeling naturally have the same performance (e.g., capacity) under QPSK modulation.

To further analyze the CM and BICM capacities of the QPSK, 8PSK, and 16QAM with the above four labelings, consider again Fig. 3 where the Shannon capacity is also included. It can be observed that the Gray labeling achieves the best capacity among all the four labelings in the BICM-NI system. Moreover, the Gray-labeled BICM-NI has capacities closely approaching its corresponding BICM-ID counterparts for QPSK, 8PSK and 16QAM modulations. Particularly, for the QPSK modulation, the Gray-labeled BICM-NI and BICM-ID have identical capacity, while the anti-Gray-labeled BICM-NI, SP-labeled BICM-NI, and MSEW-labeled BICM-NI have an obvious capacity gap from the BICM-ID. This indicates that Gray labeling may obtain trivial performance gain with the use of ID, while the other three types of labelings may obtain desirable performance gains in the ID scenario. Motivated by this conjecture, intensive research effort has been carried out to explore the applicability of the Gray labeling in BICM systems. Many evidences have been found to support the view that this labeling rule is only suitable for BICM-NI but is incapable of accomplishing satisfactory performance for BICM-ID [22], [58], [71], [78], [154], [205].

C. Summary

In this section, the system architecture and transmission mechanism of a general PLDPC-BICM is presented. Some relevant channel models employed in the study of PLDPC-BICM are reviewed and classified into four different categories: AWGN, Nakagami fading, Poisson PPM, and NAND flash-memory channels. Subsequently, the channel capacity for BICM is discussed, which is fundamental theoretical objective for systems design. Finally, major contributions in the development of PLDPC-BICM are summarized and commented.

III. BASIC PRINCIPLES OF PLDPC CODES

PLDPC codes represent a sophisticated class of LDPC codes, which have attracted considerable attention due to their excellent performance and simple structure [43], [65]. Motivated by these advantages, many meritorious variants of PLDPC codes have been formulated to satisfy the diverse requirements of modern communication and storage applications. Of most interest are the SC-PLDPC codes that inherit the advantages of both PLDPC codes and convolutional codes [67], [137], [138]. During the past two decades, the PLDPC codes and their SC variants have been intensively investigated and become a promising practical alternative for spectral-efficiency BICM configurations [64], [92],

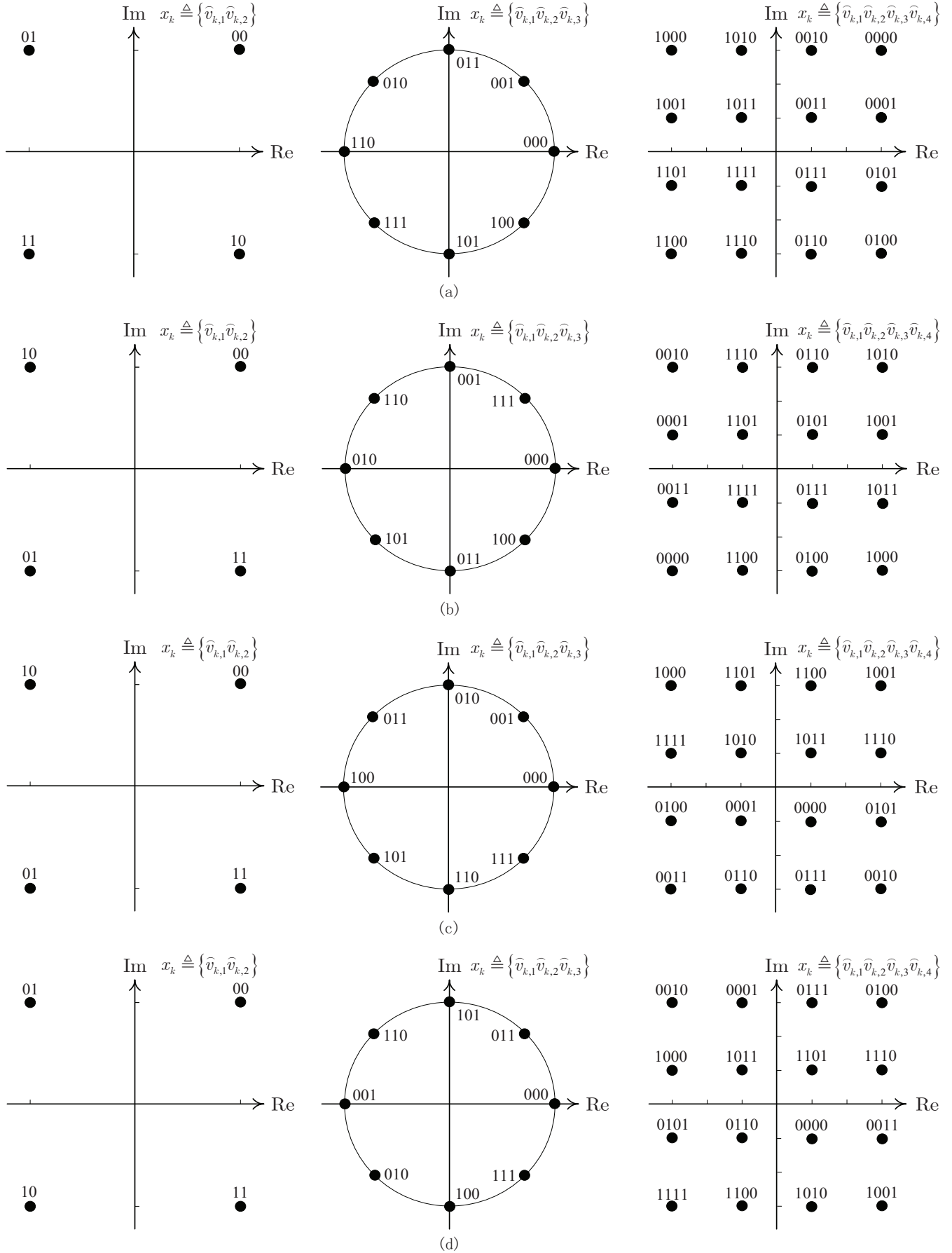


Fig. 2. Constellations for the QPSK, 8PSK, and 16QAM with (a) Gray labeling, (b) anti-Gray labeling, (c) SP labeling, and (d) MSEW labeling.

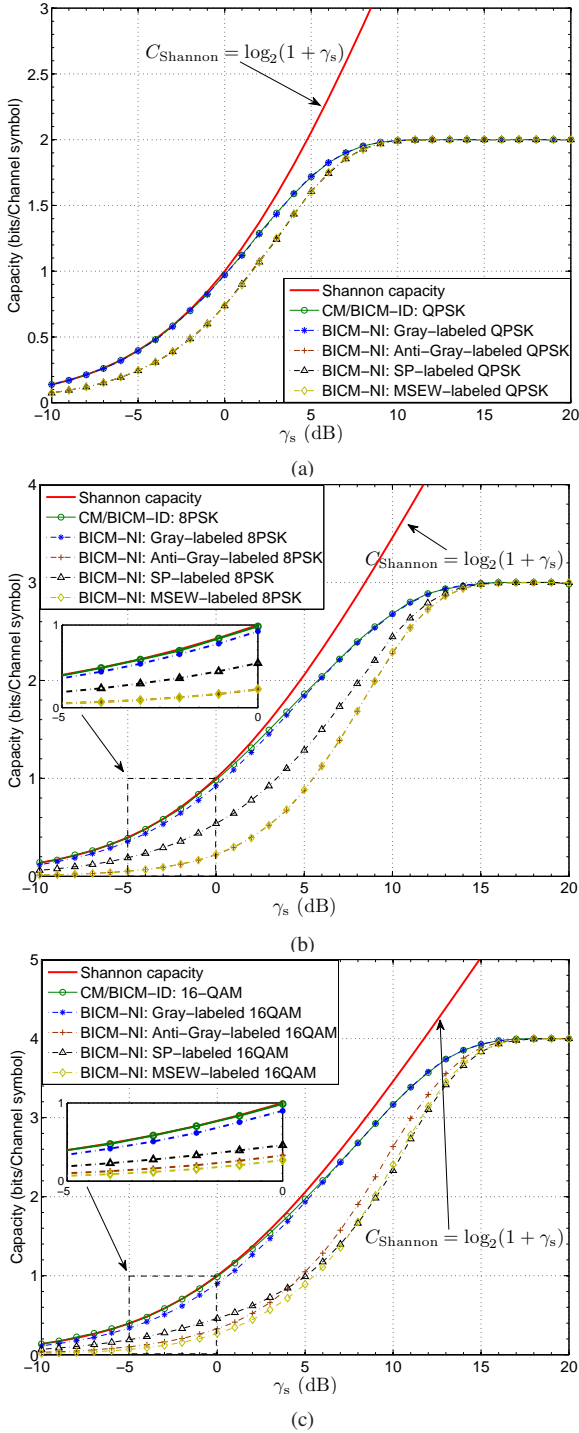


Fig. 3. CM and BICM capacities of (a) QPSK, (b) 8PSK, and (c) 16QAM over an AWGN channel with Gray labeling, anti-Gray labeling, SP labeling, and MSEW labeling.

[127]–[130], [135], [136], [149]–[156]. In the following, some basic preliminaries of PLDPC codes are presented.

A. LDPC Codes

An LDPC code Λ can be represented by either a parity-check matrix or a Tanner graph [195]. Specifically, an LDPC code Λ with N variable nodes and M check nodes can be represented by an $M \times N$ parity-check matrix $\mathbf{H} = \{h_{i,j}\}$, where $h_{i,j} \in \{0, 1\}$ is the element in the i -th row and j -th column of \mathbf{H} . Here,

$K = N - M$ is the length of information bits, and $r = K/N$ is the code rate. In particular, each variable node corresponds to one column of \mathbf{H} , while each check node corresponds to one row of \mathbf{H} . If there is an edge between the j -th variable node v_j and the i -th check node c_i , then $h_{i,j} = 1$; otherwise, $h_{i,j} = 0$. Furthermore, the degree d_{v_j} (resp. d_{c_i}) of v_j (resp. c_i) is defined as the number of its associated edges, which equals the weight of the j -th column (resp. i -th row) of \mathbf{H} . According to [27], an LDPC code can be characterized by the degree-distribution pair, i.e., $(\{d_{v_j}\}, \{d_{c_i}\})$. If both the variable-node degree and the check-node degree are constants (i.e., $d_{v_1} = d_{v_2} = \dots = d_{v_N} = d_v$ and $d_{c_1} = d_{c_2} = \dots = d_{c_M} = d_c$), then the LDPC code is called a *regular LDPC code* with a rate of $r = 1 - d_v/d_c$; otherwise, the code is called an *irregular LDPC code*. A valid LDPC codeword must satisfy the condition of $\Lambda_v \mathbf{H}^T = 0$, where the superscribe “T” indicates the transpose operation.

There exist various realizations of the parity-check matrix \mathbf{H} of an LDPC code under a given parameter setting. Typically, one can exploit progressive-edge-growth (PEG) and approximate cycle extrinsic-message-degree algorithms, to produce a well-performing parity-check matrix \mathbf{H} based on a given degree-distribution pair and a given codeword length [195]. On the basis of the parity-check matrix, a number of techniques have been proposed to construct finite-length LDPC codes for attaining capacity-approaching performance and low implementation complexity over the last half a century. Among all the existing techniques, the QC-LDPC-code-oriented construction algorithms, such as the circulant-based PEG algorithm [100], [117] and the “pre-lifted” algorithm [206], are of great interest due to the fact that they can perform using unstructured LDPC codes and possess linear-complexity encoding and higher-throughput decoding. Nonetheless, the detailed construction of QC-LDPC codes is beyond the scope of this article and hence is omitted.

B. Protograph LDPC Codes

In 2003, a novel type of structured LDPC codes, PLDPC codes, was introduced [175], which can be generated by expanding a sufficiently small graph/matrix (i.e., protograph/base matrix). Specifically, a protograph $\mathcal{G}_P = (\mathcal{V}, \mathcal{C}, \mathcal{E})$ is defined as a relatively small-size Tanner graph, which contains a set of n_P variable nodes $\mathcal{V}_P = (v_1, v_2, \dots, v_{n_P})$, a set of m_P check nodes $\mathcal{C}_P = (c_1, c_2, \dots, c_{m_P})$, and a set of ϱ_P edges $\mathcal{E}_P = \{e_{i,j}\}$, where $e_{i,j}$ denotes the edge connecting the j -th variable node v_j to the i -th check node c_i , $\varrho_P = |\mathcal{E}_P|$, and $r_P = (n_P - m_P)/n_P$ denotes the code rate [43], [65].² Moreover, the adjacency matrix of a protograph, whose columns and rows correspond to the n_P variable nodes and m_P check nodes, respectively, is defined by an $m_P \times n_P$ base matrix $\mathbf{B} = \{b_{i,j}\}$. Also, the (i, j) -th element $b_{i,j}$ of \mathbf{B} denotes the number of edges connecting v_j to c_i . To generate an $M \times N$ derived graph (i.e., Tanner graph) corresponding to an $M \times N$ parity-check matrix \mathbf{H} , one should perform the “copy-and-permute (also called *lifting*)” operation on the protograph \mathcal{G}_P , where $M = Zm_P$, $N = Zn_P$ and Z is the lifting factor. In other words, the protograph is first copied for Z times to obtain Z individual protographs; the edges of the Z

²In this article, a protograph with m_P check nodes and n_P variable nodes is referred to as an $m_P \times n_P$ protograph, with size $m_P \times n_P$.

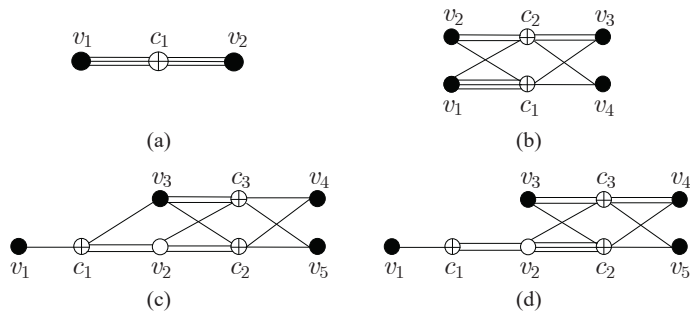


Fig. 4. Protograph structures of the rate-1/2 (a) regular PLDPC code, (b) RJA PLDPC code, (c) AR3A PLDPC code, and (d) AR4JA PLDPC code.

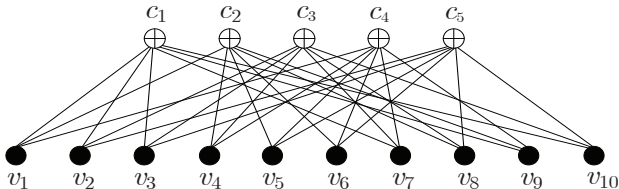


Fig. 5. Derived graph of a rate-1/2 regular-(3, 6) PLDPC code with $m_P = 1$, $n_P = 2$, $Z = 5$, $M = 5$, and $N = 10$.

individual replicas of \mathcal{G}_P are subsequently permuted within each type to produce a single derived graph under certain constraints. In particular, a type- j variable node (i.e., a replica of v_j) can only be connected to a type- i check node (i.e., a replica of c_i) via a type- (i, j) edge (i.e., a replica of $e_{i, j}$) in the lifting procedure. The resultant derived graph or parity-check matrix gives rise to a length- N PLDPC code. Unlike the conventional LDPC codes, parallel edges (i.e., multiple edges between a variable node and a check node) are permitted in a protograph, but they must be carefully permuted in the lifting process such that the derived graph only includes a single edge between any variable node and any check node [175]. Besides, punctured variable nodes may exist in the protograph to either boost the code rate or improve the convergence performance. The code rate of a punctured PLDPC code becomes

$$r_P = \frac{n_P - m_P}{n_P - n_E} = \frac{n_P - m_P}{n_T}, \quad (5)$$

where n_T and n_E are the numbers of transmitted variable nodes and punctured variable nodes of the protograph, respectively.

To date, several methods have been proposed to expand a protograph to a derived graph, among which the modified PEG algorithm is the most popular one [117], [207]. For a given lifting algorithm, the performance of a PLDPC code is determined only by the protograph, which tremendously reduces the degree of difficulty in code design and analysis. In accordance with the above reasons, the optimization of a PLDPC code is equivalent to the design of a capacity-approaching protograph associated with a small-size base matrix, which is more concise and reachable than the parity-check matrix of a conventional LDPC code. In this article, the modified PEG algorithm proposed in [117, Appendix A] is adopted to implement the lifting procedure.

Remark: As illustrated in [114], [115], the QC-LDPC codes can be treated as a special case of the PLDPC codes. A PLDPC code is exactly equivalent to a QC-LDPC code if a circulant-based PEG algorithm [100], [101], [207] is used to perform the “copy-and-permute” operation on the protograph.

Example 2: The base matrices and protographs of four conventional rate-1/2 PLDPC codes, namely regular-(3, 6) PLDPC code [65], repeat-jagged-accumulate (RJA) PLDPC code [208], accumulate-repeat-3-jagged-accumulate (AR3A) PLDPC code [209], and accumulate-repeat-by-4-jagged-accumulate (AR4JA) PLDPC code [67], are presented in (6) and Fig. 4, respectively. In this figure, the blank circles represent the punctured variable nodes. Among the four codes, the AR3A and AR4JA codes are two prestigious types of PLDPC codes because they can respectively achieve excellent performance in the low- and high-SNR regions over AWGN channels. As shown in [65], [209], introducing a small fraction of punctured variable nodes to the protographs can boost the transmission rates of PLDPC-systems and also improve their decoding thresholds in certain scenarios. The basic principle of puncturing for PLDPC codes is available in [43], [117], [141], [209].

$$\mathbf{B}_{\text{REG}} = \begin{bmatrix} 3 & 3 \end{bmatrix}, \quad \mathbf{B}_{\text{RJA}} = \begin{bmatrix} 3 & 1 & 1 & 1 \\ 1 & 2 & 2 & 1 \end{bmatrix},$$

$$\mathbf{B}_{\text{AR3A}} = \begin{bmatrix} 1 & 2 & 1 & 0 & 0 \\ 0 & 2 & 1 & 1 & 1 \\ 0 & 1 & 2 & 1 & 1 \end{bmatrix}, \quad \mathbf{B}_{\text{AR4JA}} = \begin{bmatrix} 1 & 2 & 0 & 0 & 0 \\ 0 & 3 & 1 & 1 & 1 \\ 0 & 1 & 2 & 2 & 1 \end{bmatrix}. \quad (6)$$

As a further advance, with the lifting factor $Z = 5$, one can promptly obtain the derived graph (i.e., Fig. 5) corresponding to a length-10 regular-(3, 6) PLDPC code by performing a randomly lifting operation [44], [65] on the protograph in Fig. 4(a).

C. Spatially-Coupled PLDPC Codes

As a meritorious variant of PLDPC codes, SC-PLDPC codes are capable of achieving desirable convolutional gains without sacrificing the dominant feature of protographs [67], [208]. In general, there are two major categories of SC-PLDPC codes, i.e., *TE-SC-PLDPC codes* and *TB-SC-PLDPC codes*.

1) *Terminated SC-PLDPC Codes:* A TE-SC-PLDPC code can be constructed by employing an edge-spreading rule to couple together L_{SC} disjoint replicas of a protograph into a single coupled chain, where L_{SC} is defined as the coupling length. One can proceed the construction by replicating a protograph L_{SC} times, where these individual protographs are indicated with a time index t ($t = 1, 2, \dots, L_{SC}$). Suppose that the PLDPC code consists of n_P variable nodes, m_P check nodes, and ϱ_P edges. The ϱ_P edges emanating from the n_P variable nodes at time instant t are spread over the $(\varsigma+1)m_P$ check nodes at time instants $t, t+1, \dots, t+\varsigma$, according to a predefined edge-spreading rule, where $0 < \varsigma < L_{SC}$ is the coupling width or edge-spreading factor. Owing to the termination effect, ςm_P additional check nodes are inserted at time instants $L_{SC}+1, L_{SC}+2, \dots, L_{SC}+\varsigma$ of the TE-SC protograph, which leads to a lower code rate with respect to the uncoupled PLDPC code. In other words, the code rate of a TE-SC-PLDPC code equals

$$r_{\text{TE-SC}} = 1 - \frac{(L_{SC} + \varsigma)m_P}{L_{SC}n_P} = r_P - \frac{\varsigma m_P}{L_{SC}n_P}, \quad (7)$$

where r_P is the code rate of the uncoupled PLDPC code. Moreover, $\nu_{SC} = (\varsigma + 1)Zn_P$ is defined as the constraint length of the TE-SC-PLDPC code, where Z is the lifting factor. Alternatively, a TE-SC-PLDPC code can be obtained by directly terminating the coupled chain of a convolutional PLDPC code

with a finite coupling length. Although TE-SC-PLDPC codes are able to asymptotically achieve the optimal MAP decoding thresholds of the underlying uncoupled PLDPC codes with BP decoding (called “*threshold saturation*”) due to the structured irregularity, they suffer from non-trivial code-rate loss with a finite coupling length [67], [206]. The rate loss of such codes can be an arbitrarily small value if the coupling length approaches infinity (i.e., $L_{SC} \rightarrow +\infty$), but this leads to extremely long codeword lengths. The above drawback severely restricts the practical applications of TE-SC-PLDPC codes.

On the other hand, the edge spreading of a protograph is equivalent to the division of a base matrix. In particular, the base matrix \mathbf{B} of a protograph is split to $\varsigma + 1$ sub-base matrices during the edge-spreading procedure, denoted by $\mathbf{B} = \mathbf{B}_{S,1} + \mathbf{B}_{S,2} + \dots + \mathbf{B}_{S,\varsigma+1}$, where $\mathbf{B}_{S,\mu}$ is the μ -th ($\mu = 1, 2, \dots, \varsigma + 1$) sub-base matrix, and the sizes of all the sub-base matrices are identical to that of the original base matrix. Analogously to the protograph construction, combining L_{SC} groups of $\varsigma + 1$ sub-base matrices results in an $m_P(L_{SC} + \varsigma) \times n_P L_{SC}$ base matrix of the TE-SC-PLDPC code, as shown in [67, eq. (8)].

2) *Tail-biting SC-PLDPC Codes*: To tackle the rate-loss weakness, a tail-biting method was introduced instead of the direct termination method to terminate the coupled chain [67], which yields a new type of SC-PLDPC codes, named *TB-SC-PLDPC codes*. Specifically, a TB-SC-PLDPC code can be constructed on the basis of a TE-SC-PLDPC code by combining the check nodes at time instants $t = L_{SC} + 1, L_{SC} + 2, \dots, L_{SC} + \varsigma$ with the check nodes at time instants $t = 1, 2, \dots, \varsigma$, into ς check nodes. As a result, the total number of check nodes decreases to $m_P L_{SC}$ and the code rate of the TB-SC-PLDPC code becomes $r_{TB-SC} = 1 - m_P/n_P = r_P$. The TB-SC-PLDPC code shares an identical structure and degree-distribution pair as the uncoupled PLDPC code because of the tail-biting operation; but the former possesses a relatively better property of linear and minimum-distance growth, due to the spatially coupling operation. Yet, the “*threshold saturation*” phenomenon is no longer retained for a TB-SC-PLDPC code as the irregularity feature vanishes [67].

Recently, some novel techniques have been proposed to enhance the convergence performance of TB-SC-PLDPC codes, making them a desirable choice for practical systems [144].

Example 3: Fig. 6(a) shows a simple edge-spreading rule with $\varsigma = 2$ for a rate-1/2 regular-(3, 6) PLDPC code. As a further advance, the protograph structures of the regular TE-SC-PLDPC code and TB-SC-PLDPC code, constructed from the regular-(3, 6) PLDPC code by using the above edge-spreading rule, are presented in Fig. 6(b) and Fig. 6(c), respectively. Supposing $L_{SC} = 5$, the regular TE-SC-PLDPC code and TB-SC-PLDPC code have rates $r_{TE-SC} = 3/10$ and $r_{TB-SC} = 1/2$, respectively. In comparison, TB-SC-PLDPC codes are more likely to realize high spectral-efficiency communication and storage than their TE relatives in finite-coupling-length scenarios.

D. Theoretical-Analysis Tools

Designing and implementing capacity-approaching PLDPC-BICM is a major objective for communication and storage. To achieve this goal, it is important to develop efficient theoretical tools and performance metrics tailored for such serially concatenated schemes [24]. Initially, some prestigious numerical

analysis techniques, such as density evolution [38] and EXIT function [36], [37], were deployed to characterize the convergence performance of all the components (e.g., encoder, constellation, interleaver, and decoder) of PLDPC-BICM systems in the low-SNR region. As a complementary analysis tool, AWE was designed to predict the convergence performance of PLDPC codes in BICM systems in the high-SNR region [65], [208]. Especially, the combination of the EXIT/DE and AWE acts as a complete analytical configuration for the PLDPC codes in BICM systems, which is able to accurately measure the asymptotic performance in the whole SNR region. Besides, harmonic mean of the minimum squared Euclidean distance (HMMSED) was introduced as a secondary analytical metric for the PLDPC-BICM systems, which is of great usefulness for estimating the attainable performance of constellations [46], [88]. Although some other theoretical tools have been developed for BICM systems, the EXIT, AWE and HMMSED analyses have drawn perhaps the greatest attention from the field of PLDPC-BICM because they provide accurate performance estimates, and also facilitate the system design.

1) *PEXIT Algorithm*: In 2001, the DE algorithm [38] was developed to analyze the convergence performance of LDPC codes in an iterative decoding processor. Despite the accurate characterization of the convergence performance, the DE algorithm must track the entire PDF of LLRs and thus suffers from high computational complexity. By contrast, EXIT algorithm takes the MI into account and produces a visualized extrinsic-MI-convergence chart to determine the decoding thresholds under iterative decoding [36], [37]. Building upon the MI metric, the EXIT algorithm can greatly simplify the threshold calculation of LDPC-systems without deteriorating the accuracy. Moreover, it has strong robustness against the variation of channel conditions. The EXIT algorithm can be directly applied to a large variety of channels, modulations and decoders, with only slight modifications. Also, it is very convenient to use the EXIT algorithm to characterize the decoding trajectories of concatenated systems, including BICM and non-binary CM systems. Thanks to the above superiorities, EXIT algorithms have been used as the dominant theoretical tool for analysis and design of BICM systems [51], [63], [64], [78]–[80], [88]–[90], [210].

However, the standard EXIT algorithm, which yields two-dimensional extrinsic-MI-convergence charts and calculates the decoding thresholds for conventional LDPC codes, is not applicable to the PLDPC codes in BICM systems. More precisely, the PLDPC codes may contain some degree-1 variable nodes, punctured variable nodes, and parallel edges in the corresponding base matrices, which are generally not allowed in conventional LDPC codes [65]. Moreover, some PLDPC codes possessing different base-matrix representations may share the same degree-distribution pair [40]. The standard EXIT algorithm was developed based on the degree-distribution pairs and hence does not have the capability to deal with the above issues. To address this issue, a multi-dimensional EXIT algorithm, called *PEXIT algorithm*, was developed to analyze the statistical convergence property of PLDPC codes [40], [211]. In particular, the PEXIT algorithm tracks the convergence behavior of extrinsic MIs for each variable node and check node in the protograph, but not their average MIs specified by the degree-distribution pair. In

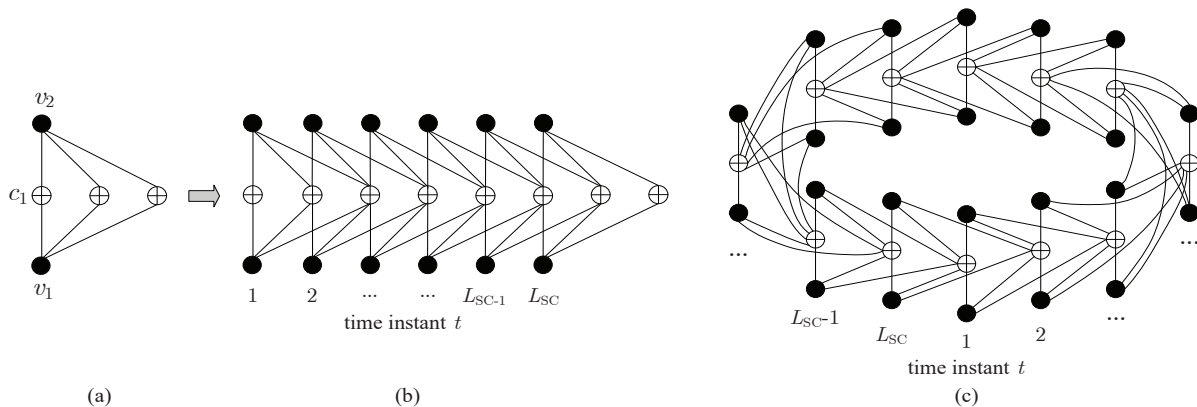


Fig. 6. Protograph structures of the regular-(3, 6) SC-PLDPC codes: (a) edge-spreading rule, (b) TE-SC-PLDPC code, and (c) TB-SC-PLDPC code, where the coupling width is $\zeta = 2$ and coupling length is L_{SC} .

TABLE III

DECODING THRESHOLDS $(E_b/N_0)_{th}$ (dB) OF THE REGULAR-(3, 6) PLDPC CODE IN BICM SYSTEMS WITH FOUR DIFFERENT LABELING SCHEMES OVER AN AWGN CHANNEL. THE MAXIMUM NUMBERS OF GLOBAL ITERATIONS IN THE NI AND ID CASES ARE SET AS $t_{GL,max} = 1$ AND $t_{GL,max} = 8$, RESPECTIVELY, WHILE THE MAXIMUM NUMBER OF THE LOCAL ITERATIONS IS SET AS $t_{BP,max} = 25$.

Modulation Type \ Constellation Type	Gray	Anti-Gray	SP	MSEW
NI: 8PSK	2.587	6.195	5.013	6.188
ID: 8PSK	2.323	4.307	3.049	4.429
NI: 16QAM	3.415	5.927	6.687	6.514
ID: 16QAM	3.201	4.385	4.724	5.027

spite of a lack of visualized MI-convergence chart, the PEXIT algorithm can yield accurate decoding thresholds by dealing with a small-size protographs [71], [179]. In parallel with the asymptotic PEXIT algorithms, some finite-length PEXIT algorithms were proposed for estimating the finite-length performance of PLDPC codes [44], [209]. Interested readers are referred to [71], [154] for the detailed steps of the PEXIT algorithm.

Remark: The decoding threshold of a PLDPC code in a BICM-ID system is determined by the types of code, constellation as well as the interleaver used. In this sense, the PEXIT algorithm can be effectively used to guide the design of the BICM-ID systems with these three components.

Example 4: Table III presents the decoding thresholds of the regular-(3, 6) PLDPC code derived by the PEXIT algorithm in BICM systems with four different constellations over an AWGN channel. As seen, the Gray labeling exhibits the lowest decoding threshold among all the four labelings, irrespective of the modulation order and receiver type. However, for a fixed modulation order, the threshold difference between the ID and NI for the Gray labeling is much smaller than those for the other three labelings, which indicates that the former can only achieve a trivial iterative gain. It was demonstrated in [22], [71], [205] that the Gray labeling is best suited to BICM-NI, but is not well suited to BICM-ID, in various transmission environments.

2) *Asymptotic-Weight-Enumerator Analysis:* According to [43], [44], [65], [195], the AWE can effectively estimate the minimum Hamming weight (or Hamming distance) and its distribution of a PLDPC code ensemble, which are of great usefulness in predicting the asymptotic performance of a PLDPC code in the high-SNR region. Moreover, PLDPC code ensembles, which have the desirable minimum-distance property, possess relatively

fewer pseudocodewords and trapping sets compared with the ensembles that do not have such a property [141], [208]. As illustrated in [43], [116], the PLDPC codes drawn from the ensembles having minimum distance and growing linearly with the codeword length (i.e., the linear-minimum-distance-growth property) always possess low error floors under BP decoding. Many theoretical and experimental evidences have suggested a performance tradeoff between the low-SNR region and high-SNR region for a PLDPC code [67], [145].

(1) **AWE Analysis for PLDPC Codes:** Consider a PLDPC-BICM system with the same parameters as in Section III-B. The normalized logarithmic AWE function of the PLDPC code ensemble is defined as

$$r(\delta) = \lim_{N_T \rightarrow \infty} \sup (\ln(\mathcal{A}_{\omega_{HAM}}) / N_T), \quad (8)$$

where $\sup(\cdot)$ is the supremum operation, δ is the normalized weight, $\mathcal{A}_{\omega_{HAM}}$ is the ensemble weight enumerator, $\omega_{HAM} = \delta N_T$ is the Hamming weight (or distance), and N_T is the transmitted codeword length. One can easily examine the AWE function to identify the existence of the property of linear minimum-distance growth and to derive the *minimum-Hamming-distance growth rate* (MHDGR). Assume that the AWE begins with the first zero-crossing at $\delta = 0$ and has the second zero-crossing at $\delta = \delta_{HAM} > 0$. If $r(\delta) < 0$ for all $\delta \in (0, \delta_{HAM})$, then δ_{HAM} is called the MHDGR of the code ensemble. Under this condition, the minimum Hamming distance grows linearly with the transmitted codeword length with an arbitrarily high probability in an asymptotic fashion. Hence, the PLDPC code ensembles with valid MHDGRs are superior to their counterparts that do not have this property in the high-SNR region. Furthermore, a larger MHDGR always leads to a better asymptotic performance in the high-SNR region [115].

Example 5: Fig. 7 shows the AWE curves of the rate-1/2 regular PLDPC code, RJA code, AR3A code, and AR4JA code. It is apparent that the AR3A code does not have the property of linear minimum-distance growth, due to the lack of positive zero-crossing, while the other three types of PLDPC codes have such a property. In particular, the MHDGRs of the regular PLDPC code, RJA code and AR4JA code are 0.023, 0.013 and 0.014, respectively. This suggests that the AR3A code is more prone to error-floor behavior with respect to other three types of codes.

(2) **AWE Analysis for SC-PLDPC Codes:** Consider an SC-PLDPC-BICM system, in which the channel code is constructed

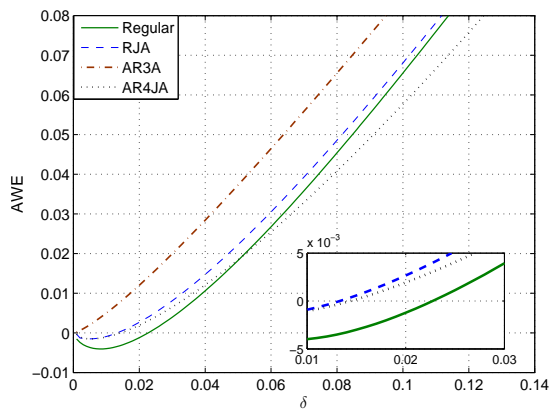


Fig. 7. AWE curves of the rate-1/2 regular-(3, 6) PLDPC code, RJA code, AR3A code, and AR4JA code.

by combining a group of disjoint protograph replicas together into a spatially-coupled chain. In contrast to the uncoupled PLDPC codes, the constraint length (i.e., $\nu_{SC} = (\zeta + 1)Zn_P$) of an SC-PLDPC code specifies the maximum number of variable nodes associated with the check nodes at any time instant t in its corresponding derived graph. Precisely speaking, the constraint length for an SC-PLDPC code is equivalent to the codeword length for an uncoupled PLDPC code.

As illustrated in [208], the minimum free distance d_{free} is more appropriate for evaluating the asymptotic performance of SC-PLDPC codes in the high-SNR region with respect to the minimum Hamming distance. Here, the minimum free distance of an SC-PLDPC code ensemble is defined as the minimum Hamming distance between any two individual codewords drawn from this code ensemble. An SC-PLDPC code ensemble is said to be asymptotically good in the high-SNR region if its minimum free distance grows linearly with the constraint length (i.e., $d_{free}(L_{SC}) = \delta_{free}(L_{SC})\nu_{SC}$) with an arbitrarily high probability, where $\delta_{free}(L_{SC})$ is defined as the *minimum free-distance growth rate* (MFDGR) for the code ensemble with a coupling length $L_{SC} > \zeta$. Benefiting from the convolutional effect, the SC-PLDPC codes usually possess better minimum-distance property than the corresponding uncoupled PLDPC codes. In the following, both the minimum free distance and minimum Hamming distance are referred to as *minimum distance* unless ambiguity may arise.

It was pointed out in [67] that the SC-PLDPC codes can retain the linear-minimum-distance-growth property if their uncoupled PLDPC codes have such a property. The average minimum free distance of the TE-SC-PLDPC code ensemble is upper-bounded by the average minimum Hamming distance of its corresponding block-code ensemble, while that of the TB-SC-PLDPC code ensemble is lower-bounded by the average minimum Hamming distance of its corresponding block-code ensemble [208]. With this property, the upper bound and lower bound of the MFDGRs for TE- and TB-SC-PLDPC codes can be respectively derived as [208, eqs. (18)] and [208, eqs. (19)]. The above two bounds will converge to the same value as L_{SC} becomes large enough.

Remark: The minimum-distance metrics are only relevant to the type of code ensemble, but irrelevant to other components of PLDPC-BICM. Moreover, there exists a trade-off between the decoding threshold and minimum distance for a PLDPC code.

Example 6: Fig. 8 illustrates the MFDGR bounds of the rate-

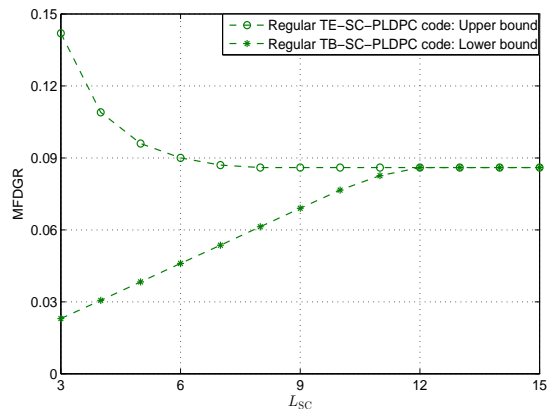


Fig. 8. MFDGR bounds of the regular-(3, 6) SC-PLDPC codes with $\zeta = 2$.

1/2 regular-(3, 6) SC-PLDPC codes. It can be observed that the upper bound and lower bound on MFDGRs of the regular SC-PLDPC code ensembles converge to the same value (i.e., $\delta_{free}(L_{SC}) = 0.086$) when the coupling length exceeds 12, which is much larger than the MHDGR ($\delta_{HAM} = 0.023$) of their uncoupled PLDPC code ensemble. Similar conclusion can be made for the RJA SC-PLDPC code ensembles [67], [140].

3) *Harmonic Mean of Minimum Squared Euclidean Distance Analysis:* Aiming to analyze the constellation performance in BICM systems, Euclidean distance was introduced in [20]. In the past two decades, several constellation design methods were proposed to maximize the minimum squared Euclidean distance (MSED) [78]. However, the MSED metric cannot ensure an accurate BER bound. Consequently, the harmonic mean of the MSED (i.e., HMMSED) was put forward to serve as a more relevant cost function for the BER bound of BICM systems [46], [88], [90]. Especially, the asymptotic performance of the signal constellations in BICM systems can be inherently interpreted by the HMMSED. Specifically, the Hamming/free distance and HMMSED are two dominant factors affecting the performance of BICM, where the former and the latter control the slope and horizontal gain of the asymptotic BER curve in the high-SNR region, respectively. In fact, the HMMSED metrics can be utilized to optimize the asymptotic performance of signal constellations, which is independent of the code design. To facilitate the design of signal constellations in PLDPC-BICM systems, the HMMSED analysis is discussed below.

Consider an M -ary modulation with a constellation χ and a labeling rule ϕ . The HMMSED is expressed as [46]

$$d_{h,A}^2(\chi, \phi) = \left(\frac{1}{w2^w} \sum_{\mu=1}^w \sum_{b=0}^1 \sum_{x \in \chi_{\mu}^b} \frac{1}{|x - \tilde{x}_A|^2} \right), \quad (9)$$

where $A \in \{NI, ID\}$, $w = \log_2 M$ is the number of labeling bits within a signal point (or a modulated symbol), χ_{μ}^b is the constellation subset of signal points with the μ -th labeling bit value $b \in \{0, 1\}$, x is a signal point belonging to χ_{μ}^b , and $\tilde{x}_A \in \bar{\chi}_{\mu}^b$ represents the signal point closest to x in the complementary set of χ_{μ}^b in the case of BICM-NI, and also represents the signal point with the same labeling-bit value as those in x except the μ -th labeling bit in the case of BICM-ID with error-free feedback. In the following, $d_{h,NI}^2(\chi, \phi)$ and $d_{h,ID}^2(\chi, \phi)$ are referred to as *NI-HMMSED* and *ID-HMMSED*, respectively. Based on the two HMMSED metrics, one can promptly obtain the offset gain as

TABLE IV
 NI-HMMSED $d_{h,NI}^2(\chi, \phi)$, ID-HMMSED $d_{h,ID}^2(\chi, \phi)$, AND OFFSET GAIN G_h (dB) OF THE 16QAM CONSTELLATIONS WITH THE GRAY LABELING, ANTI-GRAY LABELING, SP LABELING, AND MSEW LABELING.

Constellation Type	Gray	Anti-Gray	SP	MSEW
$d_{h,NI}^2(\chi, \phi)$	0.492	0.400	0.441	0.400
$d_{h,ID}^2(\chi, \phi)$	0.514	0.993	1.119	2.364
G_h	0.190	3.050	3.569	6.817

$$G_h = 10 \log_{10} \frac{d_{h,ID}^2(\chi, \phi)}{d_{h,NI}^2(\chi, \text{Gray})} \text{ (in dB)}, \quad (10)$$

which specifies the asymptotic iterative gain attained by an ideal BICM-ID with respect to the optimal Gray-labeled BICM-NI.

Actually, the ID-HMMSED is derived based on an ideal BICM-ID framework in which perfect *a priori* LLRs of the labeling bits are fed back to the demodulator. This assumption is unrealistic and may degrade the accuracy of performance evaluation for BICM-ID systems. From the design point of view, it is advisable to choose a constellation exhibiting a good balance between the NI-HMMSED and the ID-HMMSED, such that the BICM is able to achieve sufficiently good performance in both NI and ID scenarios after a few global iterations [180]. Moreover, a powerful resistance to the feedback errors is particularly important for the constellation shaping in BICM-ID systems.

Example 7: The NI-HMMSED $d_{h,NI}^2(\chi, \phi)$, ID-HMMSED $d_{h,ID}^2(\chi, \phi)$ and offset gain G_h (dB) of four classic 16QAM constellations are shown in Table IV. As observed, the Gray labeling achieves the largest $d_{h,NI}^2(\chi, \phi)$, but the smallest $d_{h,ID}^2(\chi, \phi)$ and G_h . This phenomenon reveals that the Gray labeling may not be suitable for BICM-ID systems. On the contrary, MSEW labeling suffers from the smallest $d_{h,NI}^2(\chi, \phi)$, but benefits from the largest $d_{h,ID}^2(\chi, \phi)$, which indicates that it may outperform other three labelings in BICM-ID scenario with perfect *a priori* information. However, the MSEW labeling may not achieve the best performance in the case with feedback errors.

E. Summary

In this section, the basic principles of PLDPC codes and SC-PLDPC codes are first reviewed. Then, three types of prevailing theoretical-analysis tools are introduced for the PLDPC-BICM, which can be used to develop system design and optimization methods. Specifically, the PEXIT algorithm, AWE analysis, and HMMSED analysis are discussed, which respectively yield three critical performance metrics, i.e., decoding threshold, minimum distance rate, and HMMSED, for the PLDPC-BICM.

IV. DESIGN OF PLDPC-BICM OVER AWGN CHANNELS

This section summarizes the current research achievements in the design of PLDPC-BICM systems over AWGN channels, which can be used to model various communication scenarios, e.g., deep-space communication systems [42], [65], satellite broadcasting systems [102], [121], optical communication systems [122], [150], [151]. As discussed in Section II-A, the BICM design developed over AWGN channels usually perform well over other memoryless channels if they have similar input-output MIs. Hence, the AWGN channel is considered as a proper surrogate channel for some complex channel models.

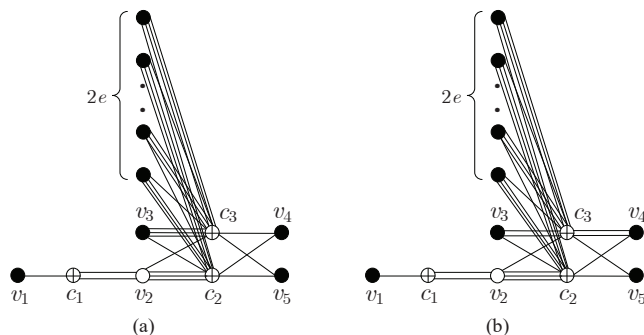


Fig. 9. Structures of (a) AR4A code [65] and (b) AR4JA code [122], with a code rate of $r_P = (e + 1)/(e + 2)$ ($e = 0, 1, 2, \dots$).

A. Design of PLDPC-BICM Systems

1) *Code Construction:* In PLDPC-BICM systems, most related works exploited computer search methods to construct capacity-approaching PLDPC codes with linear-minimum-hamming-distance-growth property based on the PEXIT algorithm and AWE analysis. The first attempt was made in [116] to carry out a joint design of PLDPC codes and high-order modulation. Motivated by this pioneering work, the majority of coding efforts turned to investigating the interplay between the PLDPC codes and high-order modulations as well as the concatenation of these two types of techniques. For instance, a family of AR4A codes (see Fig. 9(a)) were applied to the BICM-NI systems with various high-order modulations over AWGN channels [118], [122], [170]. These studies concentrated on the optimization of bit-mapping schemes but not on PLDPC codes. In the following, several PLDPC-code constructions in BICM systems over different channels are discussed.

(1) **Code Design for PSK/QAM-aided BICM-NI:** To ensure the capacity-approaching performance of BICM-NI systems with *MPSK/MQAM* modulations, a family of RC PLDPC codes, called *AR4JA codes*, were constructed in [116], with the structure shown in Fig. 9(b). Referring to this figure, the AR4JA codes cover a wide range of rate from $1/2$ to $1 - \epsilon$, where ϵ is an arbitrarily small positive value. The higher-rate AR4JA codes are formulated by repeatedly adding $2e$ ($e = 0, 1, 2, \dots$) degree-4 variable nodes into the rate- $1/2$ AR4JA code and then connecting them to the two highest-degree check nodes c_2 and c_3 (see Fig. 9(b)). The AR4JA codes possess both desirable decoding thresholds and linear-minimum-Hamming-distance-growth property. Meanwhile, a novel bit-mapping scheme, i.e., *VDMM scheme* was constructed by combining the AR4JA code with 16QAM modulation, which improves the spectral efficiency of PLDPC-based BICM-NI systems. The details of VDMM scheme will be further discussed in Section IV-A3.

(2) **Code Design for ASK-aided BICM-NI:** In parallel with the above research progress, a systematic study on the code construction and analysis of PLDPC-BICM-NI systems with probabilistic signal shaping was carried out in [171], [172]. In classic BICM-NI systems, the transmitted symbols are always assumed to follow a uniform distribution and the w labeling bits within a given symbol are always treated as mutually independent, which leads to a non-trivial gap from the channel capacity. To overcome this weakness, a new symbol-distribution optimization scheme, called *probabilistic amplitude shaping (PAS)*, was proposed in

[183] to approach the capacity of BICM-NI with the use of rate- $(n_P - 1)/n_P$ PLDPC codes and ASK modulations. Based on the PAS-aided BICM-NI framework, a PEXIT-based design scheme was developed in [171], [172] to construct outstanding PLDPC codes operating within 0.39 ~ 0.45 dB to the channel capacities.

Specifically, consider a BICM-NI system with a rate- $(n_P - 1)/n_P$ PLDPC code and an M -ary ASK modulation. To achieve the PAS goal, the protograph corresponding to the PLDPC code should include $n_P = w$ variable nodes and $m_P = w - 1$ check nodes, where $w = \log_2 M$. The PLDPC code $\Lambda = (v_1, v_2, \dots, v_N)$ of length $N = Zn_P$ is first mapped to an ASK-modulated symbol sequence $\mathbf{x} = (x_1, x_2, \dots, x_{N'})$ of length N' , where $N' = N/w = Z$, $x_k \triangleq (\hat{v}_{k,1}, \hat{v}_{k,2}, \dots, \hat{v}_{k,w}) \in \chi$ is the k -th ($k = 1, 2, \dots, N'$) modulated symbol, $\hat{v}_{k,\mu}$ is the μ -th ($\mu = 1, 2, \dots, w$) labeling bit within the k -th symbol, and $\chi = \{\pm 1, \pm 3, \dots, \pm(2^w - 1)\}$ is the constellation set.

Totally, there are $Z(w - 1)$ information bits and Z parity bits in a PLDPC code of length $N = Zw$ in such a BICM-NI system. During the systematic encoding process, the $K = Z(w - 1)$ independent and identically distributed (i.i.d.) information bits $\mathbf{s} = (s_1, s_2, \dots, s_K)$ are passed through a distribution matcher [171], so as to yield Z groups of labeling bits $\{\hat{v}_{k,2}, \hat{v}_{k,3}, \dots, \hat{v}_{k,w} \mid k = 1, 2, \dots, Z\}$ with $A_k = \sum_{\mu=2}^w \hat{v}_{k,\mu} \cdot 2^{w-\mu}$ being the amplitude of the k -th group. Due to the effect of the distribution matcher, the $w - 1$ resultant labeling bits in each group are no longer i.i.d., but follow a non-uniform discrete distribution, which are mutually dependent. Furthermore, the Z parity bits $\Lambda_P = (v_{K+1}, v_{K+2}, \dots, v_{K+Z})$ can be promptly generated according to the checksum constraint $\Lambda \mathbf{H}^T = (\mathbf{s}, \Lambda_P) \mathbf{H}^T = \mathbf{0}$, which controls the relationship between a systematic codeword $\Lambda = (\mathbf{s}, \Lambda_P)$ and its corresponding parity-check matrix \mathbf{H}^T . The Z parity bits are appended to the information bits to constitute the overall systematic PLDPC code. They are consecutively employed to indicate the sign of the amplitudes of the Z labeling-bit groups to form the overall transmitted symbols $\{x_k \triangleq (\hat{v}_{k,1}, \hat{v}_{k,2}, \dots, \hat{v}_{k,w}) \mid k = 1, 2, \dots, Z\}$. Here, the first labeling bit of the k -th symbol $\hat{v}_{k,1} = \text{sign}(x_k)$ is uniformly mapped from the k -th parity bits v_{K+k} . Thus, $x_k = +A_k$ if $\hat{v}_{k,1} \triangleq v_{K+k} = 0$, and $x_k = -A_k$ otherwise. In the end, the distribution of M different signal points belonging to the Gray-labeled MASK constellation is optimized, so as to maximize the channel input-output MI and approach the constellation-unconstrained capacity with Gaussian-distributed symbols. The above technique is referred to as PAS. Especially, the PAS technique concatenates a probabilistic-shaping-aided distribution matcher with a systematic PLDPC encoder at the transmitter, and exploits a bit-metric BP decoder at the receiver.

To simplify the design of PLDPC codes in PAS-aided BICM systems, a surrogate channel was considered in [171]. A channel is said to be a *proper surrogate channel* if the code optimized for such a channel cannot be further improved over the target BICM channel by varying the bit-mapping scheme. Through simulations, the binary-input AWGN channel was found to be proper surrogate for each bit-channel of an MASK-aided BICM-NI channel with uniformly distributed input and PAS (non-uniform) input. Then, a novel PEXIT algorithm was developed for constructing the near-capacity PLDPC codes.

Example 8: Utilizing the PEXIT-aided computer search

TABLE V
DECODING THRESHOLDS $(E_b/N_0)_{\text{th}}$ (dB) AND CAPACITY GAPS Δ OF THE OPTIMIZED PLDPC CODES FOR THREE DIFFERENT MASK-AIDED BICM-NI SYSTEMS WITH UNIFORM INPUT AND PAS INPUT, WHERE THE GRAY LABELING IS USED.

Modulation Scheme	4ASK-U	8ASK-PAS	64ASK-PAS
$(E_b/N_0)_{\text{th}}$	5.57	7.77	25.52
Capacity	5.27	7.34	25.31
Δ	0.30	0.43	0.39

method, the rate- $(w - 1)/w$ PLDPC codes can be optimized for MASK-aided BICM-NI systems with uniform input and PAS input under the Gray-labeling. The base matrices and thresholds of the optimized PLDPC codes for such frameworks with three different modulation orders (i.e., different values of M) are illustrated in (11) and Table V, respectively. As a baseline, the capacities and the capacity gaps are also included in the table.

$$\begin{aligned} \mathbf{B}_{4\text{ASK-U}} &= \begin{bmatrix} 2 & 1 & 1 & 2 & 1 & 4 \\ 1 & 1 & 1 & 2 & 2 & 5 \\ 1 & 0 & 2 & 1 & 0 & 6 \end{bmatrix}, \\ \mathbf{B}_{8\text{ASK-PAS}} &= \begin{bmatrix} 1 & 1 & 1 & 1 & 1 & 6 \\ 2 & 2 & 1 & 1 & 2 & 6 \end{bmatrix}, \\ \mathbf{B}_{64\text{ASK-PAS}} &= \begin{bmatrix} 2 & 2 & 2 & 1 & 2 & 2 & 6 & 2 & 2 & 0 & 6 & 6 \\ 1 & 1 & 1 & 2 & 1 & 1 & 6 & 1 & 0 & 2 & 6 & 6 \end{bmatrix}. \quad (11) \end{aligned}$$

The rate-1/2 4ASK-U PLDPC code, rate-2/3 8ASK-PAS PLDPC code, and rate-5/6 64ASK-PAS PLDPC code are optimized for the 4ASK modulation with uniform input, 8ASK modulation with PAS input, and 64ASK modulation with PAS input, respectively. As observed, all the three optimized PLDPC codes enjoy very desirable decoding thresholds, which are within 0.43 dB from the channel capacities. The design method can be easily extended to the PLDPC codes with rates higher than $(w - 1)/w$ for a given modulation order, such as $r_P = 3/4$ for 4ASK [171]. For simplicity, the result is omitted here.

(3) Code Design for CPSSK-aided BICM-ID: In [121], a new PEXIT function was proposed, tailored for the bilayer (i.e., $L = 2$) root-PLDPC codes in the MCPSK-aided BICM-ID context. Then, a series of two-layer root-PLDPC codes were constructed for the BICM-ID systems to increase the transmission throughput and reduce the data-processing time for the next generation of global navigation satellite systems. Recall that the MCPSK modulation is an M -ary direct-sequence spread-spectrum (DSSS) modulation, which exploits a maximum-length pseudo-noise (PN) sequence with β chips to carry $w = \log_2 M$ coded bits. Thus, a length- N PLDPC code $\Lambda = (v_1, v_2, \dots, v_N)$ is first converted to a length- N' non-binary codeword $\Lambda_{\text{NB}} = (v_{\text{NB},1}, v_{\text{NB},2}, \dots, v_{\text{NB},N'})$. Later on, each non-binary symbol is represented by a circular shift of the pre-generated length- β PN sequence φ_{CPSK} . In this setting, the MCPSK constellation set is constituted by M different circular-shift versions of φ_{CPSK} .

As a type of maximum-distance separable (MDS) codes, root-PLDPC codes were initially proposed in [179], [212], [213] to achieve full diversity and outage-limit-approaching performance over block-fading channels. It was demonstrated in [71] that the structure of root-PLDPC codes perfectly matches the characteristics of block-fading channels. Here, the root-PLDPC-code design for MCPSK-aided BICM systems over AWGN channels is discussed, without getting into details of such codes. The construction principle of root-PLDPC codes will be discussed in

Section V-B1, where the research progress relevant to the root-PLDPC-BICM over block-fading channels will be presented.

Example 9: Aiming to obtain a desirable optimized bilayer root-PLDPC code for 4CPSK-aided BICM-ID systems over an AWGN channel, a 4×8 base matrix is initialized, as

$$\mathbf{B} = \begin{bmatrix} 1 & 0 & 0 & 0 & b_{1,5} & b_{1,6} & b_{1,7} & b_{1,8} \\ 0 & 1 & 0 & 0 & b_{2,5} & b_{2,6} & b_{2,7} & b_{2,8} \\ b_{3,1} & b_{3,2} & b_{3,3} & b_{3,4} & 1 & 0 & 0 & 0 \\ b_{4,1} & b_{4,2} & b_{4,3} & b_{4,4} & 0 & 1 & 0 & 0 \end{bmatrix}, \quad (12)$$

where the value of the (i, j) -th element is assumed to be $b_{i,j} \in \{0, 1, 2, 3\}$ in order to keep relatively low computational complexity for code optimization and construction, with $i \in \{1, 2, 3, 4\}$ and $j \in \{1, 2, 3, 4, 5, 6, 7, 8\}$. Note that the structure of the base matrix (12) strictly follows the definition of root-PLDPC codes given in Section V-B1. After a PEXIT-aided search procedure, the base matrix corresponding to the optimized bilayer root-PLDPC code can be obtained, as

$$\mathbf{B}_{\text{OPT-ROOT}} = \begin{bmatrix} 1 & 0 & 0 & 0 & 0 & 1 & 2 & 1 \\ 0 & 1 & 0 & 0 & 1 & 0 & 2 & 0 \\ 1 & 3 & 1 & 2 & 1 & 0 & 0 & 0 \\ 0 & 1 & 3 & 0 & 0 & 1 & 0 & 0 \end{bmatrix}. \quad (13)$$

Both theoretical and simulation results demonstrated that the optimized bilayer root-PLDPC code accomplishes a remarkable gain of more than 0.5 dB over the L1 civil LDPC codes adopted in the 4CPSK-aided global positioning system [121].

(4) Code Design for CPM-aided BICM-ID: As another promising power- and bandwidth-efficiency modulation scheme, CPM has attracted enthusiastic interest in wireless communication systems due to its constant-envelope characteristic [214]. Inspired by this appealing advantage, the joint design of the PLDPC codes and CPM modulations was investigated in [166] by exploiting a modified PEXIT algorithm within the context of BICM-ID. Specifically, consider a CPM-aided BICM-ID system. A length- N PLDPC code $\mathbf{\Lambda} = (v_1, v_2, \dots, v_N)$ is interleaved and then processed by an M CPM modulator to generate a length- N' M -ary symbol sequence $\mathbf{x} = (x_1, x_2, \dots, x_{N'})$, where $N' = N/w$ and $x_k \triangleq (\hat{v}_{k,1}, \hat{v}_{k,2}, \dots, \hat{v}_{k,w})$ is the k -th ($k = 1, 2, \dots, N'$) modulated symbol; particularly, x_k is taken value from the set $\chi = \{\pm 1, \pm 3, \dots, \pm(2^w - 1)\}$. According to a given symbol sequence \mathbf{x} , a CPM signal transmitted over an AWGN channel can be generated as

$$\varphi_{\text{CPM}}(\tau, \mathbf{x}) = \sqrt{2E_s/T} \cos(2\pi f_0 \tau + \Upsilon(\tau, \mathbf{x}) + \Upsilon_0), \quad (14)$$

where E_s is the average symbol energy, T is the symbol duration, f_0 and Υ_0 are the carrier frequency and initial phase shift, respectively, and $\Upsilon(\tau, \mathbf{x})$ is the information-carrying phase. Based on the CPM-aided BICM-ID framework, the extrinsic MI functions for the outer decoder and inner demodulator were derived, which can facilitate the PLDPC-code optimization. Subsequently, a simple search method was proposed in [166] to construct a series of capacity-approaching rate-1/2 PLDPC codes in this framework.

Example 10: Aiming to minimize the decoding threshold of a PLDPC code in the CPM-aided BICM-ID system, a 4×8 base matrix with three degree-2 variable nodes and three degree-1 variable nodes is initialized, as

$$\mathbf{B} = \begin{bmatrix} 1 & 1 & 0 & 0 & 0 & 0 & b_{1,7} & b_{1,8} \\ 0 & 1 & 1 & 0 & 1 & 0 & b_{2,7} & b_{2,8} \\ 0 & 0 & 1 & 1 & 0 & 1 & b_{3,7} & b_{3,8} \\ 0 & 0 & 0 & 1 & 0 & 0 & b_{4,7} & b_{4,8} \end{bmatrix}, \quad (15)$$

where the seventh and eighth columns correspond to the variable nodes with degrees at least 3. To limit the search space and lower the encoding complexity, the value of $b_{i,j}$ ($i \in \{1, 2, 3, 4\}, j \in \{7, 8\}$) is assumed to satisfy $0 \leq b_{i,j} \leq 3$. Then, under three different CPM schemes, i.e., binary Gaussian minimum shift keying (GMSK, $M = 2$), Gray-labeled quaternary raised-cosine (QRC, $M = 4$), and Gray-labeled octal rectangular (OREC, $M = 8$), the base matrices of optimized PLDPC codes can be obtained after a computer-based search [166], as (16).

For comparison, the decoding thresholds and capacity gaps of the rate-1/2 optimized PLDPC codes, AR3A code and AR4JA code in the CSK-aided BICM-ID systems are summarized in Table VI. Obviously, the three optimized PLDPC codes have gaps of only 0.65 dB, 0.74 dB, and 1.54 dB to the channel capacities under GMSK, QRC, and OREC modulations, respectively, which are much smaller than those of AR3A and AR4JA codes. Moreover, the optimized PLDPC codes have decoding thresholds nearest to the capacities, while the AR4JA code has decoding thresholds farthest from the capacities.

$$\begin{aligned} \mathbf{B}_{\text{GMSK}} &= \begin{bmatrix} 1 & 1 & 0 & 0 & 0 & 0 & 1 & 2 \\ 0 & 1 & 1 & 0 & 1 & 0 & 2 & 1 \\ 0 & 0 & 1 & 1 & 0 & 1 & 1 & 1 \\ 0 & 0 & 0 & 1 & 0 & 0 & 1 & 1 \end{bmatrix}, \\ \mathbf{B}_{\text{ORC}} &= \begin{bmatrix} 1 & 1 & 0 & 0 & 0 & 0 & 1 & 1 \\ 0 & 1 & 1 & 0 & 1 & 0 & 2 & 2 \\ 0 & 0 & 1 & 1 & 0 & 1 & 1 & 1 \\ 0 & 0 & 0 & 1 & 0 & 0 & 1 & 1 \end{bmatrix}, \\ \mathbf{B}_{\text{OREC}} &= \begin{bmatrix} 1 & 1 & 0 & 0 & 0 & 0 & 1 & 1 \\ 0 & 1 & 1 & 0 & 1 & 0 & 3 & 3 \\ 0 & 0 & 1 & 1 & 0 & 1 & 1 & 1 \\ 0 & 0 & 0 & 1 & 0 & 0 & 1 & 1 \end{bmatrix}. \end{aligned} \quad (16)$$

Remark: The above works are restricted to the PLDPC-code design for regular-mapped BICM with different modulation schemes. By a glance at this issue for irregular-mapped BICM [215], relevant studies are still in infancy.

2) *Constellation Shaping:* Since the inception of BICM, a great deal of research effort has been devoted to investigating constellation shaping in order to enhance the performance in both NI and ID scenarios. Of particular interest are the works that investigated the APSK constellation optimization for LDPC-BICM systems [68], [69], [76], [77], [80], proposing desirable constellations under different environments. In contrast to the BICM-NI scenario, the trade-off between the NI-HMMSED and ID-HMMSED has to be carefully taken into account when optimizing the constellations for BICM-ID. For instance, some innovative methods were proposed in [68], [76] to design APSK constellations having excellent HMMSEDs for achieving good performance in LDPC-BICM-ID systems.

Yet, the constellation shaping for PLDPC-BICM systems is relatively unexplored. To fill this gap, an adaptive 16QAM constellation is proposed here for the PLDPC-BICM-ID systems by modifying the subset-partition rule on the Gray-labeled 16QAM constellation. Fig. 10 displays the structure of the proposed

TABLE VI
DECODING THRESHOLDS $(E_b/N_0)_{\text{th}}$ (dB) AND CAPACITY GAPS Δ OF THE RATE-1/2 OPTIMIZED PLDPC CODES, AR3A CODE, AND AR4JA CODE IN THREE DIFFERENT CSK-AIDED BICM-ID SYSTEMS OVER AN AWGN CHANNEL, WITH GRAY LABELING.

Modulation Type	Code Type	Optimized PLDPC		AR3A		AR4JA		Capacity
		$(E_b/N_0)_{\text{th}}$	Δ	$(E_b/N_0)_{\text{th}}$	Δ	$(E_b/N_0)_{\text{th}}$	Δ	
GMSK		-2.11	0.65	-0.45	2.31	-0.20	2.56	-2.76
QRC		1.36	0.74	3.36	2.74	3.68	3.06	0.62
OREC		3.79	1.54	7.29	5.04	7.92	5.67	2.25

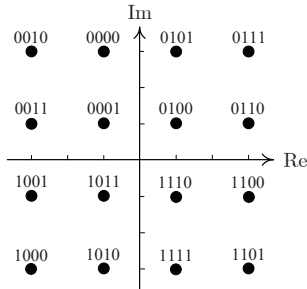


Fig. 10. Constellation of the adaptive Gray-labeled 16QAM modulation.

adaptive Gray-labeled 16QAM constellation. Analysis confirms that the adaptive Gray-labeled constellation possesses the same NI-HMMSSED (i.e., $d_{\text{h,NI}}^2(\chi, \phi) = 0.492$) with respect to the Gray-labeled counterpart, with a relatively larger ID-HMMSSED (i.e., $d_{\text{h,ID}}^2(\chi, \phi) = 0.615$). This implies that the adaptive Gray-labeled constellation can obtain better performance than the Gray counterpart in the ID setting.

As a further progress, a generalized design method was proposed in [215] to construct an adaptive constellation based on an initial constellation with any labeling format (e.g., Gray and anti-Gray) and any modulation order. The designed adaptive constellation can be seamlessly combined with its corresponding initial constellation to formulate a powerful irregular mapping (IM) scheme, which can enhance the performance of the PLDPC-BICM-ID system over AWGN channels. Note that the principle of IM and its corresponding design guideline are ignored here, which will be discussed in the next subsection.

3) *Bit-Mapper (Interleaver) Design*: Given a well-constructed PLDPC code and a well-shaped constellation, the interface between these two components is also of great importance in determining the overall performance of BICM systems. The interface between a binary code and a high-order constellation is commonly called *bit mapper or bit interleaver*.

(1) Regular Mapping: In 2005, two VDMM schemes, i.e., *water-filling and reverse water-filling VDMMs*, were proposed in [116] for Gray-labeled 16QAM-modulated BICM-NI systems. Considering a given constellation, the principle of both VDMM schemes is that the coded bits within a codeword are assigned to different labeling-bit positions within a modulated symbol according to the variable-node degree distribution of the PLDPC code. In the water-filling VDMM, the variable nodes (i.e., coded bits) with the highest degrees are assigned to the labeling-bit positions with the highest protection degrees (i.e., the highest MI), while those with the lowest degrees are assigned to the labeling-bit positions with the lowest protection degrees. On the contrary, in the reverse water-filling VDMM, the mapping between the variable nodes and the labeling bits is assigned in a reverse order. Simulation results suggest that the water-filling VDMM scheme performs as good as the random bit-mapping (interleaving) scheme, while the reverse water-filling VDMM

TABLE VII
DECODING THRESHOLDS $(E_b/N_0)_{\text{th}}$ (dB) AND CAPACITY GAPS OF THE WATER-FILLING VDMM SCHEME, OPTIMIZED VDMM SCHEME, AND THE TSLM SCHEME IN THE BICM-NI SYSTEMS OVER AN AWGN CHANNEL, WHERE A RATE-1/2 AR4JA CODE AND GRAY-MAPPED 16QAM MODULATION ARE USED.

Bit-Mapping Scheme	$(E_b/N_0)_{\text{th}}$	Δ	Capacity
Water-filling VDMM [116]	2.853	0.567	2.286
Optimized VDMM [118]	2.714	0.428	
TSLM [83]	2.812	0.526	

scheme performs worse than the random bit-mapping scheme by at least 0.1 dB. However, neither the water-filling VDMM nor the random mapping schemes can achieve optimal performance in PLDPC-BICM-NI systems. To address this issue, a PEXIT-assisted optimization strategy was developed to enhance the performance of VDMM in PLDPC-BICM-NI systems with 16QAM modulation [118], where all possible permutations for the mapping between the variable nodes with different degrees in a protograph and the labeling bits with different protection degrees in an M -ary symbol are enumerated so as to achieve the lowest decoding threshold. The optimized VDMM attains a considerable performance gain over the conventional VDMM at the expense of a higher computational complexity.

There are two drawbacks for the VDMM schemes [83], [119]:

- The VDMM schemes are not effective if the number of variable nodes in a protograph is not equal to the number of labeling bits in a modulated symbol.
- The VDMM schemes are not effective if all the variable nodes have the same degree.

Hence, the conventional and optimized VDMM schemes can only work well for irregular PLDPC-BICM systems when, and only when $n_P = w = \log_2 M$. This severely limits the application of such techniques to practical BICM systems. To break this limitation, a more feasible bit-mapping scheme, referred to as *TSLM scheme*, was developed in [83]. The proposed TSLM scheme begins by permuting the original protograph with an initial lifting factor $z = w$, which is much smaller than the lifting factor used for producing a PLDPC code.

Accordingly, a $w n_P \times w n_P$ intermediate protograph can be formulated, with variable nodes distributed on w different planes. Particularly, each plane corresponds to a replica of the protograph and comprises of n_P variable nodes. Now, all the n_P variable nodes of the μ -th ($\mu = 1, 2, \dots, w$) plane are mapped to n_P replicas of the μ -th labeling bit within an M -ary modulated symbol, such that the $w n_P$ variable nodes of the intermediate protograph can be mapped to n_P symbols. After that, the BICM framework is realized based on the intermediate protograph, which is convenient for further optimization. One can then expand the intermediate protograph to a PLDPC code with an expected codeword length (or symbol length). For instance, if the codeword length is $N = Z n_P$, the secondary lifting factor for the expansion of the intermediate protograph

becomes $Z' = \frac{N}{wn_P} = \frac{Z}{w}$. Note that the proposed TSLM scheme is applicable to any protograph structure with any modulation order. Assuming that the PLDPC-BICM-NI systems use a rate- $\frac{1}{2}$ AR4JA code and Gray-mapped 16QAM modulation, Table VII presents the decoding thresholds of the water-filling VDMM [116], optimized VDMM [118], and the TSLM schemes [83]. As seen, the decoding threshold of the TSLM scheme is slightly smaller than that of the water-filling VDMM, but is slightly higher than that of the optimized VDMM. In fact, the optimized VDMM scheme resorts to a brute-force search, which requires much higher computational complexity than the TSLM scheme. It was shown in [83] that the TSLM scheme allows the PLDPC-BICM-NI to attain close-to-capacity decoding thresholds in a wide range of code rates and modulation orders with relatively low computational complexity.

Apart from the TSLM scheme, a generalized VDMM scheme was developed in [119] for PLDPC-BICM-NI systems with MAPSK modulation, which can also be applied to combine any protograph structure with any modulation order. Specifically, the n_P types of variable nodes in a PLDPC codeword are first re-ranked in a descending order according to their degrees, while the w types of labeling bits in a symbol sequence are re-ranked in a descending order according to their protection degrees. In the sequel, the variable nodes are artificially divided into w groups, which are successively mapped to the w types of labeling bits. By this method, a water-filling-like procedure can be realized and thus desirable convergence and error performance can be achieved. As a further advance, a simplified optimization scheme for the generalized VDMM scheme was constructed to obtain optimal mapping performance with relatively lower complexity than the brute-force search-aided method [118]. Also, the generalized VDMM scheme was applied to the PLDPC-RGB-LED-based BICM-VLC systems in [122].

In parallel with the VDMM-related scheme, another novel optimized bit-mapping scheme, referred to as *variable-node fractional-allocation mapping (VNFAM) scheme*, was proposed in [149] for BICM-NI fiber-optical communication systems. In these systems, polarization-multiplexed (PM) MQAM signals are adopted for transmission. The proposed VNFAM scheme utilizes a modified PEXIT algorithm to search for an unrestricted matching between the variable nodes in a protograph and the labeling bits within a PM-MQAM modulated symbol. Results demonstrated that the PLDPC-BICM-NI with the VNFAM scheme can accomplish performance gains up to 0.25 dB over its counterpart with the consecutive mapping scheme.

Remark: The generalized VDMM scheme is applicable only to irregular codes, while the TSLM and VNFAM schemes are applicable to both regular and irregular codes.

(2) Irregular Mapping: In the traditional BICM frameworks, only one signal constellation is employed to modulate the PLDPC code, which is referred to as a *regular mapping*. With the development of BICM techniques, efforts have been made to explore more flexible mapping schemes in order to increase the degree of freedom of system design and to enhance the link adaption ability. As an alternative mapping scheme, IM that employs more than one constellation to modulate a codeword was proposed for BICM-ID systems in order to improve the convergence performance [216]. It was verified that the deploy-

TABLE VIII
DECODING THRESHOLDS $(E_b/N_0)_{th}$ (dB) OF FOUR DIFFERENT IM SCHEMES (χ_1 : GRAY-LABELED CONSTELLATION, χ_2 : ANOTHER CONSTELLATION) AND GRAY-LABELED REGULAR MAPPING SCHEME IN THE 16QAM-AIDED BICM-ID SYSTEMS OVER AN AWGN CHANNEL, WHERE THE RATE-1/2 REGULAR-(3,6) PLDPC CODE IS USED.

Code Type χ_2	Anti-Gray	MSEW	ABSA [90]	Adp-Gray	Gray
Regular	3.442	4.053	3.160	3.108	3.211

ment of IM in BICM-ID systems can have desirable capacity-approaching performance [93]. Yet, how to devise excellent IM schemes with acceptable computational complexity remains to be a challenging issue for further investigation.

In 2011, a novel IM scheme was proposed in [90] by exploiting a modified adaptive binary switch algorithm (ABSA), which is able to achieve near-capacity performance in LDPC-BICM-ID systems with MQAM. In this IM scheme, the ABSA is exploited to search for a new constellation based on a given constellation (e.g., Gray- or quasi-Gray-labeled constellation). Then, both constellations are employed to modulate the LDPC code with a fixed mixing ratio. The mixing-ratio vector of the IM is defined as $\eta = (\eta_1, \eta_2)$, where $\eta_\kappa = N_\kappa/N$ is the ratio between the number of coded bits mapped to the κ -th ($\kappa = 1, 2$) constellation and the codeword length.

As the first attempt to investigate the IM-PLDPC-BICM-ID over an AWGN channel, by mixing the adaptive Gray-labeled 16QAM constellation (see Fig. 10) with its mother constellation (i.e., Gray-labeled 16QAM constellation), a novel IM scheme, referred to as *protograph-based adaptive irregular mapping (PAIM) scheme*, was developed in [215]. It was shown that the PAIM scheme can significantly accelerate the decoding convergence of PLDPC codes in BICM-ID systems.

Example 11: Assuming a Gray-labeled constellation (denoted by χ_1) and a mixing-ratio vector $\eta = (1/2, 1/2)$, the decoding thresholds of the IM schemes are now compared with four different realizations of the second component constellation (denoted by χ_2) in the PLDPC-BICM-ID systems over an AWGN channel, where the channel code and modulation used are the rate-1/2 regular-(3,6) PLDPC code and 16QAM, respectively. In the comparison, each IM scheme is composed of the constellations χ_1 and χ_2 . The Gray-labeled regular mapping (i.e., χ_2 : Gray-labeled constellation) is also included as a benchmark. As seen from Table VIII, the IM scheme employing both Gray- and adaptive-Gray-labeled constellations exhibits the best decoding threshold among the four schemes. Moreover, the IM scheme obviously outperforms the Gray-labeled regular-mapping scheme, which achieves optimal performance in the NI scenario. Hence, the Gray- and adaptive-Gray-labeled constellations constitute a promising IM scheme for the PLDPC-BICM-ID systems.

B. Design of SC-PLDPC-BICM Systems

1) *Code Construction:* During the past decade, SC-PLDPC codes have been extensively applied to BICM systems. With the advancement of the design methodologies for SC-PLDPC codes, their BICM relatives gradually stood out as a predominant bandwidth-efficient transmission solution for communication and storage systems. For example, based on the SC-PLDPC codes, a variety of BICM design paradigms were proposed for different

TABLE IX
DECODING THRESHOLDS $(E_b/N_0)_{th}$ (dB) OF THE RATE-3/4
CONVENTIONAL REGULAR TE-SC-PLDPC CODE, ASYMMETRIC REGULAR
TE-SC-PLDPC CODE, AND THREE OPTIMIZED IRREGULAR LDPC CODES IN
THE 16QAM-AIDED BICM-ID SYSTEMS OVER AN AWGN CHANNEL,
WHERE THE GRAY, SP, AND M16A LABELINGS ARE CONSIDERED. THE
CAPACITY LIMIT IS 4.528 dB, AND THE PARAMETERS USED FOR THE
TE-SC-PLDPC CODES ARE $\varsigma = 1$ AND $L_{SC} = 100$.

Code Type \ Constellation	Gray	SP	M16a [23]
Conv. regular TE-SC-PLDPC	4.695	5.001	5.260
Asym. regular TE-SC-PLDPC	4.712	4.577	4.745
Opt. irregular LDPC-A (for Gray)	4.600	6.217	6.344
Opt. irregular LDPC-B (for SP)	> 7	4.739	4.983
Opt. irregular LDPC-C (for M16a)	> 7	4.729	4.959

constellation formats, modulation orders and code rates, with the aim to provide diverse requirements for practical applications and services [102], [153]–[155], [162], [166], [178]. In the following, several representative works are discussed.

(1) Code Design for PSK/QAM-aided BICM-NI: A so-called “universal” design method was developed in [178] for TE-SC-PLDPC codes, which not only achieves capacity-approaching performance under high-order modulations regardless of the labeling format but also has very low complexity. To facilitate the design and analysis, two convergence regions, i.e., *macro-convergence and micro-convergence regions*, are defined. The macro-convergence and micro-convergence regions are dominated by the degree distribution and spatial coupling effect of the TE-SC-PLDPC code, respectively. According to the theoretical analysis, some regular TE-SC-PLDPC codes with a proper edge-spreading rule can perform very well under different labeling formats, even perform better than the optimized LDPC codes. Assume that the TE-SC-PLDPC code is generated from a regular PLDPC code with a base matrix $\mathbf{B} = \mathbf{B}_{S,1} + \mathbf{B}_{S,2} + \dots + \mathbf{B}_{S,\varsigma+1}$, where $\mathbf{B}_{S,\mu}$ is the μ -th sub-base matrix yielded by the “matrix division” operation. To trigger an asymmetric “decoding wave” phenomenon from both the left-hand and the right-hand sides of the SC protograph, it is needed to introduce some irregularity to the $\varsigma + 1$ sub-base matrices.³ The above simple operation can significantly accelerate the MI convergence of the TE-SC-PLDPC codes in the BICM-ID systems. Analytical and simulation results demonstrated that the *asymmetric* regular TE-SC-PLDPC codes can attain capacity-approaching decoding thresholds in the BICM-ID systems with various labelings. More importantly, the asymmetric TE-SC-PLDPC codes are superior to the conventional irregular LDPC codes optimized for the BICM-ID systems.

Example 12: Based on a rate-3/4 (4, 16)-regular protograph with base matrix $\mathbf{B} = [4 \ 4 \ 4 \ 4]$, one can construct different asymmetric regular TE-SC-PLDPC codes with coupling width $\varsigma = 1$. For one realization, the two sub-base matrices split from the original base matrix \mathbf{B} are expressed as $\mathbf{B}_1 = [3 \ 2 \ 3 \ 2]$ and $\mathbf{B}_2 = [1 \ 2 \ 1 \ 2]$, respectively. According to its convolutional structure, the resultant asymmetric regular TE-SC-PLDPC code can be viewed as a regular code if the coupling length is sufficiently large. As observed, the structures of the sub-base

³The “decoding wave” phenomenon is that the variable nodes associated with the lower-degree check nodes at both ends of the coupled chain converge faster than the variable nodes in the middle under BP decoding, leading to a wave-like decoding phenomenon [67].

matrices for the asymmetric regular TE-SC-PLDPC code are quite different from those of the conventional regular TE-SC-PLDPC code (i.e., as $\mathbf{B}_1 = [2 \ 2 \ 2 \ 2]$ and $\mathbf{B}_2 = [2 \ 2 \ 2 \ 2]$), which lead to different decoding-wave behaviors. Table IX compares the decoding thresholds of the two TE-SC-PLDPC codes in the 16QAM-aided BICM-ID systems with three different labeling schemes, where $L_{SC} = 100$. As benchmarks, three irregular LDPC codes are considered, which are particularly optimized for the Gray, SP, and M16a labelings. One can observe that the conventional regular TE-SC-PLDPC code has good performance only for Gray labeling, while the asymmetric regular counterparts have excellent performance for all the three labelings. On the other hand, the irregular LDPC-A, LDPC-B, and LDPC-C codes are unable to exhibit universally good performance for all the three labelings. Thereby, the asymmetric regular TE-SC-PLDPC code can be treated as a universally desirable candidate for BICM-ID systems, regardless of the labeling scheme. In addition, the decoding-wave analysis in [178] also verified the merit of the asymmetric regular TE-SC-PLDPC code.

Apart from the TE-SC-PLDPC code design, an efficient design method was developed in [155] for the TB-SC-PLDPC codes in MPSK/MQAM-aided BICM-NI systems with shuffled BP decoding. An appealing feature of the TB-SC-PLDPC codes is that the non-negligible rate loss incurred by the termination effect can be avoided, especially in the finite-coupling-length scenario. Different from most existing design methods, the proposed method constructs a novel type of TB-SC-PLDPC codes from two mother PLDPC codes to inherit the performance advantages of both codes. This type of TB-SC-PLDPC codes is referred to as *TB-SC double-PLDPC (DPLDPC) codes*. Assume that two PLDPC codes \mathcal{A} and \mathcal{B} correspond to the same-size $m_P \times n_P$ base matrices \mathbf{B}_A and \mathbf{B}_B , respectively. The proposed code-design method includes a hybrid edge-spreading scheme and an EXIT-based degree-distribution optimization scheme. More precisely, the hybrid edge-spreading scheme is composed of a uniform edge-spreading rule and a replicative edge-spreading rule. The uniform edge-spreading rule is exploited to divide the base matrix of code \mathcal{A} into two sub-base matrices $\mathbf{B}_{A,1}$ and $\mathbf{B}_{A,2}$ (i.e., coupling width $\varsigma = 1$), while the replicative edge-spreading rule is used to divide the base matrix of code \mathcal{B} into another set of two sub-base matrices $\mathbf{B}_{B,1}$ and $\mathbf{B}_{B,2}$. To guarantee the TB-SC-DPLDPC codes constructed from the above four sub-base matrices can combine both degree distributions of the two mother PLDPC codes \mathcal{A} and \mathcal{B} , $\mathbf{B}_{B,1}$ must equal $\mathbf{B}_{A,1}$ (i.e., $\mathbf{B}_{B,1} = \mathbf{B}_{A,1}$) in the replicative edge spreading. Using this hybrid edge-spreading scheme, the TB-SC-DPLDPC codes can inherit the superiorities of the two mother PLDPC codes. To achieve an additional performance gain, one can optimize the structure of the sub-base matrices based on the PEXIT algorithm to formulate an improved TB-SC-DPLDPC (I-TB-SC-DPLDPC) code. The I-TB-SC-DPLDPC code benefits from both the hybrid edge-spreading and degree-distribution optimization, compared to the two mother PLDPC codes.

Example 13: Based on the rate-1/2 AR4JA code (code \mathcal{A}) and AR3A code (code \mathcal{B}) in Example 2, one can readily divide the base matrix \mathbf{B}_{AR4JA} into two sub-base matrices $\mathbf{B}_{AR4JA,1}$ and $\mathbf{B}_{AR4JA,2}$ via the uniform edge-spreading rule, and divide the base matrix \mathbf{B}_{AR3A} into another two sub-base matrices

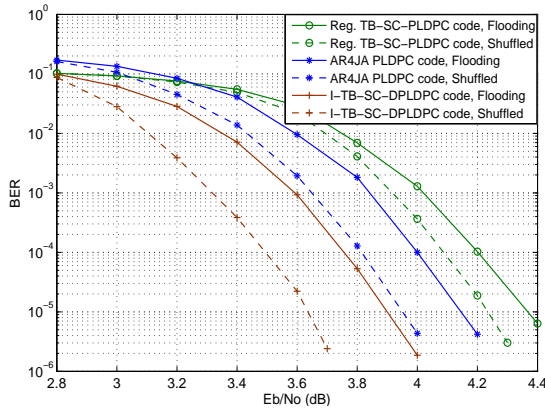


Fig. 11. BER curves of the rate-1/2 I-TB-SC-DPLDPC, regular-(3, 6) TB-SC-PLDPC, and AR4JA codes in a Gray-mapped 16QAM-aided BICM-NI system over AWGN channels with $\zeta = 1$, $L_{SC} = 4$, $N_T = 3840$, and $t_{BP,max} = 25$.

$\mathbf{B}_{AR3A,1}$ and $\mathbf{B}_{AR3A,2}$ via the replicative edge-spreading rule. Assuming the coupling length $L_{SC} = 4$, the base matrix of TB-SC-DPLDPC code is formulated as [155]

$$\mathbf{B}_{TB-SC-DP} = \begin{bmatrix} \mathbf{B}_{AR4JA,1} & \mathbf{0} & \mathbf{0} & \mathbf{B}_{AR3A,2} \\ \mathbf{B}_{AR4JA,2} & \mathbf{B}_{AR3A,1} & \mathbf{0} & \mathbf{0} \\ \mathbf{0} & \mathbf{B}_{AR3A,2} & \mathbf{B}_{AR4JA,1} & \mathbf{0} \\ \mathbf{0} & \mathbf{0} & \mathbf{B}_{AR4JA,2} & \mathbf{B}_{AR3A,1} \end{bmatrix}, \quad (17)$$

where $\mathbf{B}_{AR4JA,2}$ is derived in [155, eq.(9)]. Moreover, one has $\mathbf{B}_{AR3A,1} = \mathbf{B}_{AR4JA,1} = \mathbf{B}_{AR4JA} - \mathbf{B}_{AR4JA,2}$ and $\mathbf{B}_{AR3A,2} = \mathbf{B}_{AR3A} - \mathbf{B}_{AR3A,1}$. In particular, the variable nodes corresponding to the second columns of all the four sub-base matrices are punctured.

As is well known, the degree of the punctured variable nodes has a significant effect on the performance of the PLDPC codes. One can further optimize the degree of the punctured variable node in $\mathbf{B}_{AR4JA,2}$ so as to improve the decoding threshold of the TB-SC-DPLDPC code. To keep the encoding complexity low, the value of each element is assumed to be smaller than or equal to 3. After a simple search, the improved version of $\mathbf{B}_{AR4JA,2}$ is obtained as (18). Hence, the base matrix of the *improved TB-SC-DPLDPC* (I-TB-SC-DPLDPC) code is obtained by replacing $\mathbf{B}_{AR4JA,2}$ in (17) with $\mathbf{B}_{I-AR4JA,2}$.

$$\mathbf{B}_{I-AR4JA,2} = \begin{bmatrix} 1 & 1 & 0 & 0 & 0 \\ 0 & 1 & 1 & 0 & 0 \\ 0 & 1 & 1 & 1 & 1 \end{bmatrix} \quad (18)$$

As illustrated in [155], the I-TB-SC-DPLDPC code possesses better convergence performance than the TB-SC-DPLDPC code, which further has better performance than the two mother PLDPC codes. Fig. 11 compares the BER performance of the I-TB-SC-DPLDPC code, regular TB-SC-PLDPC code, and AR4JA code in a Gray-mapped 16QAM-aided BICM-NI system over an AWGN channel. As shown, the I-TB-SC-DPLDPC code is superior to the regular TB-SC-PLDPC code and the AR4JA code under both schedules, which commendably verifies the merit of the proposed design. Specifically, at a BER of 10^{-5} , the I-TB-SC-DPLDPC code has additional gains of about 0.3 and 0.5 dB over the AR4JA code and regular TB-SC-PLDPC code, respectively, under both BP decoding schedules.

Aiming to realize more efficient implementation of SC-PLDPC codes without loss of their performance superiority, the QC structure was taken into account in developing new

code-construction methods. On the one hand, a couple of time-invariant code-construction methods were proposed to further reduce the encoding and decoding complexity of the traditional SC-PLDPC codes in the past five years [217]. On the other hand, circulant-based PEG (i.e., circulant-based “lifting”) algorithm was seamlessly combined with the protographs in order to generate QC-PLDPC codes, which not only enable the linear encoding complexity with the aid of simple shift registers, but also produce similar error performance as the unstructured PLDPC codes [101], [218]. Inspired by the above advantages, an in-depth study was carried out in [102] on the QC SC-PLDPC codes in BICM-ID systems, which achieves both high performance and efficient implementation in practical broadcasting applications. Specifically, a novel construction method was developed for the finite-coupling-length QC-TE-SC-PLDPC codes in BICM-ID systems with QPSK modulation over AWGN channels. With this method, a base-matrix optimization scheme was developed for the variable-node degree distribution and edge-spreading pattern of the original PLDPC codes to improve the decoding thresholds and minimum distance. Then, a two-step lifting algorithm was designed, which includes a pre-lifting procedure and a post-lifting procedure, to construct the QC structure and to improve the finite-length performance of the resultant QC-TE-SC-PLDPC codes. Results demonstrated that the proposed QC-TE-SC-PLDPC codes are capable of exhibiting excellent error performance in the BICM-ID context. However, the design method was carried with QPSK modulation only.

(2) Code Design for ASK-aided BICM-NI: Although the TB-SC-PLDPC codes can overcome the rate-loss issue of the TE-SC-PLDPC codes, the former is incapable of triggering the decoding wave without a termination operation [144]. In [153], the TB-SC-LDPC-BICM-NI systems with 4ASK modulation were investigated, attempting to resolve the “decoding wave” problem with minimum code-rate loss over AWGN channels. Specifically, a random shortening technique was proposed for the TB-SC-LDPC codes to trigger a wave-like decoding behavior and to approach the performance of the TE-SC-LDPC codes with relatively smaller rate loss in the 4ASK-aided BICM-NI systems. In that technique, the codeword is shortened by setting some coded bits to zero. Through such an operation, some *a priori* knowledge can be used to initiate the wave-like convergence under BP decoding. This technique is also applicable to the TB-SC-PLDPC codes, which may achieve similar performance in such a BICM framework. Although the shortening technique can improve the convergence performance of TB-SC-LDPC-BICM systems, it slightly decreases the code rate.

Following the works of [171], [172], in [162] the ASK-aided TE-SC-PLDPC-BICM-NI systems with PAS were studied, regarding especially the quantized BP decoder design. Specifically, a quaternary BP decoding algorithm was proposed for the rate- $(w-1)/w$ TE-SC-PLDPC codes in PAS-aided BICM-NI system with *MASK* ($M \geq 4$) modulation, where $w = \log_2 M$. To ease the analysis of the proposed quantized decoding algorithm, a modified DE algorithm was developed. Analyses and simulations revealed that the proposed decoding algorithm ensures the TE-SC-PLDPC codes to achieve desirable decoding thresholds and error performance over *MASK*-aided BICM-NI with PAS. Hence, the PAS-aided TE-SC-PLDPC-BICM possesses great

potential to be a high-throughput transmission solution for optical communications. Note that the above work considered only regular TE-SC-PLDPC codes, but not the irregular TE-SC-PLDPC-BICM-NI systems. Differing from [171], it did not study the code optimization, but only the decoder design.

(3) Code Design for CPM-aided BICM-ID: In [167], a new type of SC-PLDPC codes, called *DT-SC-PLDPC codes*, was developed for CPM-aided BICM-ID systems. The DT-SC-PLDPC code was constructed in an analogous way to that of a TB-SC-PLDPC code, in order to avoid rate loss. Yet, in a DT-SC-PLDPC code, one must directly cut off all the $m_P\zeta$ check nodes at the last ζ time instants and their associated edges from the SC protograph, instead of combining them with those at the first ζ time instants. With this operation, the base matrix of a DT-SC-PLDPC code is obtained as [167, eq. (10)], which includes $m_P L_{SC}$ rows and $n_P L_{SC}$ columns, leading to a code rate of $r_{DT-SC} = 1 - m_P/n_P = r_P$. The DT-SC-PLDPC codes can preserve most convolutional benefits of the conventional TE-SC-PLDPC codes since the structure in the left-hand side of the protograph is unchanged. It was verified that the DT-SC-PLDPC code can retain the rate advantage of its original protograph code by slightly degrading the decoding threshold.

To boost the performance of CPM-aided PLDPC-BICM-ID system in [166], two regular DT-SC-PLDPC codes with $\zeta = 1, 2$ were constructed in [167] based on the rate-1/2 regular-(3,6) PLDPC code. As benchmarks, a series of regular TE-SC-PLDPC codes with $\zeta = 1, 2$ were formulated based on the rate-1/2 regular-(3,6) PLDPC code. It was demonstrated that, with a relatively large coupling length (i.e., $L_{SC} = 50$) in the GMSK-aided BICM-ID systems, the regular DT-SC-PLDPC code with $\zeta = 1$ can achieve an identical decoding threshold to the corresponding TE-SC-PLDPC code, which is much smaller than that of their original PLDPC code. However, the regular DT-SC-PLDPC code with $\zeta = 2$ suffers from an obvious threshold degradation, compared with the TE-SC-PLDPC code. Due to the performance and rate advantages, the regular DT-SC-PLDPC code with $\zeta = 1$ may serve as a preferable candidate over the TE counterpart in M-CPM-aided BICM-ID systems.

2) *Constellation Shaping:* Constellation shaping was commonly exploited to boost either the channel capacity of BICM-NI or the iterative performance of BICM-ID. A constellation is universally good for both BICM-NI and ID systems if it can simultaneously realize the above-mentioned two objectives. In spite of a surge of publications on constellation design of BICM systems appeared in the past two decades [26], [69], [79], [80], [87], [95], the investigation tailored for SC-PLDPC codes remains to be explored. As a supplement to the existing constellations, a novel type of constellations was proposed in [154] for the TB-SC-PLDPC-BICM-ID systems over AWGN channels, which can achieve both desirable BICM-NI capacity and BICM-ID performance. Based on this work, the TB-SC-PLDPC-hierarchical modulated (HM) BICM-ID systems were further studied and a type of structural quadrant (SQ) constellations was devised for such systems [180]. The design principles for the current constellation shaping schemes in the above transmission scenarios are further discussed below.

(1) Traditional Modulation: It was proved, in a variety of research works, that the Gray constellation as an optimal con-

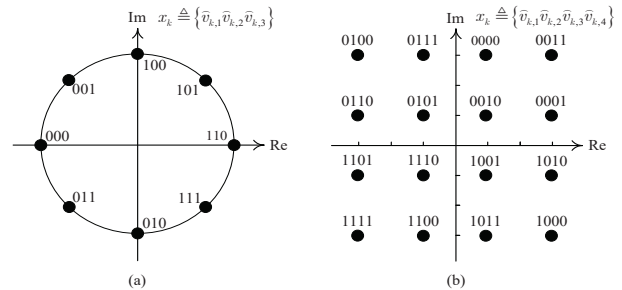


Fig. 12. Constellations of the LBPM schemes: (a) 8PSK and (b) 16QAM.

TABLE X
DECODING THRESHOLDS $(E_b/N_0)_{th}$ (dB) OF THE REGULAR-(3,6) TB-SC-PLDPC CODE IN THE 8PSK/16QAM-AIDED BICM-ID SYSTEMS WITH FOUR DIFFERENT CONSTELLATIONS OVER AWGN CHANNELS. THE PARAMETERS ARE

$r_P = 1/2$, $\zeta = 2$, $L_{SC} = 12$, $t_{GL,max} = 8$, and $t_{BP,max} = 25$.

8PSK	SP	MSEW	anti-Gray	LBPM
$(E_b/N_0)_{th}$	3.049	4.429	4.307	2.480
16QAM	SP	MSEW	anti-Gray	LBPM
$(E_b/N_0)_{th}$	4.724	5.027	4.385	3.626

stellation scheme in BICM-NI systems is generally unsuitable for BICM-ID systems due to its trivial iterative gain. Aiming at improving the performance of SC-PLDPC-BICM-ID systems over AWGN channels, a two-step design method was proposed in [154] to construct a novel type of constellations, called *labeling-bit-partial-match (LBPM) constellations*. The detailed procedure of the LBPM scheme is outlined as follows.

Step 1: For a given M -ary PSK/QAM modulation, the k -th signal point x_k belonging to a constellation is denoted as $x_k \triangleq \{\hat{v}_{k,1}, \hat{v}_{k,2}, \dots, \hat{v}_{k,w}\}$, where $\hat{v}_{k,\mu}$ is the μ -th labeling bit within the k -th modulated symbol, $w = \log_2 M$, $k = 1, 2, \dots, N'$, $N' = N/w$, and $\mu = 1, 2, \dots, w$. Especially, an M -ary constellation can be viewed as w parallel independent and binary input memoryless sub-channels. Then, the labeling bits with the maximum average MI are referred to as *high protection-degree labeling bits* and the remaining labeling bits are referred to as *low protection-degree labeling bits* [154]. By analyzing the labeling-bit distribution, the number of high protection-degree labeling bits can be calculated as $w' \in (0, w)$. Hence, the high protection-degree labeling bits are set as the first w' positions (i.e., $\{\hat{v}_{k,1}, \hat{v}_{k,2}, \dots, \hat{v}_{k,w'}\}$) within the modulated symbol, to attain excellent performance in the non-ID context.

Step 2: The remaining $w - w'$ low protection-degree labeling bits are processed sequentially and then placed in the last $w - w'$ positions within the modulated symbol. In particular, one should reasonably set each low protection-degree labeling bit to maximize the Hamming distance between the adjacent signal points in the constructed constellation. This operation is of great importance to boost the iterative gain of the constellation.

Note that the first and second steps of the LBPM constellation are executed to improve the performance in the NI and ID scenarios, respectively. Based on the design method, the LBPM constellations can be easily constructed.

Example 14: The LBPM constellations for the 8PSK and 16QAM are shown in Fig. 12. In order to verify the superiority of the two LBPM constellations, the decoding thresholds of the regular-(3,6) TB-SC-PLDPC code in BICM-ID systems are calculated with results shown in Table X, where the 8PSK and

16QAM modulations are considered. As benchmarks, three state-of-the-art constellations, i.e., anti-Gray-labeled, SP-labeled, and MSEW-labeled constellations, are included in the same table. It is observed that the (3, 6) TB-SC-PLDPC code with the LBPM constellation exhibits smaller decoding threshold than those of the other three constellations.

(2) Hierarchical Modulation: Aiming to satisfy the diverse quality-of-service requirement in emerging wireless-communication applications, such as IoT, the HM has been extensively studied. Furthermore, the HM-BICM can retain the spectral-efficiency benefit of BICM and can also realize UEP for different transmitted data streams. Inspired by these appealing characteristics, a large volume of research works related to the HM-BICM have been carried out [180], [205].

Distinguished from the traditional BICM systems, HM-BICM systems can be considered as layered systems, with constellations decomposed into several different layers in order to deal with different data streams. Thus, the existing constellation design methods may not work well for HM-BICM systems. Owing to this issue, several constellations, e.g., MSED [205], MSED-B [205], M3 [219], and hierarchical bandwidth modulation (HBM) constellations [220], were proposed in the context of HM. There is still room for further improvement of the existing HM constellations because they do not substantially consider the effect of the ID framework. Recently, a two-step design method was proposed [180] to construct a novel type of constellations, i.e., SQ constellations, which are applicable to any M -ary HM-BICM system. Analytical and simulation results demonstrate that the proposed SQ constellation outperforms the existing MSED, MSED-B, M3, and HBM constellations in both HM-BICM and HM-BICM-ID systems over AWGN channels.

3) Bit-Mapper (Interleaver) Design: Before 2015, there seemed to have no research work addressing the bit-mapping design for SC-PLDPC codes. Then, a couple of efficient bit-mapping schemes were developed for SC-PLDPC-BICM systems [150], [154]. The design frameworks in [150] and [154] have great potential for bandwidth-efficient fiber-optical systems and wireless-communication systems, respectively.

(1) Regular Mapping: In [150], a systematic study was proposed on the bit-mapping optimization for SC-PLDPC-BICM-NI systems over AWGN channels. In these systems, both TE- and TB-SC-PLDPC codes are considered as channel codes, while the Gray-labeled PM- M QAM is considered as a modulation scheme. Two different optimized bit-mapping schemes were proposed for TE- and TB-SC-PLDPC codes based on the UEP property offered by the different labeling bits within a PM- M QAM-modulated symbol. More precisely, the fast convergence of SC-PLDPC codes in these BICM systems is attributed to the optimized bit-mapping schemes that proportionally assign the coded bits located in different positions of the coupled chain to the labeling bits with different protection degrees.

On the one hand, for a TE-SC-PLDPC code, the lower-degree check nodes at both ends of the TE-SC protograph must pass more reliable messages to their associated variable nodes, which significantly accelerate the decoding convergence of such variable nodes. In this sense, the variable nodes at the beginning and the end of the TE-SC protograph should converge faster than the variable nodes in the middle. Consequently, the decoding

wave can be triggered by default from both ends to the middle of the coupled chain due to the inherent termination boundary. It was illustrated in [150] that the decoding-wave phenomenon can be dramatically strengthened by assigning the variable nodes at the beginning and end of the TE-SC protograph to the labeling bits with low protection degrees within a modulated symbol, while assigning the variable nodes in the middle area to the labeling bits with high protection degrees. This technique is referred to as *optimized TE bit-mapping scheme* for the BICM-NI systems. Note that in the optimized TE bit-mapping scheme, the proportion of VNs at the beginning and the end of the coupled chain that are assigned to the low protection-degree labeling bits must be optimized so as to guarantee the excellent performance, which induces an additional computational overhead.

On the other hand, for a TB-SC-PLDPC code, the variable nodes in the TB-SC protograph (i.e., coupled chain) possess the same convergence behavior as those in its corresponding original protograph. In particular, all the variable nodes of a regular TB-SC-PLDPC code must have identical convergence performance regardless of the coupling length. Inspired by the inherent convergence feature of the TE-SC-PLDPC codes, the UEP offered by the w labeling bits within an M -ary symbol can be utilized to create an artificial termination boundary, which is of great significance to triggering the wave-like decoding convergence of the TB-SC-PLDPC code. Assume that the BP (or the windowed BP) decoding algorithm starts from the first time instant of the coupled chain. In the *optimized TB bit-mapping scheme* [150], the coded bits at the beginning of the TB-SC protograph are mostly assigned to the high protection-degree labeling bits within a symbol. Accordingly, the remaining coded bits in other areas (i.e., in the middle and at the end) of the coupled chain can be decoded in a more efficient way by using reliable soft information of such coded bits at the beginning of the coupled chain. As a result, a locally improved decoding convergence is ensured using the above mapping scheme, which is able to initiate the wave-like decoding behavior.

However, it was found that allocating the coded bits at the beginning of the coupled chain to the labeling bits with relatively high protection degree [150] is not able to completely trigger the decoding wave. In fact, coded bits at both the beginning and the end of the coupled chain play the same role on triggering the wave-like decoding. As an amendment to the work of [150], the effect of spatial-coupled structure of the TB-SC-PLDPC codes on the decoding convergence of the BICM systems was re-examined in [154]. To further enhance the system performance, a new bit-mapping scheme, referred to as *VNMM scheme*, was designed. The principle of the VNMM scheme is illustrated as follows.

For a given M -ary PSK/QAM LBPM constellation (see Section IV-B2), the input-output MI should be first analyzed so as to determine the protection-degree distribution of w ($w = \log_2 M \geq 3$) different labeling bits within a modulated symbol. Then, the two high protection-degree labeling bits can be found, while the remaining $w - 2$ labeling bits are referred to as the low protection-degree labeling bits. In the bit-to-symbol mapping process, an entire codeword is first divided into w blocks in a sequential order. Then, w coded bits are attracted from the w different blocks to generate an M -ary modulated symbol. Specifically, the two coded bits, which are separately extracted

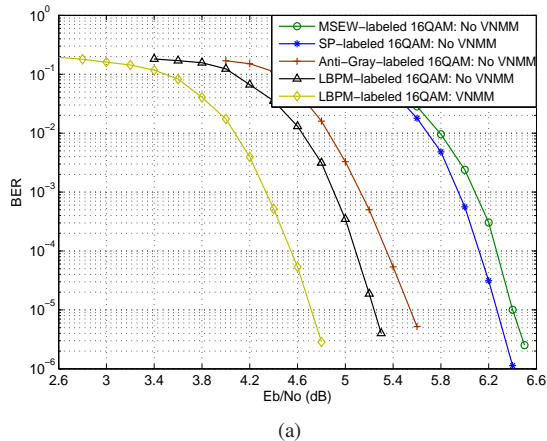


Fig. 13. BER curves of the regular-(3, 6) TB-SC-PLDPC code in the LBPM-labeled 16QAM-aided BICM-ID systems with $r_{SC} = 1/2$, $\varsigma = 2$, $L_{SC} = 12$, $N_T = 4800$, $t_{GL,max} = 8$, and $t_{BP,max} = 25$.

from the first block and the last block, will be mapped to the two high protection-degree labeling bits within the symbol. On the other hand, the remaining $w - 2$ coded bits, which are extracted from the remaining $w - 2$ blocks, will be mapped to the $w - 2$ low protection-degree labeling bits in a sequential order.

Remark: The optimized TB bit-mapping scheme in [150] and the VNMM scheme in [154] are effective for both regular and irregular codes, while the VDMM-based schemes in [116], [118], [119] are effective only for the irregular codes.

Example 15: Consider a TB-SC-PLDPC-BICM system using an LBPM-labeled 16QAM, where $w = 4$. To realize the VNMM scheme, the entire codeword is divided into w blocks in a sequential order, where each block includes $N' = \frac{N_{SC}}{w}$ coded bits. According to the LBPM-labeled 16QAM constellation in Fig. 12(b), the input-output MIs of four labeling bits satisfy $I(\hat{v}_{k,1}; y_k) = I(\hat{v}_{k,2}; y_k) > I(\hat{v}_{k,4}; y_k) > I(\hat{v}_{k,3}; y_k)$. Thereby, the high protection-degree labeling bits are $\hat{v}_{k,1}$ and $\hat{v}_{k,2}$.

In the mapping procedure, the four coded bits involved in each symbol can be extracted from the four different sub-blocks separately. Specifically, the coded bits in the first and the last blocks must be mapped to the labeling bits $\hat{v}_{k,1}$ and $\hat{v}_{k,2}$, respectively. Meanwhile, the coded bits in the second and the third blocks must be mapped to the remaining two labeling bits $\hat{v}_{k,3}$ and $\hat{v}_{k,4}$, respectively. By using the VNMM scheme, the wave-like convergence of the TB-SC-PLDPC code can be initiated similarly to that of the TE-SC-PLDPC code without any rate loss. In this BICM system, the variable nodes at both the beginning and the end of the codeword are protected with a higher priority, so as to accelerate their MI/LLR convergence.

Example 16: Fig. 13 depicts the BER curves of the regular-(3, 6) TB-SC-PLDPC code in the 16QAM-aided BICM-ID systems with different labelings and bit-mapping schemes. The results demonstrate that the LBPM labeling achieves gains of about 0.3, 1.0 and 1.2 dB over the anti-Gray, SP and MSEW labelings, respectively, at a BER of 10^{-5} . Moreover, the TB-SC-PLDPC-BICM-ID systems with the LBPM labeling obtain an additional performance gain of about 0.5 dB by using the VNMM scheme.

(2) Hybrid Mapping: In order to trigger the decoding-wave phenomenon of TB-SC-PLDPC codes in M QAM-aided BICM-ID systems, a *hybrid mapping scheme* was proposed in [152]. This

scheme adopts an SP-labeled constellation and another optimized constellation simultaneously to deal with a given codeword. In this scheme, each codeword is divided into L_{SC} blocks according to the coupling length L_{SC} . Then, the SP-labeled constellation mapper is employed for the first T_{SC} ($T_{SC} < L_{SC}$) blocks, while another constellation mapper is adopted for the remaining $L_{SC} - T_{SC}$ blocks. In this way, for a sufficiently large T_{SC} , the BP algorithm can locally decode the more reliable code bits, which can be treated as an effective termination to trigger the wave-like decoding convergence. However, the performance of the hybrid mapping scheme is determined by the parameter T_{SC} . For any given codeword, it is necessary to search for the optimal value of T_{SC} , which leads to an additional computational overhead. Especially, if the optimized constellation is implemented by the Gray-labeled constellation, combining the TB-SC-PLDPC codes with the hybrid mapping scheme can achieve desirable performance gains over the TE-SC-PLDPC counterparts in BICM-ID scenarios, without encountering any rate loss. Owing to these advantages, the hybrid mapping scheme turned out to be a promising alternative to the regular mapping scheme for BICM systems. It should be noted that the hybrid mapping scheme is exploited only for the 16QAM-aided BICM-ID system in [152].

Remarks: The hybrid mapping scheme has a similar principle to the IM scheme [90], [93], [215], because both schemes employ two different constellations to modulate a single codeword.

C. Summary

In this section, some design paradigms for PLDPC-BICM systems over AWGN channels are discussed. First, an overview of PLDPC-code constructions, constellation and bit-mapper designs for BICM systems is presented. Furthermore, the state-of-the-art progress of the SC-PLDPC-BICM system design is reported. For the SC-PLDPC-BICM systems, sophisticated channel-coding and bit-mapping schemes are developed to trigger the wave-like decoding phenomenon, which help improve the ID performance.

V. DESIGN OF PLDPC-BICM OVER FADING CHANNELS

This section presents the recent achievements related to designing PLDPC-BICM systems over both ergodic fast-fading channels and non-ergodic block-fading (i.e., slow-fading) channels. The design techniques can be viewed as promising alternatives to realize high-spectral-efficiency transmission in a variety of wireless-communication applications.

A. System Design for Ergodic Fast-Fading Channels

Recall the discussion in Section II-A4, the PLDPC codes that perform well over an AWGN channel can also perform well over other ergodic channel models [43], [71]. For this reason, the PLDPC codes optimized for BICM systems over AWGN channels can be directly applied to ergodic fast-fading channels [83], [86], [102]. It has been shown that the AWGN-optimized PLDPC codes do exhibit excellent performance over fast-fading channels. Hence, there are a few works devoted to the PLDPC-code design for BICM systems in such scenarios. More research effort was devoted to developing bit-mapping schemes for SC-PLDPC-BICM systems [46], [62], [83], [86], [88], [102].

TABLE XI

DECODING THRESHOLDS $(E_b/N_0)_{\text{th}}$ (dB) AND CAPACITY GAPS Δ OF THE RATE-1/2 AR4JA CODE AND EAR4JA CODE IN THE BICM-NI SYSTEMS OVER A NAKAGAMI FAST-FADING CHANNEL WITH FADING DEPTH $m = 1$. THE GRAY-LABELED QPSK, 8PSK AND 16QAM MODULATIONS ARE ASSUMED.

Code Type	QPSK			8PSK			16QAM		
	$(E_b/N_0)_{\text{th}}$	Δ	Capacity	$(E_b/N_0)_{\text{th}}$	Δ	Capacity	$(E_b/N_0)_{\text{th}}$	Δ	Capacity
AR4JA	2.326	0.474	1.852	4.019	0.631	3.388	4.783	0.654	4.129
EAR4JA	2.158	0.306		3.722	0.334		4.556	0.427	

1) *Design of PLDPC-BICM Systems:* It was proved that the AR4JA code possesses both excellent decoding threshold and MHDGR, and thus performs well in both low- and high-SNR regions over AWGN channels [65]. Based on the structure of the rate-1/2 AR4JA code in Fig. 4(d), an *EAR4JA code* was constructed in [83], by adding two variable nodes and one check node into the protograph. The base matrix of the rate-1/2 EAR4JA code is shown in (19), where the variable node corresponding to the second column is punctured. Using the PEXIT algorithm, one can easily calculate the decoding threshold of the EAR4JA code as 0.395 dB over a BPSK-modulated AWGN channel, which has a gap of only 0.208 dB to the channel capacity. However, no work discussed bit-mapper design for PLDPC-BICM over ergodic fast-fading channels.

$$\mathbf{B}_{\text{EAR4JA}} = \begin{bmatrix} 1 & 2 & 0 & 0 & 1 & 0 & 0 \\ 0 & 3 & 1 & 1 & 1 & 0 & 1 \\ 0 & 1 & 2 & 2 & 2 & 1 & 1 \\ 0 & 2 & 0 & 0 & 0 & 2 & 0 \end{bmatrix} \quad (19)$$

Example 17: Table XI compares the decoding thresholds and capacity gaps of the rate-1/2 AR4JA code and EAR4JA code in the *MPSK/MQAM*-aided BICM-NI systems over a Nakagami fast-fading channel. As seen, AR4JA-coded BICM-NI systems possess decoding thresholds of about 0.47 ~ 0.66 dB to the corresponding capacity limits. Moreover, the EAR4JA code that outperforms the AR4JA code over an AWGN channel also preserves its advantage over a fast-fading channel. For example, the EAR4JA code not only has gains of about 0.17 ~ 0.30 dB over the AR4JA code, but also operates about 0.3 ~ 0.43 dB away from the corresponding capacity limits. These demonstrate that there is no need to re-optimize the PLDPC codes over ergodic fast-fading channels.

2) *Design of SC-PLDPC-BICM Systems:* In the current literature, there did not seem to be much work on designing BICM systems deploying SC-PLDPC codes over fast-fading channels. **(1) Code Construction:** In recent progress, a new QC-SC-PLDPC-BICM scheme was proposed in [102] using a conventional pseudo-random interleaver to support efficient and reliable transmission of QPSK-aided BICM-ID systems. In particular, a new construction method, which consists of a base-matrix optimization scheme and a two-step lifting scheme, was developed for the QC-TE-SC-PLDPC codes to achieve capacity-approaching performance over both AWGN channels and ergodic fast-fading channels. More precisely, the design of capacity-approaching QC-TE-SC-PLDPC codes proposed in [102] was formulated over an AWGN channel. Subsequently, the designed codes were applied to ergodic fast-fading channels under the same framework. BER and word error rate (WER) simulations were performed, which demonstrated that the QC-TE-SC-PLDPC codes designed over the AWGN channel also exhibit desirable performance over the Nakagami fast-fading channel. It

was further conjectured that the QC-TE-SC-PLDPC codes are able to universally achieve near-capacity performance in BICM-ID systems even for the case of higher-order modulation. As such, the QC-TE-SC-PLDPC-BICM-ID appears to be a good attractive transmission scheme for practical wireless systems due to its low implementation complexity. The details of the design, especially the base-matrix optimization scheme and two-step lifting scheme, has been discussed in Section IV-B1.

(2) Bit-Mapper Design: According to [67], the coded bits in the middle area of the coupled chain are much more difficult to converge than those at the beginning and the end for a TE-SC-PLDPC code when the coupling length L_{SC} is a finite value. Motivated by this property, a position-based bit-mapping scheme was proposed for the TE-SC-PLDPC codes in BICM-NI systems [150]. Yet, this scheme is not well suited for irregular TE-SC-PLDPC codes (e.g., the RJA TE-SC-PLDPC codes [67] and RA TE-SC-PLDPC codes [145]), in which some coded bits at the beginning and the end of the coupled chain may converge slower than those in the middle. This is one salient property of the irregular TE-SC-PLDPC codes distinguished from the regular TE-SC-PLDPC codes. To overcome the weakness of the work of [150], a spatial-position matched mapping (SPMM) scheme was constructed in [86] for the TE-SC-PLDPC-BICM-NI system based on MI analysis. The SPMM can enhance the decoding-wave phenomenon and accelerate the convergence of TE-SC-PLDPC-BICM systems irrespective of the code structure.

Now, consider a TE-SC-PLDPC-BICM-NI system with Gray-labeled *MPSK/MQAM*. The principle of the SPMM scheme can be summarized as follows. Assume that the length of the TE-SC-PLDPC code is $N = Zn_{\text{SC}} = Zn_{\text{P}}L_{\text{SC}}$, where Z is the lifting factor, n_{SC} and n_{P} are the numbers of the variable nodes of the TE-SC protograph and the uncoupled original protograph, respectively, L_{SC} is the coupling length, and the codeword length N is a multiple of $w = \log_2 M$ (i.e., $N' = N/w$). At the beginning, the entire codeword is divided into n_{SC} blocks in a sequential order, i.e., $\mathcal{V}_{\text{SC}} = \{\mathcal{V}_{\text{B},1}, \mathcal{V}_{\text{B},2}, \dots, \mathcal{V}_{\text{B},n_{\text{SC}}}\}$, where $\mathcal{V}_{\text{B},j}$ is the j -th block that includes all the Z variable nodes at the j -th position. Subsequently, the n_{SC} blocks $\mathcal{V}_{\text{B},1}, \mathcal{V}_{\text{B},2}, \dots, \mathcal{V}_{\text{B},n_{\text{SC}}}$ are re-ranked to $\mathcal{V}_{\text{B},i(1)}, \mathcal{V}_{\text{B},i(2)}, \dots, \mathcal{V}_{\text{B},i(n_{\text{SC}})}$ in a descending order of their *a posteriori* MIs output from the outer decoder. Furthermore, the n_{SC} re-ranked blocks are consecutively converted to w intermediate blocks $\mathcal{V}_{\text{G},1}, \mathcal{V}_{\text{G},2}, \dots, \mathcal{V}_{\text{G},w}$, where $\mathcal{V}_{\text{G},\mu}$ contains n_{SC}/w blocks (i.e., N' variable nodes), and $\mu = 1, 2, \dots, w$. Finally, aiming to balance the convergence speeds of the MIs for all the variable nodes as much as possible in the bit-to-symbol mapping procedure, the w intermediate blocks $\mathcal{V}_{\text{G},1}, \mathcal{V}_{\text{G},2}, \dots, \mathcal{V}_{\text{G},w}$ are consecutively mapped to the w labeling bits within a modulated symbol in an ascending order of their protection degrees. Specifically, all the variable nodes in $\mathcal{V}_{\text{G},\mu}$ are mapped to the labeling bits with the μ -th lowest protection degree within the length- N' M -ary modulated symbol

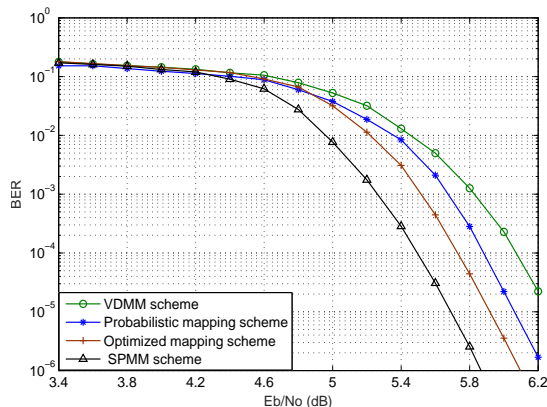


Fig. 14. BER curves of the RJA TE-SC-PLDPC code with four different bit-mapping schemes in the Gray-labeled 16QAM-aided BICM-ID systems over a Nakagami fast-fading channel with $m = 1$, $r_{SC} = 5/12$, $\varsigma = 1$, $L_{SC} = 6$, $N_T = 4800$, and $t_{BP,max} = 100$.

sequence. Based on this mapping procedure, the variable nodes with relatively slower convergence speed can be protected with relatively higher protection degrees, and thus the decoding-wave effect of the TE-SC-PLDPC code can be further enhanced. As such, the SPMM scheme is a more feasible and precise method with respect to the bit-mapping optimization scheme in [150], because the former substantially uses the MI distribution of the coded bits to accelerate the decoding convergence.

Example 18: Consider the BICM-NI systems deploying the rate-5/12 RJA TE-SC-PLDPC code and Gray-labeled 16QAM modulation. Fig. 14 compares the performance of the SPMM scheme with the VDMM scheme [116], the probabilistic mapping scheme [87], and the optimized mapping scheme [82]. As observed from this figure, the SPMM needs an SNR of about 5.6 dB to achieve a BER of 2×10^{-5} , while the optimized mapping, probabilistic mapping and VDMM need SNRs of about 5.85 dB, 6.0 dB and 6.2 dB to do so, respectively. The results verify the superiority of the SPMM scheme.

Finally, it is noted that there does not seem to be any work on the design of signal constellations for the SC-PLDPC-BICM systems over ergodic fast-fading channels.

B. System Design for Non-Ergodic Block-Fading Channels

The block-fading channel has attracted considerable attention during the past three decades because it can be used to model many communication scenarios with slowly varying fading, such as orthogonal frequency division multiplexing systems, free-space optical systems, cooperative communication systems, and cellular networks [52], [72], [212]. In this channel model, the fading gain remains constant on each symbol block but randomly varies on different blocks. As a type of non-ergodic channel, block-fading channel possesses some salient features quite different from those in ergodic AWGN and fast-fading channels. Of particular significance is that the block-fading channel is not information stable. For this reason, the information outage-probability limit, instead of the Shannon capacity limit, is utilized to characterize the fundamental performance limit of block-fading channels [174], [213]. In recent years, PLDPC codes along with their BICM schemes have been recommended for such non-ergodic channels [71], [99], [179], [212], [213], which

are obviously superior to the previously-proposed convolutional- and turbo-coded counterparts [89], [174], [194].

Assuming a BICM system deploying an M -ary modulation and a rate- r PLDPC code, the achievable diversity order of a PLDPC code over a block-fading channel is bounded by $d \leq m(1 + \lfloor L(1 - R_{SE}/\log_2 |\chi|) \rfloor)$ [71], where L is the number of fading blocks, m is the fading depth, $R_{SE} = r \log_2 M = rw$ is the spectral efficiency, and χ is the signal constellation set. This bound implies an optimal trade-off between the spectral efficiency (or code rate) and the diversity order. A PLDPC code is said to have full diversity if and only if $d = mL$. As a result, the highest achievable spectral efficiency (resp. code rate) for a full-diversity PLDPC-BICM system over a BF channel is $R_{SE,max} = \log_2 |\chi|/L = w/L$ (resp. $r_{max} = \frac{1}{L}$). Accordingly, designing a rate- $\frac{1}{L}$ full-diversity PLDPC code and an appropriate M -ary modulation is indispensable in realizing high-efficiency transmissions over BICM block-fading channels [72], [194].

1) *Design of PLDPC-BICM Systems:* In the past five years, a flurry of research activities took place in devising PLDPC-BICM systems over block-fading channels. In [71], PLDPC-BICM systems were carefully investigated over M PSK/ M QAM-modulated Nakagami block-fading channels from the perspectives of code construction, modulation-strategy design, and bit-mapper optimization. Besides, a number of works studied the M -ary chaos-based SS BICM systems, i.e., M DCSK-aided BICM systems, with the use of PLDPC codes over such channels [64], [92], [128]–[130], [156]. In the following, these PLDPC-BICM designs over block-fading channels will be discussed.

(1) **PSK/QAM-aided PLDPC-BICM Design:** To achieve full diversity over block-fading channels, several types of powerful LDPC codes, including root-LDPC codes [221], [222] and root-PLDPC codes [99], [179], [213], were proposed. Although all these LDPC codes are able to attain outage-limit-approaching performance with the maximum code rate (i.e., $r_{max} = 1/L$) over block-fading channels, the conventional root-LDPC codes are randomly constructed and thus suffer from relatively high encoding and decoding complexity. On the contrary, the structured root-PLDPC codes emerged to be a more desirable choice for such environments, because they possess both advantages of full diversity and simple implementation. As a special type of check nodes, rootchecks are the key component in root-PLDPC codes, which guarantees full diversity for all the information-bearing coded bits. However, it is very challenging for the root-PLDPC codes to adapt to the high-order modulations without losing full diversity [53], [71], [194]. Here, the principle of root-LDPC codes is briefly introduced, followed by some discussions on their feasibility to BICM-ID framework.

Consider an L -layer root-PLDPC code transmitted over a block-fading channel. A type- l ($l = 1, 2, \dots, L$) *rootcheck* is defined as a check node having one edge connecting to an information-bearing variable node transmitted on the l -th fading gain α_l , and the remaining edges connecting to other variable nodes are transmitted on another fading gain $\alpha_{l'}$ ($l' \neq l$). The maximum achievable code rate for a full-diversity PLDPC code in such a scenario is $r_{max} = 1/L$. To guarantee full diversity and maximum rate, an L -layer root-PLDPC code must include L different types of rootchecks. Also, to achieve full diversity of the information-bearing variable nodes, each type- l rootcheck set

must be composed of $L-1$ different rootchecks, which separately span the remaining $L-1$ fading blocks [179].

Based on the principle of rootcheck, one can easily construct an L -layer root-PLDPC code $\mathbf{A} = (\mathcal{V}_1, \mathcal{V}_2, \dots, \mathcal{V}_L)$ based on an $m_P \times n_P$ protograph, as follows. At the beginning, the n_P/L information bits are uniformly divided into L subsets, in which the l -th subset is transmitted on the l -th fading gain α_l . Meanwhile, the $(L-1)n_P/L$ parity bits are uniformly divided into L subsets, to effectively protect the information bits in each fading block. The l -th information-bit subset and l -th parity-bit subset constitute the l -th code block, and the L different blocks constitute the overall variable-node set of the root-PLDPC code. To achieve full diversity, each information-bearing variable node in the l -th block must be simultaneously connected to all the $L-1$ rootchecks belonging to the type- l rootcheck set with $L-1$ single edges. On the other hand, the parity-check variable nodes in the l -th block must be connected to other $L-1$ types of rootchecks. The L different types of rootcheck sets constitute the overall check-node set of the root-PLDPC code. As a consequence, a full-diversity L -layer root-PLDPC code can be constructed by combining the variable-node set, check-node set, and their associated edges, into a single entity.

According to the above construction procedure, the number of variable nodes in a root-PLDPC protograph must be $n_P = L^2$ in order to ensure the lowest encoding complexity. In the root-PLDPC code, the information bits rather than the parity bits can realize full diversity, which is called *UEP*. The root-PLDPC codes are capable of achieving excellent performance because only the information bits are counted in performance measurement. Moreover, one can clearly distinguish the information bits from the parity bits in a root-PLDPC code [99].

Example 19: According to the concepts of root-PLDPC codes, one can easily derive the base matrices of the rate-1/2 regular-(3,6) bilayer root-PLDPC code and the rate-1/3 regular-(4,6) three-layer root-PLDPC code, as (20). To simplify the exposition, the regular-(3,6) bilayer root-PLDPC code and the regular-(4,6) three-layer root-PLDPC code are called *RP-2 code* and *RP-3 code*, respectively. It was proved in [179] that the above two types of root-PLDPC codes can achieve full diversity over BPSK-modulated block-fading channels with $L=2$ and $L=3$, respectively. Likewise, full-diversity irregular root-PLDPC codes can be constructed by varying the row/column weights of the base matrix while keeping the rootcheck structure unchanged.

$$\mathbf{B}_{\text{RP-2}} = \begin{bmatrix} 1 & 0 & 0 & | & 1 & 2 & 2 & | & 0 & 0 & 0 \\ 1 & 0 & 0 & | & 0 & 0 & 0 & | & 1 & 2 & 2 \\ 1 & 2 & 2 & | & 1 & 0 & 0 & | & 0 & 0 & 0 \\ 0 & 0 & 0 & | & 1 & 0 & 0 & | & 1 & 2 & 2 \\ 1 & 2 & 2 & | & 0 & 0 & 0 & | & 1 & 0 & 0 \\ 0 & 0 & 0 & | & 1 & 2 & 2 & | & 1 & 0 & 0 \end{bmatrix}, \mathbf{B}_{\text{RP-3}} = \begin{bmatrix} 1 & 0 & 0 & | & 1 & 2 & 2 & | & 0 & 0 & 0 \\ 1 & 0 & 0 & | & 0 & 0 & 0 & | & 1 & 2 & 2 \\ 1 & 2 & 2 & | & 1 & 0 & 0 & | & 0 & 0 & 0 \\ 0 & 0 & 0 & | & 1 & 0 & 0 & | & 1 & 2 & 2 \\ 1 & 2 & 2 & | & 0 & 0 & 0 & | & 1 & 0 & 0 \\ 0 & 0 & 0 & | & 1 & 2 & 2 & | & 1 & 0 & 0 \end{bmatrix}. \quad (20)$$

However, when the modulation order M varies from 2 to 2^w ($w \geq 2$), the root-PLDPC codes are unable to achieve full diversity. To overcome this weakness, a novel modulation strategy was proposed in [71] to determine the order of *MPSK/MQAM*, which guarantees full-diversity order and maximum spectral efficiency for the root-PLDPC-BICM systems.

Suppose that an L -layer root-PLDPC code is deployed in an *MPSK/MQAM*-aided BICM system over a block-fading channel. Then, as demonstrated in [179], the modulation order

must satisfy $M = 2^w = 2^{zL}$ in order to enable the root-PLDPC-BICM system to achieve full diversity with both maximum code rate and maximum spectral efficiency, where z is a positive integer. For simplicity, one may assume that $z = 1$ when developing a bit-mapping scheme or related techniques.

In addition, a UEP-based bit-mapping scheme was developed in [71] to further accelerate the decoding convergence of root-PLDPC-BICM over block-fading channels. Consider the scenario that an L -layer root-PLDPC code is transmitted over a block-fading channel in an *MPSK/MQAM*-aided BICM system, where the protograph size is $(L-1)L \times L^2$, and $M = 2^w = 2^L$. Here, the l -th variable-node set transmitted on the l -th fading gain α_l is expressed as $\mathcal{V}_l = (v_{il,1}, v_{pl,1}, v_{pl,2}, \dots, v_{pl,L-1})$, which can be exactly mapped to an M -ary symbol $x_k \triangleq (\hat{v}_{k,1}, \hat{v}_{k,2}, \dots, \hat{v}_{k,w})$ transmitted with the same fading gain, where $v_{il,l}$, $v_{pl,\mu'}$, and $\hat{v}_{k,\mu}$ are the single information-bearing variable node in \mathcal{V}_l , the μ' -th parity-check variable node in \mathcal{V}_l , and the μ -th labeling bit within x_k , respectively, $k = 1, 2, \dots, N'$. In the UEP-based bit-mapping scheme, the information-bearing variable node $v_{il,1}$ should be mapped to the lowest protection-degree labeling bit within the symbol, while the $L-1$ parity-check variable nodes $v_{pl,1}, v_{pl,2}, \dots, v_{pl,L-1}$ should be mapped to the remaining $w-1$ labeling bits within the symbol. The UEP-based bit-mapping scheme can realize the best combination between the root-PLDPC code and the *MPSK/MQAM* modulation because it exploits the UEP property of both high-order modulation and rootcheck structure. As illustrated in [179], the anti-Gray labeling achieves a significant performance gain over the Gray-labeling in the root-PLDPC-BICM-ID system over block-fading channels, while the former is slightly inferior to the latter without ID. Hence, the anti-Gray labeling is a better choice than the Gray labeling in this scenario.

Example 20: Fig. 15 shows the WER curves of the bilayer RP-2 code, regular-(3,6) PLDPC code, and irregular AR4JA code in the BICM-ID systems over a Nakagami block-fading channel. Among the three types of PLDPC codes, only the RP-2 code can achieve full diversity and outage-limit-approaching performance. Additionally, simulations on the RP-3 code over the BICM block-fading channels verified its excellent performance.

(2) DCSK-aided PLDPC-BICM Design: DCSK modulation is a non-coherent SS-modulation scheme that benefits from excellent anti-fading robustness, powerful near-far resilience, and low implementation complexity. During the past two decades, a great deal of research effort has been devoted to optimizing the performance of DCSK as well as their high-order counterparts (i.e., *MDCSK*) and to facilitating their implementation [223], [224]. Based on the current research advancements, *MDCSK* has become an appealing modulation technique for low-power and low-complexity wireless applications, such as wireless personal area networks and wireless sensor networks. To realize high-reliability and high-throughput transmission in such short-range wireless-communication systems, the joint design of PLDPC codes and *MDCSK* was carefully investigated over block-fading channels [64], [92], [126], [156], [225], [226].

More precisely, there are two types of *MDCSK* modulations, i.e., Walsh-code-based *MDCSK* and constellation-based *MDCSK*, which can construct M -ary chaotic signals with

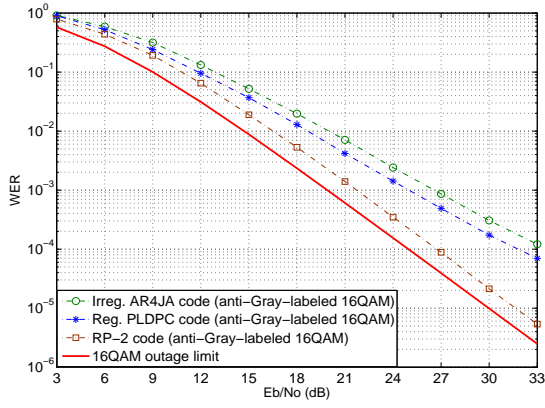


Fig. 15. WER curves of the root-PLDPC-BICM-ID system and two conventional PLDPC-BICM-ID systems over a Nakagami block-fading channel. The codes used are the bilayer RP-2 code, regular-(3, 6) PLDPC code, and irregular AR4JA code, the modulation used is anti-Gray-labeled 16QAM, respectively, and the parameters used are $m = 1$, $L = 2$, $r_P = 1/2$, $N_T = 1024$, $t_{GL,max} = 5$, and $t_{BP,max} = 50$.

the M -order Walsh code and M -ary constellation, respectively [126], [225]. Both M DCSK modulations can be used to formulate robust PLDPC-BICM systems over block-fading channels.

In the BICM-ID system with a Walsh-code-based M -DCSK modulation, a length- N PLDPC codeword $\Lambda = (v_1, v_2, \dots, v_N)$ is first converted to a length- N' non-binary codeword $\Lambda_{NB} = (v_{NB,1}, v_{NB,2}, \dots, v_{NB,N'})$, where $v_{NB,k} \in \{0, 1, \dots, M-1\}$ is the k -th non-binary coded symbol, with $w = \log_2 M$ and $k = 1, 2, \dots, N'$. The M possible values of non-binary symbol will be utilized to select their corresponding row indices of an M -order Walsh code, so as to guarantee the orthogonality of the M different transmitted chaotic signals. In particular, a 2^w -order orthogonal Walsh code is introduced, as [126]

$$\overline{\mathbf{W}}_{2^w} = \begin{bmatrix} \overline{\mathbf{W}}_{2^{w-1}} & \overline{\mathbf{W}}_{2^{w-1}} \\ \overline{\mathbf{W}}_{2^{w-1}} & -\overline{\mathbf{W}}_{2^{w-1}} \end{bmatrix} = [\omega_1, \omega_2, \dots, \omega_M]^T, \quad (21)$$

where $\overline{\mathbf{W}}_{2^0} = \overline{\mathbf{W}}_1 = 1$, $\omega_\mu = [\omega_{\mu,1}, \omega_{\mu,2}, \dots, \omega_{\mu,M}]$ is the μ -th row vector of the Walsh code, $\mu = 1, 2, \dots, M$.

Assume that $\mathbf{c}_k = [c_{k,1}, c_{k,2}, \dots, c_{k,\beta}]$ is the reference-chaotic fragment for the M -DCSK modulation with a spreading factor β . Then, the transmitted M DCSK-modulated signal \mathbf{x}_k corresponding to the non-binary symbol $v_{NB,k}$ can be formulated by multiplying the elements of the $(v_{NB,k} + 1)$ -th row vector $\omega_{v_{NB,k}+1}$ in the Walsh code with the M delayed replicas of reference-chaotic fragment \mathbf{c}_k , which can be expressed as $\mathbf{x}_k = [\omega_{v_{NB,k}+1,1}\mathbf{c}_k, \omega_{v_{NB,k}+1,2}\mathbf{c}_k, \dots, \omega_{v_{NB,k}+1,M}\mathbf{c}_k]$. As a consequence, a Walsh-code-based M DCSK signal consists of M chaotic fragments, which will result in a global spreading factor of $M\beta$. At the receiver, a generalized-maximum-likelihood (GML) energy detector is employed to demodulate the ‘‘corrupted’’ non-binary symbol output from the block-fading channel [126].

In 2015, the AR4JA PLDPC codes were applied to the Walsh-code-based M DCSK system in [128], and the interaction between channel coding and modulation was investigated. Furthermore, a turbo-like iterative receiver was constructed, comprising a GML demodulator and a PLDPC decoder, to improve the performance of the BICM framework. Following the above work, a simple computer-search method was developed in [156] to obtain a family of *improved ARA (IARA) codes* that possess

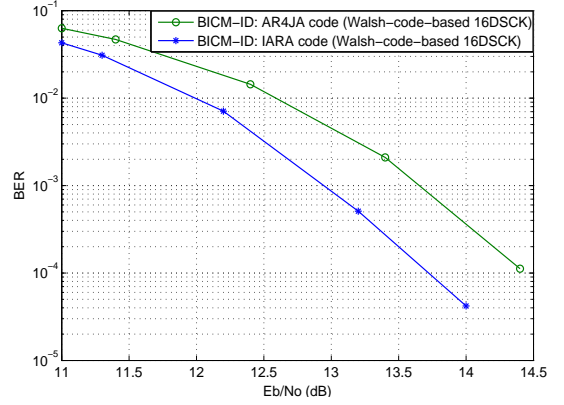


Fig. 16. BER curves of the rate-1/2 IARA code and AR4JA code in the Walsh-code-based 16DCSK-aided BICM-ID system over a Nakagami block-fading channel with $m = 1$, $N_T = 4096$, $\beta = 40$, $t_{GL,max} = 5$, and $t_{BP,max} = 40$.

desirable decoding thresholds and MHDGRs over block-fading channels with code rates ranging from $1/2$ to $1 - \epsilon$. The base matrix of a rate- $(e+1)/(e+2)$ IARA code is obtained as

$$\mathbf{B}_{\text{IARA}} = \begin{bmatrix} & & & & \overbrace{0 \ 0 \ \dots \ 0 \ 0}^{2e} & & \\ 1 & 2 & 0 & 0 & 0 & 0 & \dots & 0 & 0 \\ 0 & 2 & 2 & 1 & 1 & 1 & 2 & \dots & 1 & 2 \\ 0 & 1 & 1 & 2 & 1 & 2 & 1 & \dots & 2 & 1 \end{bmatrix}, \quad (22)$$

where the variable node corresponding to the first column is punctured. Both analyses and simulations demonstrated that the IARA codes significantly outperform the AR4JA codes in the Walsh-code-based M DCSK-aided BICM-ID systems over Nakagami block-fading channels, as shown in Fig. 16.

According to [126], the Walsh codes realize high-order M DCSK modulations by introducing $M - 1$ radio-frequency delay lines and M chaotic fragments (i.e., a length- $M\beta$ DCSK signal), which dramatically decrease the transmission throughput and increase the implementation complexity. To relax these limitations, a constellation-based M DCSK modulation scheme was proposed in [225], which can modulate w coded bits into a length- 2β DCSK signal for transmission. In other words, the constellation-based M -DCSK enables higher efficiency and lower complexity, as compared with the Walsh-coded-based counterpart, and turns out to be a more promising choice for bandwidth-limited wireless communication applications.

In the BICM-ID system with a constellation-based M DCSK modulation, a length- N PLDPC codeword $\Lambda = (v_1, v_2, \dots, v_N)$ is first uniformly converted to a length- N' complex-valued symbol $\mathbf{g} = (g_1, g_2, \dots, g_{N'})$ based on a given M -ary signal constellation, such as the M PSK/ M QAM constellation shown in Fig. 2, where $N' = N/\log_2 M = N/w$. The real part and imaginary part of the k -th M -ary symbol g_k are denoted as $g_{RE,k}$ and $g_{IM,k}$, respectively, $k = 1, 2, \dots, N'$. Based on a length- β reference-chaotic fragment \mathbf{c}_k and its β -delayed signal $\mathbf{c}_{R,k}$, one can construct its orthogonal signal $\mathbf{c}_{\Gamma,k}$ by performing a Hilbert transform [126], [225], where $\mathbf{c}_{\Gamma,k} \cdot (\mathbf{c}_{R,k})^T = 0$. The information-bearing fragment can be generated through a linear combination of the quadrature chaotic signals $\mathbf{c}_{R,k}$ and $\mathbf{c}_{\Gamma,k}$ weighted by the fractions $g_{RE,k}$ and $g_{IM,k}$, respectively, i.e., $\mathbf{d}_k = g_{RE,k}\mathbf{c}_{R,k} + g_{IM,k}\mathbf{c}_{\Gamma,k}$. As such, the length- 2β M -DCSK signal is obtained as $\mathbf{x}_k = [\mathbf{c}_k \ \mathbf{d}_k]$, and then transmitted over the block-fading channel. At the receiver, a modified energy

detector is used to retrieve the original symbol g_k . Specifically, the two corrupted orthogonal signals $\tilde{\mathbf{c}}_{R,k}$ and $\tilde{\mathbf{c}}_{\Gamma,k}$ can be easily attained from the noisy reference-chaotic signal $\tilde{\mathbf{c}}_k$. These two signals correlate with the corrupted information-bearing signal $\tilde{\mathbf{d}}_k$, thereby generating two energy-based metrics $z_{R,k}$ and $z_{\Gamma,k}$, respectively, which will be finally utilized to make the decision and yield the retrieved symbol \tilde{g}_k for g_k [225].

In [92], the capacity-approaching AR4JA codes were applied to the constellation-based M -DCSK-aided BICM-ID system over block-fading channels. According to the analyses and simulations, the proposed PLDPC- M DCSK-aided BICM-ID system significantly boosts the anti-noise and anti-multipath-fading capability compared to the BICM-NI counterpart. Furthermore, the impact of several critical parameters, such as the spreading factor and number of global iterations, on the performance of PLDPC-BICM-ID systems with constellation-based M DCSK was discussed, aiming to optimize the overall performance. However, this work did not focus on the code design, which deserves further exploration towards practical applications.

(3) PLDPC-PNC BICM Design: Inspired by the desirable advantages of PLDPC-BICM, its application was extended to other emerging systems, including TWR communication systems with PNC [58]. Compared with the convolutional codes, PLDPC codes are more likely to approach the BICM capacity over PNC-aided TWR channels. For this reason, in [135], [227] the M PSK-aided PLDPC-BICM-ID was studied over PNC-aided TWR block-fading channels. This was perhaps the first attempt to apply the AR3A PLDPC-BICM-ID scheme to PNC-aided TWR communication systems, which can help boost the transmission throughput and error performance over block-fading channels. Besides, the effect of signal labelings on the performance of PLDPC-BICM-ID was investigated over block-fading channels. Interestingly, as illustrated through analyses and simulations, the Gray-labeled BICM-ID is able to achieve a considerable performance gain over its BICM-NI counterpart over PNC-aided TWR channels, which is in contrast to the observation in the point-to-point scenario. This phenomenon suggests that the Gray labeling has great potential for application in PLDPC-PNC BICM-ID systems over block-fading channels.

2) *Design of SC-PLDPC-BICM Systems:* According to [43], [194], the non-ergodic block-fading channel can be treated as a type of memory channel since its fading gain remains constant during the entire transmission period of each code block. As mentioned in V-B1, the code rate of a full-diversity root-PLDPC code is $r_P = 1/L$ over a BICM block-fading channel with L fading blocks. However, how to improve the diversity order of their SC counterparts (i.e., SC-PLDPC codes) over such a channel is still a challenging issue for the coding community. In [212], the performance of SC-PLDPC codes over the BPSK-aided block-fading channel with $L = 2$ was carefully evaluated. As a type of convolutional-like codes, SC-PLDPC codes may find their great potential for transmission over block-fading channels. In fact, the inherent memory feature of the SC-PLDPC codes makes them a powerful choice for slowly-varying fading wireless communications. It was demonstrated in [212] that the diversity order of a TE-SC-PLDPC code can be improved by increasing the constraint length without a sophisticated design, which is determined by the coupling width and the codeword

length of its original PLDPC code (i.e., $\nu_{SC} = (\zeta + 1)Zn_P$). In other words, based on a length- N PLDPC code, the diversity order of its corresponding TE-SC-PLDPC code can be significantly boosted by increasing the coupling width ζ over a block-fading channel at the price of a small rate loss. More importantly, unlike the root-PLDPC codes [71], the TE-SC-PLDPC codes are capable of achieving full diversity without the need of any specific design. Although no high-order modulation has been considered, the above feature may be further exploited to boost the diversity order of SC-PLDPC-BICM systems over M PSK/ M QAM-modulated block-fading channels.

C. Summary

In this section, the recent development and contributions in PLDPC-BICM systems over wireless fading channels are reviewed. First, the code and bit-mapper design for such systems over ergodic fast-fading channels are described. Then, some typical research works concerning the design of PLDPC-BICM systems are introduced, under the M PSK/ M QAM and M DCSK modulations over non-ergodic block-fading channels. Finally, the application of PLDPC codes to PNC BICM systems over TWR block-fading channels is discussed.

VI. DESIGN OF PLDPC-BICM OVER POISSON PPM CHANNELS

Poisson channel is considered as a channel model that can suitably describe the statistic characteristics of optical deep-space and free-space links [228], [229]. PPM is a popular alternative for such applications, which not only allows simple bit-to-symbol mapping but also possesses near-optimal channel capacity. To realize power-efficiency transmissions in free-space optical communication systems, it makes sense to combine capacity-approaching codes (e.g., PLDPC codes) with PPM over Poisson channels. However, the PLDPC codes constructed for M PSK/ M QAM-aided BICM systems over AWGN and fading channels do not work well for Poisson PPM channels.

During the past decade, a variety of code-design and performance-analysis methodologies have been developed for PLDPC-BICM systems over Poisson PPM channels, where the receiver includes an inner PPM demodulator and an outer PLDPC decoder [54], [55], [123], [124], [177]. On the contrary, the application of SC-PLDPC codes to the Poisson PPM channels and their design approaches are relatively unexplored. For this reason, in the following only the PLDPC-BICM systems over Poisson PPM channels are discussed.

A. Principles of PPM and Poisson Channels

Distinguished from conventional M PSK/ M QAM modulations, PPM is a type of position-aware modulation scheme, in which each transmitted signal is represented by an M -slot PPM symbol. For each PPM symbol, only one single pulse is transmitted in one of the M slots, while the remaining $M - 1$ slots keep silent. In other words, an M -ary PPM symbol can be defined as a vector $\mathbf{x}_k = [x_{P,k,0}, x_{P,k,1}, \dots, x_{P,k,M-1}]$ of size $1 \times M$, where $x_{P,k,\mu} \in \{0, 1\}$, $k = 1, 2, \dots, N'$, $\mu = 0, 1, 2, \dots, M - 1$, $N' = N/w = N/\log_2 M$, and each symbol has only one element equal to 1 (i.e., one active pulse). In

a PLDPC-BICM-ID system with M PPM, a length- N PLDPC codeword $\mathbf{\Lambda} = (v_1, v_2, \dots, v_N)$ is first converted to a length- N' non-binary codeword $\mathbf{\Lambda}_{\text{NB}} = (v_{\text{NB},1}, v_{\text{NB},2}, \dots, v_{\text{NB},N'})$, where $v_{\text{NB},k} \in \{0, 1, \dots, M-1\}$. Subsequently, the non-binary codeword is modulated into an M -ary PPM symbol sequence $\mathbf{X} = (\mathbf{x}_1, \mathbf{x}_2, \dots, \mathbf{x}_{N'})$, where the k -th PPM symbol \mathbf{x}_k is mapped from the k -th non-binary coded symbol $v_{\text{NB},k}$ in accordance with its value. Specifically, the μ -th element $x_{\text{P},k,\mu}$ of \mathbf{x}_k equals 1 (i.e., $x_{\text{P},k,\mu} = 1$) if and only if $v_{\text{NB},k} = \mu$.

Consider a Poisson PPM channel. The received signal can be described by a $1 \times M$ vector $\mathbf{y}_k = [y_{\text{P},k,0}, y_{\text{P},k,1}, \dots, y_{\text{P},k,M-1}]$, where $y_{\text{P},k,\mu} = \alpha_{\text{P},k,\mu} x_{\text{P},k,\mu} + n_{\text{P},k,\mu}$, $\alpha_{\text{P},k,\mu}$ and $n_{\text{P},k,\mu}$ are i.i.d. Poisson random variables with means λ_α and λ_n , respectively, where λ_α and λ_n are the average power per pulsed slot and of background radiation, respectively. In consequence, the conditioned PDF of the μ -th element in the k -th channel output is written as

$$f(y_{\text{P},k,\mu} | x_{\text{P},k,\mu}) = \frac{(\lambda_\alpha x_{\text{P},k,\mu} + \lambda_n)^{y_{\text{P},k,\mu}}}{y_{\text{P},k,\mu}!} \exp(-(\lambda_\alpha x_{\text{P},k,\mu} + \lambda_n)), \quad (23)$$

where the average SNR per symbol in the M PPM Poisson channel is defined as $\lambda_\alpha / (M\lambda_n)$.

B. PLDPC-Code Design for PPM-aided BICM Systems

In 2010, the first attempt to design and analyze the PLDPC codes in M PPM-aided BICM-ID systems over Poisson channels was carried out in [177]. Specifically, the PEXIT algorithm was generalized to facilitate the optimization of the PLDPC codes in such transmission scenarios. Using the generalized PEXIT algorithm, one can get a rate-1/2 optimized PLDPC code, referred to as *PPM-PLDPC-A code*, for the 64PPM-aided BICM-ID system based on certain constraints after a computer search. The protograph corresponding to the PPM-PLDPC-A code includes 88 non-punctured variable nodes and 44 check nodes. In detail, there are 66 degree-3 variable nodes, 21 degree-2 variable nodes, and 1 degree-24 variable node among all the 88 variable nodes. On the other hand, all the 44 check nodes have a constant degree of 6. Simulation results showed that at a BER of 10^{-5} , the PPM-PLDPC-A code achieves a remarkable gain of about 0.8 dB on the AR4A code in the BICM-ID system over a Poisson PPM channel with $M = 64$ and $\lambda_n = 0.2$. More importantly, the PPM-PLDPC-A code has a gap of only 1 dB to the channel capacity. Although the PPM-PLDPC-A-coded BICM is slightly inferior to the convolutional-coded serially concatenated PPM, it is amenable to lower decoding latency (i.e., parallel decoding) with better rate compatibility.

As can be observed, the protograph size corresponding to the PPM-PLDPC-A code is a bit large, which leads to relatively complicated representation and implementation. Actually, it is preferred to design a smaller protograph tailored for BICM system over Poisson PPM channels. For this reason, another notable contribution related to PLDPC-code design over Poisson PPM channels was presented in [54], where the drawbacks of the 3×5 protograph corresponding to a rate-1/2 AR4A code (see Fig. 9(a)) were identified. Then, a 2×4 protograph was optimized within the context of 64PPM, in which the maximum number of edges connecting a variable node to a check node is limited to 3. After a simple search, an optimized PLDPC code

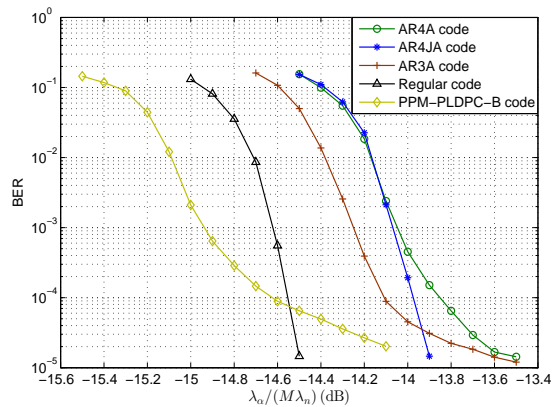


Fig. 17. BER curves of the rate-1/2 PPM-PLDPC-B code, AR4A code, AR4JA code, AR3A code, and regular-(3, 6) PLDPC code in the BICM-ID system over a Poisson PPM channel with $N_T = 8160$, $M = 64$, $\lambda_n = 0.2$, $t_{\text{GL,max}} = 8$, and $t_{\text{BP,max}} = 25$.

(referred to as *PPM-PLDPC-B code*) that exhibits the lowest decoding threshold can be obtained, with a base matrix

$$\mathbf{B}_{\text{PPM-B}} = \begin{bmatrix} 1 & 1 & 0 & 1 \\ 1 & 2 & 2 & 2 \end{bmatrix}. \quad (24)$$

Example 21: Considering a BICM-ID system over a Poisson PPM channel with $M = 64$ and $\lambda_n = 0.2$, one can compare the decoding thresholds and MHDGRs of the rate-1/2 PPM-PLDPC-B code and AR4A code by using the PEXIT and AWE analyses. It has been shown that the PPM-PLDPC-B code has a decoding threshold of -14.98 dB, which is much smaller than that of the AR4A code (i.e., -14.13 dB). Furthermore, the decoding threshold of the former is only about 0.6 dB away to the channel capacity. However, both codes do not have effective MHDGRs because they have too many (i.e., more than 40%) degree-2 variable nodes, which implies that they may suffer from error-floor behavior in the high-SNR region [43].

To have more insight, the BER performances of the rate-1/2 PPM-PLDPC-B code and AR4A code in the BICM-ID system over a Poisson PPM channel are compared in Fig. 17. For reference, three classic rate-1/2 PLDPC codes, i.e., AR4JA code, AR3A code, and regular-(3, 6) PLDPC code, are included in the same figure. It can be clearly seen that the PPM-PLDPC-B code significantly outperforms the other four types of PLDPC codes in the low-SNR region with respect to the capacity-approaching decoding threshold. Also, the PPM-PLDPC-B code, AR4A code, and AR3A code encounter severe error-floor issues in the high-SNR region. Particularly, the PPM-PLDPC-B code becomes inferior to the regular PLDPC code once the SNR exceeds -14.55 dB. Therefore, it is desirable to design more robust PLDPC codes that have both excellent decoding thresholds and MHDGRs in the context of M PPM, to meet the ultra-high-reliability requirement of optical communication applications.

More recently, a novel design method was proposed in [124] to construct capacity-approaching punctured non-binary PLDPC codes for Poisson PPM channels with the usage of a surrogate erasure channel model. It was shown that the non-binary PLDPC-CM schemes outperform the binary PLDPC- and convolutional- BICM schemes. Although the non-binary PLDPC codes can combine with M PPM in a more seamless fashion compared with the binary PLDPC codes, they have much higher

implementation complexity. Thus, the binary PLDPC-BICM is usually more preferable for practical Poisson PPM applications with respect to the non-binary PLDPC-CM.

C. Summary

In this section, the majority of contributions in the PLDPC-BICM design over Poisson PPM channels were reviewed. In particular, the structures of two types of optimized PLDPC codes, i.e., PPM-PLDPC-A and PPM-PLDPC-B codes, are described, which exhibit excellent decoding thresholds in the BICM-ID frameworks over Poisson PPM channels. However, both types of codes do not enjoy the benefit of the linear-minimum-distance-growth rates, and hence may suffer from severe error floors in the high-SNR region.

VII. DESIGN OF PLDPC-BICM OVER NAND FLASH-MEMORY CHANNELS

As an excellent non-volatile memory technique, NAND flash memory indicates a revolutionized paradigm shift in the evolution of modern data-storage devices. With respect to conventional hard disk drives (HDDs), flash-memory-based solid state drives (SSDs) benefit from faster access speed, less power consumption, and higher storage capacity, and thus have become a mainstream data-storage scheme [193], [230]. Nowadays, flash-memory-based storage techniques have been ubiquitously used in most electronic and communication systems, including smart devices and enterprise data centers. To increase the data-storage density, the conventional single-level-cell (SLC) technique has been replaced by MLC, TLC, and QLC techniques, for which the storage density gradually increases from 1 bit/cell to 4 bit/cell [191], [192]. However, due to the continual increase in storage density, the flash-memory systems suffer from severer noise and interference, which give rise to more errors during the read/write procedure. As compared with the conventional algebraic codes [193], PLDPC codes can significantly enhance the reliability of such high-density flash-memory devices, which make capacity-approaching data storage attainable [158]–[160], [231].

The voltage levels stored in the cell of an MLC/TLC/QLC flash memory can be regarded as a 4PAM/8PAM/16PAM signal [159]. In this sense, a multiple-level-cell flash memory deploying the PLDPC code can be regarded as a BICM system. Yet, due to the impact of various circuit-level noise, the conventional PLDPC codes designed for communication systems may not perform well in such environments. In addition, high code rate (i.e., $r \geq 4/5$) is required in order to meet the high-storage-efficiency demand of flash-memory devices. During the past few years, some research effort has been made to formulate robust design of high-rate PLDPC codes and bit-mapping schemes for MLC flash memory [232]. However, relevant investigation in this field is still in its infancy, where many challenging problems have to be resolved. Here, several design paradigms are introduced for the PLDPC-BICM over MLC flash-memory channels in order to take advantage of the potential benefits of these frameworks. Within this context, the proposed designs may also be applicable to TLC and QLC scenarios with appropriate modifications.

In general, a flash-memory channel model can be modeled as $v_{th} = v_w + n_r + n_c + n_w + n_u + n_p$, where v_{th} is the threshold voltage representing multiple bits (e.g., 2 bits) in a memory cell,

v_w is the write-voltage level, n_r is the data retention noise; n_c is the cell-to-cell interference; n_w is the random telegraph noise; n_u is the incremental step pulse programming noise, and n_p is the programming noise [193], [233]. To retrieve the stored data in flash memory, read voltages need to be applied to quantize the threshold voltages into several voltage regions [234], [235]. In addition, the cell-to-cell interference can be mitigated by utilizing post-compensation techniques [233], [236]. As such, the flash-memory channel can be regarded as a *discrete memoryless channel* when establishing coding criteria [73], [158], [159].

A. System Design for Regular Mapping

The first works on specific design methodologies of unpunctured and punctured PLDPC-BICM systems over flash-memory channels were presented in [57] and [73], respectively. Then, a novel combinatorial design approach, which consists of an optimal overlap partitioning and circulant power optimizer, was presented in [160] to construct superb non-binary SC-PLDPC codes over flash-memory channels. However, this work did not consider the design of binary SC-PLDPC codes and their corresponding BICM schemes, which remains an unsolved issue today. In the following, the recent progress of PLDPC-BICM systems over flash-memory channels is briefly reviewed.

1) *Design of Unpunctured PLDPC Codes:* In [57], a design and analysis of PLDPC-BICM-NI over MLC flash-memory channels was presented. As a representative contribution to this area, it first analyzed the raw BERs and MIs of the most significant bit (MSB) and least significant bit (LSB), which are located on different pages of the flash memory.⁴ It was found that the MSB and LSB pages typically exhibit unbalanced raw BERs, which may be very useful for improving the decoding performance and convergence speed of the PLDPC-MLC flash-memory systems. More precisely, the MSB page has relatively better raw BER and MI than the LSB page. Accordingly, a new bit-mapping scheme, referred to as *variable-node-degree-based mapping* (VNDM) *scheme*, was proposed for the PLDPC-coded MLC flash-memory systems. In the VNDM scheme, the n_p variable nodes in a protograph are first re-ranked in a descending order by their degrees. Subsequently, the $n_p/2$ higher-degree and $n_p/2$ lower-degree variable nodes are respectively mapped to the MSB and LSB pages in order to accelerate the decoding convergence of the MLC flash-memory system. Simulation results showed that the VNDM enables a desirable performance gain over the conventional successive and random bit-mapping scheme. Note that the VNDM can be viewed as a generalization of the VDMM [83] to the flash-memory channel, which takes into account the UEP feature between the MSB and LSB pages.

Assume a rate-1/2 unpunctured PLDPC code corresponding to a 3×6 base matrix, where the degrees of the first three variable nodes must be higher than those of the last three variable nodes, and the maximum value of each element is limited to 3. Aiming to minimize the decoding threshold without losing the linear-minimum-distance-growth property under the VNDM

⁴In an MLC flash memory, there are four possible symbols (i.e., 00, 01, 10, 11) stored in each cell. Each symbol consists of two bits, where the left-most bit and the right-most bit are called *MSB* and *LSB*, respectively [56]. The MSB and LSB within each stored symbol correspond to the high protection-degree labeling bit and the low protection-degree labeling bit within a 4PAM symbol, respectively.

scheme over MLC flash-memory channels, one can easily obtain an optimized PLDPC code, as shown in [57, eq. (5)].

However, the VNDM scheme may not achieve the best BICM performance over MLC flash-memory channels. To find an optimal bit-mapping scheme for the resultant rate- $\frac{1}{2}$ PLDPC code in order to attain the lowest decoding threshold, one can estimate the decoding thresholds of all the possible permutations for the column patterns mapped to the MSB and LSB pages. Then, the optimized VNDM scheme for the PLDPC code in [57, eq. (5)] can be obtained, i.e.,

$$\mathbf{B}_{\text{OPT-VNDM}, \frac{1}{2}} = \left[\begin{array}{ccc|ccc} 1 & 0 & 1 & 1 & 0 & 0 \\ 2 & 2 & 3 & 1 & 2 & 1 \\ 5 & 1 & 1 & 3 & 1 & 1 \end{array} \right], \quad (25)$$

$\underbrace{\hspace{3em}}_{\text{MSB}}$
 $\underbrace{\hspace{3em}}_{\text{LSB}}$

where the first three variable nodes and the last three variable nodes are mapped to the MSB and LSB pages, respectively.

According to [56], [157], [158], [193], high-rate codes are always required in practical flash-memory applications. To meet this requirement, the rate- $\frac{1}{2}$ PLDPC code in (25) was extended to a family of optimized RC-PLDPC codes in [57], called *VNDM-PLDPC codes*, by repeatedly appending the same variable-node pattern to both the MSB and LSB pages. Consequently, the base matrix of a rate- $(6e+3)/(6e+6)$ VNDM-PLDPC code is obtained, i.e.,

$$\mathbf{B}_{\text{OPT-VNDM}} = \left[\begin{array}{ccc|ccc} 1 & 0 & 1 & \overbrace{3 \ 2 \ 0 \ \dots}^{3e} & 1 & 0 & 0 & \overbrace{3 \ 2 \ 0 \ \dots}^{3e} \\ 2 & 2 & 3 & 1 \ 2 \ 1 \ \dots & 1 & 2 & 1 & 1 \ 2 \ 1 \ \dots \\ 5 & 1 & 1 & 0 \ 1 \ 3 \ \dots & 3 & 1 & 1 & 0 \ 1 \ 3 \ \dots \end{array} \right]. \quad (26)$$

$\underbrace{\hspace{3em}}_{\text{MSB}}$
 $\underbrace{\hspace{3em}}_{\text{LSB}}$

where the newly added variable-node pattern for the MSB/LSB page consists of three variable nodes with degrees 4, 5, 4, respectively. The VNDM-PLDPC codes cover various rates ranging from $1/2$ to $1 - \epsilon$. For instance, one can construct a rate-9/10 VNDM-PLDPC code by setting $e = 4$ in (26). The structure of such a variable-node pattern allows the resultant higher-rate VNDM-PLDPC codes to preserve low-decoding-threshold and linear-minimum-distance-growth benefits. The VNDM-PLDPC codes outperform the irregular LDPC codes in [159], optimized for the BICM-NI MLC flash-memory systems.

2) *Design of Punctured PLDPC Codes*: The code-design method developed in [57] has only considered unpunctured PLDPC codes and the BICM-NI framework. In fact, incorporating some punctured variable nodes into the PLDPC codes and the ID framework into BICM can improve the transmission throughput and error performance in communication applications. This motivated the employment of the punctured PLDPC codes and BICM-ID in the flash-memory systems [158]. However, due to the impact of the ID framework, the existing PLDPC codes designed for BICM-NI flash-memory systems may not preserve their superiority. For this reason, in [73] a comprehensive study was proposed on the design of punctured PLDPC-codes for BICM-ID flash-memory systems with the anti-Gray labeling.

As is well known, the PEXIT algorithm can be used to predict the asymptotic convergence performance of PLDPC codes in terms of decoding thresholds. However, there exist some problems that make the standard PEXIT algorithm unsuitable for BICM-ID flash-memory channels, as follows.

- Different from communication channels, the flash memory needs to apply the read voltages that are selected for different PE cycles and retention time to dynamically adapt to the variation of the threshold voltages.
- Due to the effect of quantization, the initial LLRs output from a flash-memory channel no longer follow a symmetric-Gaussian distribution.

To address the aforementioned issues, a voltage-sensing (VS) PEXIT algorithm was proposed for PLDPC-BICM-ID over flash-memory channels. Unlike the conventional PEXIT algorithm, the VS-PEXIT substantially takes into account the variation of the threshold voltages and the feature of the ID framework. Particularly, to deal with the variation of threshold voltages, a maximum MI (MMI) technique [159] is utilized to obtain the read-voltage levels for different numbers of PE cycles in the VS-PEXIT algorithm. Furthermore, the VS-PEXIT algorithm applies the realistic LLRs to generate the initial MI of flash-memory channel based on Monte-Carlo simulations.

Based on the VS-PEXIT analysis, it was found [73] that the conventional optimal PLDPC codes over AWGN channels cannot maintain excellent error performance over BICM-ID MLC flash-memory channels. Therefore, a new design method was proposed to construct high-rate PLDPC codes having low decoding thresholds and effective MHDGRs over such channels.

The design starts with a rate- $\frac{1}{2}$ PLDPC code. To obtain a good rate- $\frac{1}{2}$ protograph with the properties of a relatively low decoding threshold and an effective MHDGR, one can first impose some constraints on the protograph: (1) incorporate a degree-1 variable node, a punctured highest-degree variable node, and a degree-2 variable node, into the rate- $\frac{1}{2}$ protograph; (2) set the maximum number of degree-2 variable nodes to be less than the number of check nodes outside the precoding structure [43]. Through a VS-PEXIT-aided computer search, the base matrix corresponding to the optimized rate- $\frac{1}{2}$ PLDPC code with the lowest decoding threshold can be obtained, as

$$\mathbf{B}_{\text{OPT-ID}, \frac{1}{2}} = \left[\begin{array}{ccccc} 1 & 2 & 0 & 0 & 0 \\ 0 & 1 & 1 & 3 & 1 \\ 0 & 3 & 2 & 0 & 1 \end{array} \right], \quad (27)$$

where the variable node corresponding to the second column is punctured. Furthermore, it was observed that repeatedly adding a degree-3 variable-node pattern (i.e., two degree-3 variable nodes) to the designed rate- $\frac{1}{2}$ protograph can yield higher-rate protographs with relatively low decoding thresholds.

More importantly, appending VNs with degrees no less than 3 to the rate- $\frac{1}{2}$ PLDPC code can ensure the linear-minimum-distance-growth property. Therefore, an optimized rate- $\frac{e+1}{e+2}$ PLDPC code, called *optimized ARA (OARA) code* [73], is constructed, with the base matrix formulated as

$$\mathbf{B}_{\text{OARA}} = \left[\begin{array}{cccc|cccc} 1 & 2 & 0 & 0 & 0 & \overbrace{0 \ 0 \ \dots \ 0 \ 0}^{2e} \\ 0 & 1 & 1 & 3 & 1 & 1 & 2 & \dots & 1 & 2 \\ 0 & 3 & 2 & 0 & 1 & 2 & 1 & \dots & 2 & 1 \end{array} \right]. \quad (28)$$

By means of AWE analysis, it can be verified that the OARA code has an effective MHDGR. Assuming that $e = 9$, the decoding threshold of the rate- $\frac{9}{10}$ OARA code is obtained as 12.956 dB, which is lower than that of the AR4JA code, regular column-weight-3 PLDPC code and the optimized VNDM-PLDPC code

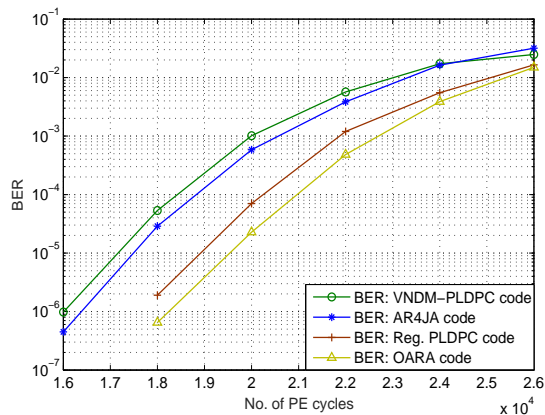


Fig. 18. BER curves of four different PLDPC codes over a BICM-ID flash-memory channel with $r_P = 9/10$, $N_T = 4200$, $t_{GL,max} = 5$, and $t_{BP,max} = 25$.

[57], and moreover has a gap of only about 0.6 dB to the capacity limit of the BICM-ID flash-memory channel. Besides, Fig. 18 plots the BERs of four different rate- $\frac{9}{10}$ PLDPC codes over a BICM-ID flash-memory channel. When the number of PE cycles is 18000, the OARA code achieves a BER of 7×10^{-7} , while the regular column-weight-3 PLDPC code, AR4JA code and optimized VNDM-PLDPC code only achieve BERs of 2×10^{-6} , 3×10^{-5} and 5×10^{-5} , respectively. This verifies that the OARA code outperforms the other three types of PLDPC codes.

B. System Design for Irregular Mapping

According to [90], [93], [237], IM is a useful technique to speed up the decoding convergence for BICM systems. However, the existing works have only considered the design of IM schemes over AWGN and fading channels, but not the flash-memory channel. To fill this gap, the IM technique was applied to the BICM-ID flash-memory systems in [120], with a specific code-design method developed for this framework.

Consider a PLDPC code corresponding to a protograph with n_P variable nodes and m_P check nodes. A length- N_P PLDPC codeword $\Lambda = (v_1, v_2, \dots, v_N)$ is grouped into n_P blocks, i.e., $\mathcal{V}_1, \mathcal{V}_2, \dots, \mathcal{V}_{n_P}$, where \mathcal{V}_j consists of $Z = N/n_P$ replicas of v_j . Furthermore, each block \mathcal{V}_j is divided into D sub-blocks $\{\mathcal{V}_{j,\kappa} | \kappa = 1, 2, \dots, D\}$ if D ($D \geq 2$) different types of constellations are employed. The length of $\mathcal{V}_{j,\kappa}$ equals $\eta_\kappa Z$, where $\eta_\kappa \in (0, 1)$ is the mixing ratio of the κ -th constellation and $\sum_{\kappa=1}^D \eta_\kappa = 1$. After processing by the interleaver, the interleaved sub-block $\hat{\mathcal{V}}_\kappa$ is generated, as illustrated in Fig. 19. Consequently, the written symbol sequence \mathbf{x}_κ is produced by the κ -th constellation to modulate $\hat{\mathcal{V}}_\kappa$.

Example 22: Assume that two constellations (i.e., Gray-labeled constellation and anti-Gray-labeled constellation, $D = 2$) with a mixing-ratio vector $\boldsymbol{\eta} = (\eta_1, \eta_2) = (1/2, 1/2)$ are applied in an IM-PLDPC-BICM-ID MLC flash-memory system. In this system, each block \mathcal{V} is divided into 2 sub-blocks. After processing by the interleaver, two interleaved coded-bit subsequences ($\hat{\mathcal{V}}_1$ and $\hat{\mathcal{V}}_2$) are produced. Then, the written symbol sequences (\mathbf{x}_1 and \mathbf{x}_2) are generated by the Gray- and anti-Gray-labeled constellations to modulate $\hat{\mathcal{V}}_1$ and $\hat{\mathcal{V}}_2$, respectively.

To satisfy the high-rate demand for flash-memory applications, high-rate PLDPC codes are constructed with two constellations

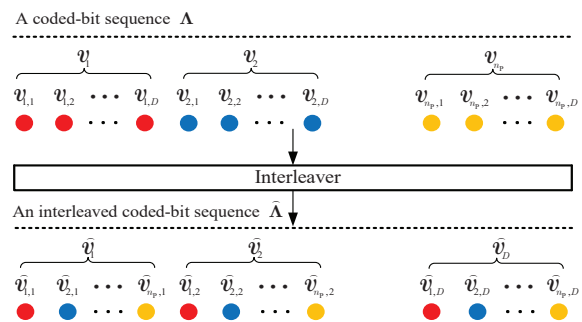


Fig. 19. Bit-interleaving process for an IM-PLDPC-BICM-ID over a flash memory channel.

(i.e., Gray-labeled constellation and anti-Gray-labeled constellation) in the IM-BICM-ID flash-memory systems in [120]. Here, the mixing-ratio vector is assumed as $\boldsymbol{\eta} = (\eta_1, \eta_2) = (1/2, 1/2)$ without loss of generality. Note that the proposed construction approach can also be applied to other mixing ratios.

Next, assume a rate- $\frac{9}{10}$ PLDPC code corresponding to a 3×21 base matrix, which includes 1 punctured variable node and 20 unpunctured variable nodes. Then, some constraints are imposed on the base matrix so as to obtain a desirable decoding threshold and an effective MHDGR for IM-BICM-ID flash-memory systems. The procedure is as follows.

- (1) Initialize a protograph with a precoding structure and a highest-degree punctured variable node.
- (2) Enable the linear-minimum-distance-growth property, where only one degree-2 variable node is allowed outside the precoding structure of the protograph.
- (3) Ensure the linear-minimum-distance-growth property by employing an extension variable-node pattern with two degree-3 variable nodes in the protograph.

Based on the above constraints, the optimized rate- $\frac{9}{10}$ PLDPC code, referred to as *irregular-mapped accumulate-repeat-accumulate (IMARA) code*, is constructed by a PEXIT-aided computer search. According to [43], [65], adding degree-3 VNs into a rate- $\frac{9}{10}$ protograph can retain the lowest complexity for its corresponding higher-rate counterparts without deteriorating the linear-minimum-distance-growth property. Hence, one can easily construct a higher-rate IMARA code by further appending the degree-3 variable-node pattern to the base matrix of rate- $\frac{9}{10}$ IMARA code. The base matrix of a rate- $r_P = \frac{e+1}{e+2}$ ($e \geq 8$) IMARA code is given by

$$\mathbf{B}_{\text{IMARA}} = \begin{bmatrix} 1 & 2 & 0 & 1 & 0 & 0 & 0 & \cdots & 0 & 0 \\ 0 & 3 & 1 & 0 & 1 & 1 & 2 & \cdots & 1 & 2 \\ 0 & 1 & 2 & 3 & 1 & 2 & 1 & \cdots & 2 & 1 \end{bmatrix}, \quad (29)$$

where the variable node corresponding to the second column is punctured.

Now, consider five different rate- $\frac{9}{10}$ PLDPC codes, i.e., IMARA code, AR4JA code, VNDM-PLDPC code, OARA code and regular column-weight-3 PLDPC code. The IMARA code not only possesses the lowest decoding threshold among the five codes (i.e., 11.483 dB), but also has a 0.182-dB gap to the capacity limit (i.e., 11.301 dB) of an IM-BICM-ID flash-memory channel. Also, it is verified by AWE analysis that the IMARA code enables the linear-minimum-distance-growth property.

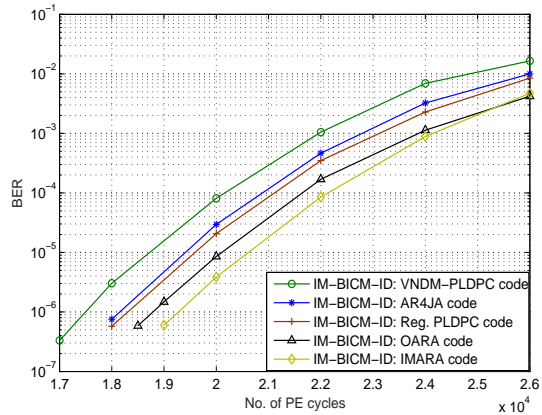


Fig. 20. BER curves of five different PLDPC codes in the IM-BICM-ID flash-memory system with $r_P = 9/10$, $N_T = 4000$, $t_{GL,max} = 6$, and $t_{BP,max} = 40$.

Example 23: Fig. 20 compares the BER performance of the rate- $\frac{9}{10}$ IMARA code, AR4JA code, VNDM-PLDPC code, OARA code and regular PLDPC code in an IM-BICM-ID flash-memory system. At a BER of 10^{-6} , the IMARA code achieves performance gains of about 500, 1000, 1100 and 1800 PE cycles over the OARA code, regular PLDPC code, AR4JA code and VNDM-PLDPC code, respectively. This demonstrates the excellent error performance of the IMARA code. Furthermore, it should be noted that the IM-IMARA-BICM-ID flash-memory system is obviously superior to its regular-mapped counterpart (Simulations are omitted here for simplicity).

C. Summary

In this section, the optimization methodologies for PLDPC-BICM flash-memory systems is reviewed. In particular, some design guidelines of PLDPC codes and bit mappers are presented for regular-mapped BICM flash-memory systems to meet the high-reliability and high-efficiency requirements. As a further advancement, a paradigmatic devise on the IM-PLDPC-BICM-ID flash-memory systems is introduced, which can achieve better error performance and lower decoding latency.

VIII. FUTURE RESEARCH DIRECTIONS

In the above sections, a thorough survey is provided for the design of PLDPC-BICM over several typical channel models. The PLDPC-BICM has attracted considerable attention in recent years because it exhibits excellent performance with a simple design and easy implementation. Despite the fruitful results in the vast volume of literature on PLDPC-BICM, a number of challenging issues still require to be addressed. Here, some potential research directions are suggested for further investigation.

A. Further Optimization of SC-PLDPC-BICM

Most existing SC-PLDPC codes reported in the literature suffer from relatively low rates (i.e., $r_{SC} \leq \frac{1}{2}$), which to some extent limit their applications in digital communications and data-storage systems [153]–[155]. Actually, high-rate codes are always preferred over low-rate codes, especially for data-storage systems. To satisfy the high-throughput requirement in practical applications, developing robust design approaches to construct

higher-rate SC-PLDPC codes (e.g., couple a series of higher-rate PLDPC codes) for BICM systems becomes an urgent task for the coding community.

Additionally, the investigation of SC-PLDPC-BICM systems has been restricted to the AWGN and fading channels. Similarly to conventional SC-LDPC codes [61], [160], [161], the SC-PLDPC codes will find more applications in optical communication systems, flash-memory systems, and underwater acoustic communication systems. Accordingly, it is expected to develop efficient SC-PLDPC-BICM frameworks enjoying the wave-like-convergence benefit in other channel models, which will support more diverse transmission/storage services.

Different from the conventional point-to-point communications, multiple access is a critical technology to the future massive IoT network. The existing orthogonal multiple access technologies divide the resource elements (e.g., time and frequency) orthogonally to avoid the inter-user interference, but sacrifice the spectrum efficiency. To circumvent this limitation, NOMA [130]–[132] becomes a promising solution, which can assign limited resource elements to support more users at the cost of inducing inter-user interference. Therefore, SC-PLDPC-BICM will be an appealing technique for boosting the error performance of NOMA-aided wireless communication systems.

B. Receiver Design of PLDPC-BICM

To date, most relevant work has been devoted to tackling design issues from the transmitter perspective for PLDPC-BICM systems. However, the optimization and implementation of receivers, including detection and decoding algorithms, have been largely ignored during the past decade. In fact, a detection/decoding algorithm is an inevitable technique to ensure high performance and hardware-friendly implementation of the BICM systems. Although there are some attempts to develop novel receiver designs for BICM systems [23], [52], [93], [97], [171], these algorithms do not consider the salient features of protograph and spatial coupling. Aiming to improve the error performance and to reduce the computational complexity, high-efficiency detection/decoding algorithms for the PLDPC-BICM are worth exploring. Besides, as receiver does not know the CSI in actual implementation, channel estimation becomes a critical issue in detector design. Then, based on the characteristics of PLDPC codes and interleaver, using the soft information (i.e., bit-level LLRs) output from the decoder to assist the channel estimator is expected to further improve the system performance. An emerging solution is to incorporate learning techniques [238] into receiver designs.

The hybrid-automatic-repeater-request (HARQ) [133] PLDPC-BICM will be a promising technique to realize high-reliability and high-throughput transmissions over non-ergodic channels. The transmitter first sends the symbols associated with the coded bits that are relatively easier to be recovered (i.e., the variable nodes with relatively high degrees in the parity check matrix). The receiver exploits the cyclic-redundancy check and HARQ to implement decoding, then the undecodable codeword in the previous transmission slot can combine with new incremental parity check bits to decode again.

The decoding performance of BICM flash-memory systems is highly dependent on the reliability of read voltages that produce

initial LLRs for the PLDPC decoder. However, the existing detection schemes, such as MMI and voltage-entropy-based detection schemes [159], [236], require the knowledge of threshold-voltage distributions in order to optimize the read voltages, and thus dramatically increase the implementation complexity. As a remedy, novel learning-aided detection schemes (e.g., read-voltage optimization schemes), which can achieve excellent performance without requiring threshold-voltage distributions, are needed to be developed for such systems.

C. New Application Scenarios of PLDPC-BICM

1) *Ultra-High-Density Flash-Memory Systems*: Although the design methodologies for high-rate PLDPC codes and bit mappers over BICM MLC flash-memory channels with regular mapping and IM have been extensively investigated, as discussed in Section VII, the optimization of PLDPC-BICM TLC/QLC flash-memory systems have not been completely studied. Since these higher-density flash-memory systems suffer from severer circuit-level noise, more errors will occur. Consequently, it is indispensable to develop excellent code-construction methods and bit-mapping schemes to guarantee the storage reliability for PLDPC-BICM TLC/QLC flash-memory systems.

Recently, three-dimensional (3D) NAND flash memory has emerged as a new non-volatile storage medium. This type of flash-memory devices have already been adopted in some electronic and communication devices. Compared with the planar flash memory, 3D flash memory can significantly increase the storage capacity and decrease the storage cost, but it is prone to severer interference and noise. LDPC codes have been demonstrated to have outstanding error-correction capability in 3D TLC flash-memory systems [239], [240], which may inspire more research efforts on the design of low-complexity PLDPC codes as well as robust BICM schemes.

2) *Underwater Acoustic Communication Systems*: Underwater acoustic channel represents another typical channel model for practical wireless communications. The underwater acoustic channel, which is commonly described as a doubly-selective fading channel, is viewed as one of the most complicated wireless-communication environments. It is extremely difficult to establish design criteria for capacity-approaching FEC codes together with their BICM schemes in such scenarios. Recently, PLDPC codes were applied to significantly enhance the robustness against fading and noise incurred by the underwater acoustic channel [61], [241]. To achieve higher throughput, the PLDPC-BICM-ID is expected to outperform the algebraic-coded counterparts [60] and to be a more favorable transmission solution for underwater acoustic communications.

D. New Types of BICM Frameworks

1) *Spatial-Modulation-aided PLDPC-BICM*: Spatial modulation can realize high spectral and energy efficiency with relatively simple design, which has been explosively investigated since 2008. In contrast to the conventional modulations, like *MPSK/MQAM*, the space-domain and other signal-domain (e.g., frequency/time/code/angle-domain) resources have been integrated into the spatial modulation, thereby achieving more desirable performance [242], [243]. Although the LDPC coding techniques have been applied to high-order spatial-modulation

systems [168]–[170], there is a lack of systematic design guideline for the BICM systems involving PLDPC codes and spatial modulations. Actually, the joint design and optimization of PLDPC code, bit-to-symbol mapping and index scheme has a significant effect on the performance of spatial-modulation systems. Therefore, it is important to conceive some sophisticated methods for intelligently integrating the PLDPC codes into spatial-modulation systems, which may yield new types of capacity-approaching BICM schemes.

2) *Joint PLDPC-and-PNC BICM*: Relay-aided cooperation is a crucial enabling technique for future wireless-communication applications, especially for PNC systems and IoT. Specifically, this technique can be exploited to enhance the spatial diversity, thus it has been widely applied in low-power and low-complexity wireless-communication systems. Inspired by these advantages, several robust constructions were developed for the PLDPC codes in BPSK-aided relay systems [98], [99], [136], [179]. While PLDPC codes have recently been deployed to PNC BICM systems over TWR channels [135], their optimization is still unexplored. Especially, how to develop capacity-approaching joint PLDPC-and-PNC algorithms tailored for BICM is still a challenging issue to be resolved.

3) *Polar-Coded BICM*: As the first type of capacity-achieving FEC codes, polar codes are superior to LDPC codes in certain cases, hence providing a promising error-correction solution for communication and storage [244]. In 2018, polar codes were selected as the coding scheme for the control channel in 5G radios. Some research efforts have been made to establish a series of polar-coded BICM systems so as to achieve bandwidth-efficient transmissions in communication and storage systems [245], [246]. In this direction, a number of research issues (e.g., encoder/decoder design, constellation and bit-mapper optimization) are waiting for further investigation to fully exploit the polarization feature towards optimal BICM performance.

IX. CONCLUDING REMARKS

This article provides an overview of an promising bandwidth-efficiency BICM technique, namely the PLDPC-BICM. During the past fifteen years, the PLDPC-BICM has drawn a great deal of attention from both academic and industrial communities as it is capable of achieving capacity-approaching performance with low implementation complexity. To offer a comprehensive review, the evolution of the PLDPC-BICM was traced from the deployment of PLDPC codes to the application of their SC-PLDPC relatives. These two types of codes can be conveniently represented by small-size protographs, which lead to easy design, analysis and implementation. The inherited benefits allow the PLDPC codes to be seamlessly combined with various high-order modulations, thus making the resultant BICM attractive for modern communication and storage systems including deep-space communication systems, satellite broadcasting systems, optical communication systems, wireless communication systems, and flash-memory-aided data-storage systems.

In order to give a full picture of this research field, most of the representative design and analysis methodologies were presented in relation to the PLDPC-BICM with many illustrative examples. The code construction, constellation shaping and bit-mapper optimization were discussed in several typical transmission

environments, including AWGN, fading, Poisson PPM, flash-memory channels, assuming a serially concatenated decoding framework which comprises a soft-decision demodulator and a BP decoder at the receiver. More than two hundred and thirty technical papers were carefully selected, so as to substantially elucidate the recent research progress and emerging development trends in the regard of PLDPC-BICM systems.

As one type of structured LDPC codes, the PLDPC codes exhibit capacity-approaching decoding thresholds and desirable linear-minimum-distance-growth property in BICM systems under different channel conditions. Although the presentation is limited to several typical channel models, the corresponding design and analysis techniques offer certain universal principles effective for more generalized channel models. Owing to the superb performance and simple implementation, PLDPC-BICM has been widely recognized as a competitive transmission scheme for a myriad of digital-communication and data-storage applications. Beyond any doubt, the PLDPC-BICM will be adopted by more emerging practical use and industry standards.

X. ACKNOWLEDGEMENTS

This work was supported in part by the NSF of China under Grants 62071131, the Guangdong Basic and Applied Basic Research Foundation under Grant 2022B1515020086, the International Collaborative Research Program of Guangdong Science and Technology Department under Grant 2022A0505050070, in part by the Open Research Fund of the State Key Laboratory of Integrated Services Networks under Grant ISN22-23, and the Industrial R&D Project of Haoyang Electronic Co., Ltd. under Grant 2022440002001494, in part by Singapore University of Technology Design under “Advanced Error Control Coding for 6G URLLC and mMTC” Grant FCP-NTU-RG-2022-020, and A*STAR under “Campus Wide V2X Integrated System Platform” Grant SERC A19D6a053.

REFERENCES

- [1] H. Ji, S. Park, J. Yeo, Y. Kim, J. Lee, and B. Shim, “Ultra-reliable and low-latency communications in 5G downlink: Physical layer aspects,” *IEEE Wireless Commun.*, vol. 25, no. 3, pp. 124–130, Jun. 2018.
- [2] M. Simsek, A. Aijaz, M. Dohler, J. Sachs, and G. Fettweis, “5G-enabled tactile internet,” *IEEE J. Sel. Areas Commun.*, vol. 34, no. 3, pp. 460–473, Mar. 2016.
- [3] C. E. Shannon, “A mathematical theory of communication,” *Bell Syst. Tech. J.*, vol. 27, no. 3, pp. 379–423, 1948.
- [4] R. W. Hamming, “Error detecting and error correcting codes,” *Bell Syst. Tech. J.*, vol. 29, no. 2, pp. 147–160, 1950.
- [5] R. G. Gallager, *Low-Density Parity-Check Codes*. Cambridge, MA: MIT Press, 1963.
- [6] Z. Ma, M. Xiao, Y. Xiao, Z. Pang, H. V. Poor, and B. Vucetic, “High-reliability and low-latency wireless communication for internet of things: Challenges, fundamentals, and enabling technologies,” *IEEE Internet Things J.*, vol. 6, no. 5, pp. 7946–7970, 2019.
- [7] D. J. Costello and G. D. Forney, “Channel coding: The road to channel capacity,” *Proc. IEEE*, vol. 95, no. 6, pp. 1150–1177, Jun. 2007.
- [8] G. Calzolari, M. Chiani, F. Chiaraluce, R. Garelo, and E. Paolini, “Channel coding for future space missions: New requirements and trends,” *Proc. IEEE*, vol. 95, no. 11, pp. 2157–2170, Nov. 2007.
- [9] J. Wozencraft and R. Kennedy, “Modulation and demodulation for probabilistic coding,” *IEEE Trans. Inf. Theory*, vol. 12, no. 3, pp. 291–297, Jul. 1966.
- [10] J. L. Massey, “Coding and modulation in digital communications,” in *Proc. Int. Zurich Sem. Digital Commun.*, Mar. 1974, pp. 1–4.
- [11] G. Ungerboeck, “Channel coding with multilevel/phase signals,” *IEEE Trans. Inf. Theory*, vol. 28, no. 1, pp. 55–67, 1982.
- [12] D. Divsalar and M. K. Simon, “The design of trellis coded MPSK for fading channels: Performance criteria,” *IEEE Trans. Commun.*, vol. 36, no. 9, pp. 1004–1012, Sep. 1988.
- [13] H. Imai and S. Hirakawa, “A new multilevel coding method using error-correcting codes,” *IEEE Trans. Inf. Theory*, vol. 23, no. 3, pp. 371–377, May 1977.
- [14] U. Wachsmann, R. F. H. Fischer, and J. B. Huber, “Multilevel codes: Theoretical concepts and practical design rules,” *IEEE Trans. Inf. Theory*, vol. 45, no. 5, pp. 1361–1391, Jul. 1999.
- [15] Y. Koganei, T. Oyama, K. Sugitani, H. Nakashima, and T. Hoshida, “Multilevel coding with spatially coupled repeat-accumulate codes for high-order QAM optical transmission,” *J. Lightw. Technol.*, vol. 37, no. 2, pp. 486–492, Jan. 2019.
- [16] C. Berrou, A. Glavieux, and P. Thitimajshima, “Near Shannon limit error-correcting coding and decoding: Turbo-codes,” in *Proc. IEEE Int. Conf. Commun. (ICC)*, May 1993, pp. 1064–1070.
- [17] S. J. Johnson, *Iterative Error Correction: Turbo, Low-Density Parity-Check and Repeat-Accumulate Codes*. Cambridge, MA: Cambridge university press, 2010.
- [18] D. J. C. MacKay, “Good error-correcting codes based on very sparse matrices,” *IEEE Trans. Inf. Theory*, vol. 45, no. 2, pp. 399–431, Mar. 1999.
- [19] E. Zehavi, “8-PSK trellis codes for a Rayleigh channel,” *IEEE Trans. Commun.*, vol. 40, no. 5, pp. 873–884, May 1992.
- [20] G. Caire, G. Taricco, and E. Biglieri, “Bit-interleaved coded modulation,” *IEEE Trans. Inf. Theory*, vol. 44, no. 3, pp. 927–946, May 1998.
- [21] X. Li and J. A. Ritcey, “Bit-interleaved coded modulation with iterative decoding,” *IEEE Commun. Lett.*, vol. 1, no. 6, pp. 169–171, Nov. 1997.
- [22] S. ten Brink, J. Speidel, and R.-H. Yan, “Iterative demapping for QPSK modulation,” *Electron. Lett.*, vol. 34, no. 15, pp. 1459–1460, Jul. 1998.
- [23] F. Schreckenbach, “Iterative decoding of bit-interleaved coded modulation,” Ph.D. dissertation, Technische Universität München, Munich, Germany, Sep 2007.
- [24] A. G. i Fàbregas, A. Martinez, and G. Caire, “Bit-interleaved coded modulation,” *Found. Trends Commun. Inf. Theory*, vol. 5, no. 1-2, pp. 1–153, Nov. 2008.
- [25] M. Franceschini, G. Ferrari, and R. Raheli, *LDPC Coded Modulations*. Berlin, Germany: Springer, 2009.
- [26] H. M. Navazi and M. J. Hossain, “Efficient multi-dimensional mapping using QAM constellations for BICM-ID,” *IEEE Trans. Wireless Commun.*, vol. 16, no. 12, pp. 8067–8076, Dec. 2017.
- [27] T. Richardson and R. Urbanke, *Modern Coding Theory*. Cambridge university press, 2008.
- [28] S. ten Brink, “Convergence behavior of iteratively decoded parallel concatenated codes,” *IEEE Trans. Commun.*, vol. 49, no. 10, pp. 1727–1737, Oct. 2001.
- [29] S. Shao, P. Hailes, T. Wang, J. Wu, R. G. Maunder, B. M. Al-Hashimi, and L. Hanzo, “Survey of turbo, LDPC, and polar decoder ASIC implementations,” *IEEE Commun. Surveys Tuts.*, vol. 21, no. 3, pp. 2309–2333, 3rd Quart. 2019.
- [30] J. M. Moualeu, W. Hamouda, H. Xu, and F. Takawira, “Multi-relay turbo-coded cooperative diversity networks over Nakagami- m fading channels,” *IEEE Trans. Veh. Technol.*, vol. 62, no. 9, pp. 4458–4470, Nov. 2013.
- [31] J. Boutros, N. Gresset, and L. Brunel, “Turbo coding and decoding for multiple antenna channels,” in *Proc. Int. Symp. Turbo Codes (ISTC)*, Sep. 2003, pp. 185–186.
- [32] S. Haykin and M. Sellathurai, “Turbo-BLAST with multi-loop feedback receiver,” in *Proc. Int. Symp. Turbo Codes (ISTC)*, Sep. 2003, pp. 195–202.
- [33] B. Lu, X. Wang, and K. Narayanan, “LDPC-based space-time coded OFDM systems over correlated fading channels: Performance analysis and receiver design,” *IEEE Trans. Commun.*, vol. 50, no. 1, pp. 74–88, Jan 2002.
- [34] J. Hou, P. Siegel, and L. Milstein, “Design of LDPC-coded MIMO systems with EXIT chart,” in *Proc. Annu. Allerton Conf. Commun., Control, Comput.*, vol. 40, no. 1, Oct. 2002, pp. 227–236.
- [35] J. Hou, P. H. Siegel, L. B. Milstein, and H. D. Pfister, “Capacity-approaching bandwidth-efficient coded modulation schemes based on low-density parity-check codes,” *IEEE Trans. Inf. Theory*, vol. 49, no. 9, pp. 2141–2155, Sep. 2003.
- [36] B. M. Hochwald and S. ten Brink, “Achieving near-capacity on a multiple-antenna channel,” *IEEE Trans. Commun.*, vol. 51, no. 3, pp. 389–399, Mar. 2003.
- [37] S. ten Brink, G. Kramer, and A. Ashikhmin, “Design of low-density parity-check codes for modulation and detection,” *IEEE Trans. on Commun.*, vol. 52, no. 4, pp. 670–678, Apr. 2004.

- [38] T. Richardson and R. Urbanke, "The capacity of low-density parity-check codes under message-passing decoding," *IEEE Trans. Inf. Theory*, vol. 47, no. 2, pp. 599–618, Feb. 2001.
- [39] J. M. F. Moura, J. Lu, and H. Zhang, "Structured low-density parity-check codes," *IEEE Signal Process. Mag.*, vol. 21, no. 1, pp. 42–55, Jan. 2004.
- [40] G. Liva, S. Song, L. Lan, Y. Zhang, S. Lin, and W. Ryan, "Design of LDPC codes: A survey and new results," *J. Commun. Softw. Syst.*, vol. 2, no. 3, pp. 191–211, Sep. 2006.
- [41] M. El-Hajjar and L. Hanzo, "EXIT charts for system design and analysis," *IEEE Commun. Surveys Tuts.*, vol. 16, no. 1, pp. 127–153, 1st Quart. 2014.
- [42] K. S. Andrews, D. Divsalar, S. Dolinar, J. Hamkins, C. R. Jones, and F. Pollara, "The development of turbo and LDPC codes for deep-space applications," *Proc. IEEE*, vol. 95, no. 11, pp. 2142–2156, Nov. 2007.
- [43] Y. Fang, G. Bi, Y. L. Guan, and F. C. M. Lau, "A survey on protograph LDPC codes and their applications," *IEEE Commun. Surveys Tuts.*, vol. 17, no. 4, pp. 1989–2016, 4th Quart. 2015.
- [44] Y. Fang, G. Han, G. Cai, and *et al.*, "Design guidelines of low-density parity-check codes for magnetic recording systems," *IEEE Commun. Surveys & Tutorials*, vol. 20, no. 2, pp. 1574–1606, 2nd Quart. 2018.
- [45] L. Michael and D. Gómez-Barquero, "Bit-interleaved coded modulation (BICM) for ATSC 3.0," *IEEE Trans. Broadcast.*, vol. 62, no. 1, pp. 181–188, Mar. 2016.
- [46] A. Chindapol and J. A. Ritcey, "Design, analysis, and performance evaluation for BICM-ID with square QAM constellations in Rayleigh fading channels," *IEEE J. Sel. Areas Commun.*, vol. 19, no. 5, pp. 944–957, May 2001.
- [47] F. Brannstrom and L. K. Rasmussen, "Classification of unique mappings for 8PSK based on bit-wise distance spectra," *IEEE Trans. Inf. Theory*, vol. 55, no. 3, pp. 1131–1145, Mar. 2009.
- [48] M. Krasicki, "Packet appending as a method of alleviating the turbo-cliff effect in BICM-ID," *IEEE Commun. Lett.*, vol. 20, no. 11, pp. 2145–2148, Nov. 2016.
- [49] A. Ashikhmin, G. Kramer, and S. ten Brink, "Extrinsic information transfer functions: Model and erasure channel properties," *IEEE Trans. Inf. Theory*, vol. 50, no. 11, pp. 2657–2673, Nov. 2004.
- [50] M. Jang, H. Lee, S. Kim, S. Myung, H. Jeong, and J. Kim, "Design of LDPC coded BICM in DVB broadcasting systems with block permutations," *IEEE Trans. Broadcast.*, vol. 61, no. 2, pp. 327–333, Jun. 2015.
- [51] J. Du, L. Yang, J. Yuan, L. Zhou, and X. He, "Bit mapping design for LDPC coded BICM schemes with multi-edge type EXIT chart," *IEEE Commun. Lett.*, vol. 21, no. 4, pp. 722–725, Apr. 2017.
- [52] A. G. D. Uchoa, C. T. Healy, and R. C. de Lamare, "Iterative detection and decoding algorithms for MIMO systems in block-fading channels using LDPC codes," *IEEE Trans. Veh. Tech.*, vol. 65, no. 4, pp. 2735–2741, Apr. 2016.
- [53] Y. Li and M. Salehi, "A new BC-BICM scheme for block-fading channels," in *Proc. Annu. Conf. Information Sciences and Systems (CISS)*, 2008, pp. 574–576.
- [54] H. Zhou, M. Jiang, C. Zhao, and J. Wang, "Optimization of protograph-based LDPC coded BICM-ID for the Poisson PPM channel," *IEEE Commun. Lett.*, vol. 17, no. 12, pp. 2344–2347, Dec. 2013.
- [55] J. Xiang, Y. Wu, X. Lu, and G. Cha, "Design of unequal error protection LDPC code in PPM and LDPC optical communication system," in *Proc. IEEE Int. Conf. Artif. Intell. Comput. Appl. (ICAICA)*, Mar. 2019, pp. 397–401.
- [56] Y. Cai, S. Ghose, E. F. Haratsch, Y. Luo, and O. Mutlu, "Error characterization, mitigation, and recovery in flash-memory-based solid-state drives," *Proc. IEEE*, vol. 105, no. 9, pp. 1666–1704, Sep. 2017.
- [57] P. Chen, K. Cai, and S. Zheng, "Rate-adaptive protograph LDPC codes for multi-level-cell NAND flash memory," *IEEE Commun. Lett.*, vol. 22, no. 6, pp. 1112–1115, Jun. 2018.
- [58] Z. Sun, L. Chen, X. Yuan, and Y. Yakufu, "Design and analysis of BICM-ID for two-way relay channels with physical-layer network coding," *IEEE Trans. Veh. Tech.*, vol. 66, no. 11, pp. 10 170–10 182, Nov. 2017.
- [59] Q. Xie, K. Peng, J. Song, and Z. Yang, "Bit-interleaved LDPC-coded modulation with iterative demapping and decoding," in *Proc. IEEE Veh. Technol. Conf. (VTC)*, Apr. 2009, pp. 1–5.
- [60] C. P. Shah, C. C. Tsimenidis, and *et al.*, "Low-complexity iterative receiver structure for time-varying frequency-selective shallow underwater acoustic channels using BICM-ID: Design and experimental results," *IEEE J. Ocean. Eng.*, vol. 36, no. 3, pp. 406–421, Jul. 2011.
- [61] S. K. Padala and J. D'Souza, "Performance of spatially coupled LDPC codes over underwater acoustic communication channel," in *Proc. National Conf. Commun. (NCC)*, Feb. 2020, pp. 1–5.
- [62] H. Niu and J. Ritcey, "Pilot-symbol-assisted LDPC coded BICM over correlated Rayleigh fading channels," *IEEE Trans. Wireless Commun.*, vol. 4, no. 5, pp. 2076–2082, Sep. 2005.
- [63] Q. Xie, Z. Yang, J. Song, and L. Hanzo, "EXIT-chart-matching-aided near-capacity coded modulation design and a BICM-ID design example for both Gaussian and Rayleigh channels," *IEEE Trans. Veh. Technol.*, vol. 62, no. 3, pp. 1216–1227, Mar. 2013.
- [64] P. Chen, L. Shi, Y. Fang, G. Cai, L. Wang, and G. Chen, "A coded DCSK modulation system over Rayleigh fading channels," *IEEE Trans. Commun.*, vol. 66, no. 9, pp. 3930–3942, Sep. 2018.
- [65] D. Divsalar, S. Dolinar, C. R. Jones, and K. Andrews, "Capacity-approaching protograph codes," *IEEE J. Sel. Areas Commun.*, vol. 27, no. 6, pp. 876–888, Aug. 2009.
- [66] L. Dolecek, D. Divsalar, Y. Sun, and B. Amiri, "Non-binary protograph-based LDPC codes: Enumerators, analysis, and designs," *IEEE Trans. Inf. Theory*, vol. 60, no. 7, pp. 3913–3941, Jul. 2014.
- [67] D. G. M. Mitchell, M. Lentmaier, and D. J. Costello, "Spatially coupled LDPC codes constructed from protographs," *IEEE Trans. Inf. Theory*, vol. 61, no. 9, pp. 4866–4889, Sep. 2015.
- [68] Z. Liu, Q. Xie, K. Peng, and Z. Yang, "APSK constellation with Gray mapping," *IEEE Commun. Lett.*, vol. 15, no. 12, pp. 1271–1273, Dec. 2011.
- [69] F. Yang, K. Yan, Q. Xie, and J. Song, "Non-equiprobable APSK constellation labeling design for BICM systems," *IEEE Commun. Lett.*, vol. 17, no. 6, pp. 1276–1279, Jun. 2013.
- [70] D. Zou and I. B. Djordjevic, "FPGA-based rate-adaptive LDPC-coded modulation for the next generation of optical communication systems," *Optics Express*, vol. 24, no. 18, pp. 21 159–21 166, 2016.
- [71] Y. Fang, G. Zhang, G. Cai, F. C. M. Lau, P. Chen, and G. Han, "Root-protograph-based BICM-ID: A reliable and efficient transmission solution for block-fading channels," *IEEE Trans. Commun.*, vol. 67, no. 9, pp. 5921–5939, Sep. 2019.
- [72] D. Duyck, J. J. Boutros, and M. Moeneclaey, "Precoding for word error rate minimization of LDPC coded modulation on block fading channels," *IEEE Trans. Wireless Commun.*, vol. 11, no. 7, pp. 2457–2467, Jul. 2012.
- [73] Y. Bu, Y. Fang, G. Han, S. Mumtaz, and M. Guizani, "Design of protograph-LDPC-based BICM-ID for multi-level-cell (MLC) NAND flash memory," *IEEE Commun. Lett.*, vol. 23, no. 7, pp. 1127–1131, Jul. 2019.
- [74] Q. Chen, L. Wang, P. Chen, and G. Chen, "Optimization of component elements in integrated coding systems for green communications: A survey," *IEEE Commun. Surveys Tuts.*, vol. 21, no. 3, pp. 2977–2999, 3rd Quart. 2019.
- [75] Y. He, M. Jiang, X. Ling, and C. Zhao, "Robust BICM design for the LDPC coded DCO-OFDM: A deep learning approach," *IEEE Trans. Commun.*, vol. 68, no. 2, pp. 713–727, Nov. 2020.
- [76] Z. Yang, Q. Xie, K. Peng, and J. Song, "Labeling optimization for BICM-ID systems," *IEEE Commun. Lett.*, vol. 14, no. 11, pp. 1047–1049, Nov. 2010.
- [77] Q. Xiao, Y. Chen, S. Lin, H. He, X. Wu, J. You, Y. Zeng, L. Zhou, and Z. Dong, "DFT-spread DMT-WDM-PON employing LDPC-coded probabilistic shaping 16QAM," *J. Lightw. Technol.*, vol. 38, no. 4, pp. 714–722, Oct. 2020.
- [78] J. Tan and G. L. Stuber, "Analysis and design of symbol mappers for iteratively decoded BICM," *IEEE Trans. Wireless Commun.*, vol. 4, no. 2, pp. 662–672, Mar. 2005.
- [79] J. Bao, Z. Ma, M. Xiao, T. A. Tsiftsis, and Z. Zhu, "Bit-interleaved coded SCMA with iterative multiuser detection: Multidimensional constellations design," *IEEE Trans. Commun.*, vol. 66, no. 11, pp. 5292–5304, Dec. 2018.
- [80] M. C. Valenti and X. Xiang, "Constellation shaping for bit-interleaved LDPC coded APSK," *IEEE Trans. Commun.*, vol. 60, no. 10, pp. 2960–2970, Jul. 2012.
- [81] S. Che and S. Tong, "Low-complexity LDPC coded BICM-ID with orthogonal modulations," *Electron. Lett.*, vol. 45, no. 16, pp. 845–846, Aug. 2009.
- [82] X. Liu, Y. Wei, and M. Jiang, "A universal interleaver design for bit-interleaved QC-LDPC coded modulation," in *Proc. Int. Conf. Wireless Commun. Signal Process. (WCSP)*, Oct. 2017, pp. 1–6.
- [83] T. V. Nguyen, A. Nosratinia, and D. Divsalar, "Threshold of protograph-based LDPC coded BICM for Rayleigh fading," in *Proc. IEEE Global Telecommun. Conf.*, Dec. 2011, pp. 1–5.
- [84] S. Lee, J. Ha, and J. Lee, "On interleaver design for BICM system with low error-floors," in *Proc. Int. Conf. Inf. Commun. Technol. Convergence (ICTC)*, 2015, pp. 765–769.
- [85] F. Kienle and N. Wehn, "Macro interleaver design for bit interleaved coded modulation with low-density parity-check codes," in *Proc. IEEE Veh. Technol. Conf. (VTC)*, 2008, pp. 763–766.
- [86] Y. Zhao, Y. Fang, and Z. Yang, "Interleaver design for small-coupling-length spatially coupled protograph LDPC-coded BICM systems over

- wireless fading channels," *IEEE Access*, vol. 8, pp. 33 500–33 510, Feb. 2020.
- [87] A. Alvarado, E. Agrell, L. Szczecinski, and A. Svensson, "Unequal error protection in BICM with QAM constellations: Interleaver and code design," in *Proc. IEEE Int. Conf. Commun. (ICC)*, Jun. 2009, pp. 1–6.
- [88] H. M. Navazi and M. J. Hossain, "Novel method for multi-dimensional mapping of higher order modulations for BICM-ID over Rayleigh fading channels," *IEEE Trans. Wireless Commun.*, vol. 18, no. 2, pp. 1142–1154, Feb. 2019.
- [89] Y. Hori and H. Ochiai, "An interleaver optimization for BICM-OFDM with convolutional codes over frequency-selective block fading channels," in *Proc. IEEE Wireless Commun. Netw. Conf. (WCNC)*, Apr. 2014, pp. 769–774.
- [90] Z. Liu, K. Peng, T. Cheng, and Z. Wang, "Irregular mapping and its application in bit-interleaved LDPC coded modulation with iterative demapping and decoding," *IEEE Trans. Broadcast.*, vol. 57, no. 3, pp. 707–712, Sep. 2011.
- [91] T. Cheng, K. Peng, Z. Liu, and Z. Yang, "Efficient receiver architecture for LDPC coded BICM-ID system," *IEEE Commun. Lett.*, vol. 19, no. 7, pp. 1089–1092, Jul. 2015.
- [92] J. Zhan, L. Wang, M. Katz, and G. Chen, "A differential chaotic bit-interleaved coded modulation system over multipath Rayleigh channels," *IEEE Trans. Commun.*, vol. 65, no. 12, pp. 5257–5265, Dec. 2017.
- [93] Q. Wang, C. Zhang, and J. Dai, "Irregular mapping design for bit-interleaved coded modulation with low complexity iterative decoding," in *Proc. Int. Conf. Electron. Inf. Emergency Commun. (ICEIEC)*, Jun. 2016, pp. 42–45.
- [94] J. Tan, Q. Wang, C. Qian, Z. Wang, S. Chen, and L. Hanzo, "A reduced-complexity demapping algorithm for BICM-ID systems," *IEEE Trans. Veh. Technol.*, vol. 64, no. 9, pp. 4350–4356, Sep. 2015.
- [95] Q. Xie, Z. Wang, and Z. Yang, "Simplified soft demapper for APSK with product constellation labeling," *IEEE Trans. Wireless Commun.*, vol. 11, no. 7, pp. 2649–2657, Jul. 2012.
- [96] J. Tan, Z. Wang, Q. Wang, and L. Dai, "BICM-ID scheme for clipped DCO-OFDM in visible light communications," *Optics Express*, vol. 24, no. 5, pp. 4573–4581, 2016.
- [97] L. Zuolo, C. Zambelli, A. Marelli, R. Micheloni, and P. Olivo, "LDPC soft decoding with improved performance in 1X-2X MLC and TLC NAND flash-based solid state drives," *IEEE Trans. Emerg. Topics Comput.*, vol. 7, no. 3, pp. 507–515, 2019.
- [98] T. Van Nguyen, A. Nosratinia, and D. Divsalar, "Bilayer protograph codes for half-duplex relay channels," *IEEE Trans. Wireless Commun.*, vol. 12, no. 5, pp. 1969–1977, May 2013.
- [99] Y. Fang, Y. L. Guan, G. Bi, L. Wang, and F. C. M. Lau, "Rate-compatible root-protograph LDPC codes for quasi-static fading relay channels," *IEEE Trans. Veh. Technol.*, vol. 65, no. 4, pp. 2741–2747, Apr. 2016.
- [100] L. Kong, L. He, P. Chen, G. Han, and Y. Fang, "Protograph-based quasi-cyclic LDPC coding for ultra-high density magnetic recording channels," *IEEE Trans. Magn.*, vol. 51, no. 11, pp. 1–4, Nov. 2015.
- [101] A. Dehghan and A. H. Banihashemi, "On the Tanner graph cycle distribution of random LDPC, random protograph-based LDPC, and random quasi-cyclic LDPC code ensembles," *IEEE Trans. Inf. Theory*, vol. 64, no. 6, pp. 4438–4451, Jun. 2018.
- [102] Y. Zhang, K. Peng, J. Song, and Y. Wu, "Quasi-cyclic spatially coupled LDPC code for broadcasting," *IEEE Trans. Broadcast.*, vol. 66, no. 1, pp. 187–194, Mar. 2020.
- [103] I. B. Djordjevic, "On the irregular nonbinary QC-LDPC-coded hybrid multidimensional OSCD-modulation enabling beyond 100 Tb/s optical transport," *J. Lightw. Technol.*, vol. 31, no. 16, pp. 2669–2675, Aug. 2013.
- [104] A. Tasdighi, A. H. Banihashemi, and M. Sadeghi, "Efficient search of girth-optimal QC-LDPC codes," *IEEE Trans. Inf. Theory*, vol. 62, no. 4, pp. 1552–1564, Apr. 2016.
- [105] G. Zhang, Y. Hu, Y. Fang, and J. Wang, "Constructions of type-II QC-LDPC codes with girth eight from Sidon sequence," *IEEE Trans. Commun.*, vol. 67, no. 6, pp. 3865–3878, Jun. 2019.
- [106] G. Zhang, Y. Fang, and Y. Liu, "Automatic verification of GCD constraint for construction of girth-eight QC-LDPC codes," *IEEE Commun. Lett.*, vol. 23, no. 9, pp. 1453–1456, Sep. 2019.
- [107] C. Chen, L. Wang, and F. C. M. Lau, "Joint optimization of protograph LDPC code pair for joint source and channel coding," *IEEE Trans. Commun.*, vol. 66, no. 8, pp. 3255–3267, Aug. 2018.
- [108] Q. Chen, L. Wang, S. Hong, and Y. Chen, "Integrated design of JSCC scheme based on double protograph LDPC codes system," *IEEE Commun. Lett.*, vol. 23, no. 2, pp. 218–221, Feb. 2019.
- [109] D. Hui, S. Sandberg, and *et al.*, "Channel coding in 5G new radio: A tutorial overview and performance comparison with 4G LTE," *IEEE Veh. Technol. Mag.*, vol. 13, no. 4, pp. 60–69, Dec. 2018.
- [110] T. Richardson and S. Kudekar, "Design of low-density parity check codes for 5G new radio," *IEEE Commun. Mag.*, vol. 56, no. 3, pp. 28–34, Mar. 2018.
- [111] CCSDS, *TC Synchronization and Channel Coding*. CCSDS 231.0-B-3, Blue Book, Sep. 2017. [Online]. Available: <https://public.ccsds.org/Pubs/231x0b3.pdf>
- [112] 3GPP, *3rd Generation Partnership Project; Technical Specification Group Radio Access Network; NR; Multiplexing and Channel Coding*. 3GPP TS 36.212 v15.1.1: Technical Specification, Apr. 2018.
- [113] M. Jang, H. Jeong, S. Myung, K.-J. Kim, J. Park, and S.-H. Kim, "Analysis and design of QC-LDPC coded BICM ensembles based on RCA density evolution," *IEEE Trans. Commun.*, vol. 70, no. 4, pp. 2183–2199, Apr. 2022.
- [114] J. Li, K. Liu, S. Lin, K. Abdel-Ghaffar, and W. E. Ryan, "An unnoticed strong connection between algebraic-based and protograph-based LDPC codes, Part I: Binary case and interpretation," in *Proc. Inf. Theory Appl. Workshop*, Feb. 2015, pp. 36–45.
- [115] R. Smarandache and P. O. Vontobel, "Quasi-cyclic LDPC codes: Influence of proto- and Tanner-graph structure on minimum Hamming distance upper bounds," *IEEE Trans. Inf. Theory*, vol. 58, no. 2, pp. 585–607, Feb. 2012.
- [116] D. Divsalar and C. Jones, "Protograph based low error floor LDPC coded modulation," in *Proc. IEEE Military Commun. Conf. (MILCOM)*, Oct. 2005, pp. 378–385.
- [117] V. Nguyen, "Design of capacity-approaching protograph-based LDPC coding systems," Ph.D. dissertation, University of Texas at Dallas, Dallas, TX, Dec. 2012.
- [118] Y. Jin, M. Jiang, and C. Zhao, "Optimized variable degree matched mapping for protograph LDPC coded modulation with 16QAM," in *Proc. Int. Symp. Turbo Codes & Iterative Inf. Process. (ISTC)*, Sep. 2010, pp. 161–165.
- [119] C. Tang, H. Shen, M. Jiang, and C. Zhao, "Optimization of generalized VDM for protograph-based LDPC coded BICM," *IEEE Commun. Lett.*, vol. 18, no. 5, pp. 853–856, May 2014.
- [120] Y. Fang, Y. Bu, and *et al.*, "Irregular-mapped protograph LDPC-coded modulation: A bandwidth-efficient solution for 6G-enabled mobile networks," *IEEE Trans. Intell. Transp. Syst.*, vol. PP, no. 99, pp. 1–14, Oct. 2021.
- [121] L. O. Espluga, C. Poulliat, M.-L. Boucheret, M. Aubault-Roudier, and H. Al-Bitar, "Binary root protograph LDPC codes for CSK modulation to increase the data rate and reduce the TTD," in *Proc. ION Global Navigation Satellite Systems (GNSS)*, Sep. 2019, pp. 193–197.
- [122] C. Tang, M. Jiang, H. Shen, and C. Zhao, "Analysis and optimization of P-LDPC coded RGB-LED-based VLC systems," *IEEE Photon. J.*, vol. 7, no. 6, pp. 1–13, Dec. 2015.
- [123] F. Zabini, B. Matuz, G. Liva, E. Paolini, and M. Chiani, "The PPM poisson channel: Finite-length bounds and code design," in *Proc. Int. Symp. Turbo Codes & Iterative Inf. Process. (ISTC)*, Aug. 2014, pp. 193–197.
- [124] B. Matuz, E. Paolini, F. Zabini, and G. Liva, "Non-binary LDPC code design for the Poisson PPM channel," *IEEE Trans. Commun.*, vol. 65, no. 11, pp. 4600–4611, Nov. 2017.
- [125] Z. Yang, Y. Fang, G. Zhang, and F. C. M. Lau, "Design and optimization of protograph LDPC-coded multipulse PPM systems over Poisson channels," *IEEE Trans. Veh. Technol.*, early access, Jun. 01, 2022, doi: 10.1109/TVT.2022.3179483.
- [126] Y. Fang, G. Han, P. Chen, F. C. M. Lau, G. Chen, and L. Wang, "A survey on DCSK-based communication systems and their application to UWB scenarios," *IEEE Commun. Surveys Tuts.*, vol. 18, no. 3, pp. 1804–1837, 4th Quart. 2016.
- [127] G. Cai, Y. Fang, P. Chen, G. Han, G. Cai, and Y. Song, "Design of an MISO-SWIPT-aided code-index modulated multi-carrier M -DCSK system for e-Health IoT," *IEEE J. Sel. Areas Commun.*, vol. 39, no. 2, pp. 311–324, Feb. 2021.
- [128] Y. Lyu, L. Wang, G. Cai, and G. Chen, "Iterative receiver for M -ary DCSK systems," *IEEE Trans. Commun.*, vol. 63, no. 11, pp. 3929–3936, Nov. 2015.
- [129] C. Zhou, W. Hu, L. Wang, and G. Chen, "Turbo trellis-coded differential chaotic modulation," *IEEE Trans. Circuits Syst.*, vol. 65, no. 2, pp. 191–195, Feb. 2018.
- [130] P. Chen, Y. Fang, K. Su, and G. Chen, "Design of a capacity-approaching chaos-based multiaccess transmission system," *IEEE Trans. Veh. Technol.*, vol. 66, no. 12, pp. 10 806–10 816, Dec. 2017.
- [131] D. Cai, P. Fan, Q. Zou, and *et al.*, "Active device detection and performance analysis of massive non-orthogonal transmissions in cellular Internet of Things," *Sci. China Inf. Sci.*, vol. 65, no. 8, pp. 1–18, Jul. 2022.

- [132] D. Cai, Y. Xu, F. Fang, and *et al.*, "On the impact of time-correlated fading for downlink NOMA," *IEEE Trans. Commun.*, vol. 67, no. 6, pp. 4491–4504, Jun. 2019.
- [133] Y. Xu, D. Cai, F. Fang, and *et al.*, "Outage constrained power efficient design for downlink NOMA systems with partial HARQ," *IEEE Trans. Commun.*, vol. 68, no. 8, pp. 5188–5201, Aug. 2020.
- [134] M. Vameghestabhanati, I. Marsland, R. H. Gohary, and *et al.*, "How does channel coding affect the design of uplink SCMA multidimensional constellations?" in *Proc. IEEE Wireless Commun. Netw. Conf. (WCNC)*, May 2020, pp. 1–6.
- [135] P. Chen, S. C. Liew, and L. Shi, "Bandwidth-efficient coded modulation schemes for physical-layer network coding with high-order modulations," *IEEE Trans. Commun.*, vol. 65, no. 1, pp. 147–160, Jan. 2017.
- [136] P. Chen, L. Shi, S. C. Liew, Y. Fang, and K. Cai, "Channel decoding for nonbinary physical-layer network coding in two-way relay systems," *IEEE Trans. Veh. Technol.*, vol. 68, no. 1, pp. 628–640, Jan. 2019.
- [137] D. J. Costello, L. Dolecek, T. E. Fuja, J. Kliewer, D. G. M. Mitchell, and R. Smarandache, "Spatially coupled sparse codes on graphs: Theory and practice," *IEEE Commun. Mag.*, vol. 52, no. 7, pp. 168–176, Jul. 2014.
- [138] S. Kudekar, T. J. Richardson, and R. L. Urbanke, "Threshold saturation via spatial coupling: Why convolutional LDPC ensembles perform so well over the BEC," *IEEE Trans. Inf. Theory*, vol. 57, no. 2, pp. 803–834, Feb. 2011.
- [139] A. R. Iyengar, P. H. Siegel, R. L. Urbanke, and J. K. Wolf, "Windowed decoding of spatially coupled codes," *IEEE Trans. Inf. Theory*, vol. 59, no. 4, pp. 2277–2292, Apr. 2013.
- [140] Z. Yang, Y. Fang, G. Han, G. Cai, and F. C. M. Lau, "Design and analysis of punctured terminated spatially coupled protograph LDPC codes with small coupling lengths," *IEEE Access*, vol. 6, pp. 36 723–36 731, 2018.
- [141] D. G. M. Mitchell, M. Lentmaier, A. E. Pusane, and D. J. Costello, "Randomly punctured LDPC codes," *IEEE J. Sel. Areas Commun.*, vol. 34, no. 2, pp. 408–421, Feb. 2016.
- [142] M. R. Sanatkar and H. D. Pfister, "Increasing the rate of spatially-coupled codes via optimized irregular termination," in *Proc. Int. Symp. Turbo Codes & Iterative Inf. Process. (ISTC)*, Sep. 2016, pp. 31–35.
- [143] P. M. Olmos and R. L. Urbanke, "A scaling law to predict the finite-length performance of spatially-coupled LDPC codes," *IEEE Trans. Inf. Theory*, vol. 61, no. 6, pp. 3164–3184, Jun. 2015.
- [144] T. Jerkovits, G. Liva, and A. Graell i Amat, "Improving the decoding threshold of tailbiting spatially coupled LDPC codes by energy shaping," *IEEE Commun. Lett.*, vol. 22, no. 4, pp. 660–663, Apr. 2018.
- [145] M. Stinner and P. M. Olmos, "On the waterfall performance of finite-length SC-LDPC codes constructed from protographs," *IEEE J. Sel. Areas in Commun.*, vol. 34, no. 2, pp. 345–361, Feb. 2016.
- [146] H. Esfahanizadeh, A. Hareedy, and L. Dolecek, "Finite-length construction of high performance spatially-coupled codes via optimized partitioning and lifting," *IEEE Trans. Commun.*, vol. 67, no. 1, pp. 3–16, Jan. 2019.
- [147] V. Aref, N. Rengaswamy, and L. Schmalen, "Finite-length analysis of spatially-coupled regular LDPC ensembles on burst-erasure channels," *IEEE Trans. Inf. Theory*, vol. 64, no. 5, pp. 3431–3449, May 2018.
- [148] C. Häger, A. G. i. Amat, A. Alvarado, F. Brännström, and E. Agrell, "Optimized bit mappings for spatially coupled LDPC codes over parallel binary erasure channels," in *Proc. IEEE Int. Conf. Commun. (ICC)*, Jun 2014, pp. 2064–2069.
- [149] C. Häger, A. G. i. Amat, F. Brännström, A. Alvarado, and E. Agrell, "Improving soft FEC performance for higher-order modulations via optimized bit channel mappings," *Optics Express*, vol. 22, no. 12, pp. 14 544–14 558, Jun. 2014.
- [150] C. Häger, A. G. i. Amat, F. Brännström, A. Alvarado, and E. Agrell, "Terminated and tailbiting spatially coupled codes with optimized bit mappings for spectrally efficient fiber-optical systems," *J. Lightw. Technol.*, vol. 33, no. 7, pp. 1275–1285, Apr. 2015.
- [151] C. Häger, "Analysis and design of spatially-coupled codes with application to fiber-optical communications," Ph.D. dissertation, Chalmers University of Technology, Gothenburg, Sweden, May 2016.
- [152] S. Cammerer, L. Schmalen, V. Aref, and S. ten Brink, "Wave-like decoding of tail-biting spatially coupled LDPC codes through iterative demapping," in *Proc. Int. Symp. Turbo Codes & Iterative Inf. Process. (ISTC)*, Sep. 2016, pp. 121–125.
- [153] S. Cammerer, V. Aref, L. Schmalen, and S. ten Brink, "Triggering wave-like convergence of tail-biting spatially coupled LDPC codes," in *Proc. IEEE Annu. Conf. Inf. Sci. Syst. (CISS)*, Mar. 2016, pp. 93–98.
- [154] Z. Yang, Y. Fang, G. Zhang, F. C. M. Lau, S. Mumtaz, and D. B. da Costa, "Analysis and optimization of tail-biting spatially coupled protograph LDPC codes for BICM-ID systems," *IEEE Trans. Veh. Technol.*, vol. 69, no. 1, pp. 390–404, Jan. 2020.
- [155] Z. Yang, Y. Fang, G. Cai, G. Zhang, and P. Chen, "Design and optimization of tail-biting spatially coupled protograph LDPC codes under shuffled belief-propagation decoding," *IEEE Commun. Lett.*, vol. 24, no. 7, pp. 1378–1382, Jul. 2020.
- [156] Q. Chen, L. Wang, Y. Lyu, and G. Chen, "Designing protograph-based LDPC codes for iterative receivers on M -ary DCSK systems," *IEEE Trans. Circuits Syst. II, Exp. Briefs*, vol. 65, no. 4, pp. 466–470, Apr. 2018.
- [157] L. Zuolo, C. Zambelli, R. Micheloni, and P. Olivo, "Solid-state drives: Memory driven design methodologies for optimal performance," *Proc. IEEE*, vol. 105, no. 9, pp. 1589–1608, Sep. 2017.
- [158] H. Lee, J. Shy, Y. Chen, and Y. Ueng, "LDPC coded modulation for TLC flash memory," in *Proc. IEEE Inf. Theory Workshop (ITW)*, Nov. 2017, pp. 204–208.
- [159] J. Wang, K. Vakilinia, T. Chen, T. Courtade, G. Dong, T. Zhang, H. Shankar, and R. Wesel, "Enhanced precision through multiple reads for LDPC decoding in flash memories," *IEEE J. Sel. Areas Commun.*, vol. 32, no. 5, pp. 880–891, May 2014.
- [160] A. Hareedy, H. Esfahanizadeh, and L. Dolecek, "High performance non-binary spatially-coupled codes for flash memories," in *Proc. IEEE Inf. Theory Workshop (ITW)*, Nov. 2017, pp. 229–233.
- [161] A. Hareedy, R. Wu, and L. Dolecek, "A channel-aware combinatorial approach to design high performance spatially-coupled codes," *IEEE Trans. Inf. Theory*, vol. 66, no. 8, pp. 4834–4852, Aug. 2020.
- [162] F. Steiner, E. Ben Yacoub, B. Matuz, and *et al.*, "One and two bit message passing for SC-LDPC codes with higher-order modulation," *J. Lightw. Technol.*, vol. 37, no. 23, pp. 5914–5925, Dec. 2019.
- [163] Z. He, K. Peng, J. Song, and Y. Zhang, "Sliding window decoding for QC-SC-LDPC codes under the constraint of implementation complexity," *IEEE Trans. Broadcast.*, vol. 68, no. 2, pp. 305–316, Jun. 2022.
- [164] P. Popovski, Č. Stefanović, J. J. Nielsen, E. de Carvalho, M. Angelichinoski, K. F. Trillingsgaard, and A. Bana, "Wireless access in ultra-reliable low-latency communication (URLLC)," *IEEE Trans. Commun.*, vol. 67, no. 8, pp. 5783–5801, Aug. 2019.
- [165] H. D. Vu, T. V. Nguyen, D. N. Nguyen, and H. T. Nguyen, "On design of protograph LDPC codes for large-scale MIMO systems," *IEEE Access*, vol. 8, pp. 46 017–46 029, 2020.
- [166] T. Benaddi, C. Poulliat, and *et al.*, "Design of unstructured and protograph-based LDPC coded continuous phase modulation," in *Proc. IEEE Int. Symp. Inf. Theory (ISIT)*, 2014, pp. 1982–1986.
- [167] T. Benaddi, C. Poulliat, M. Boucheret, B. Gadat, and G. Lesthievant, "Protograph-based LDPC convolutional codes for continuous phase modulation," in *Proc. IEEE Int. Conf. Commun. (ICC)*, 2015, pp. 4454–4460.
- [168] H. Liu, J. Zheng, J. Dou, and B. Bai, "EXIT-chart-based LDPC code design for spatial modulation," in *Proc. IEEE Int. Conf. Inf. Sci. Technol. (ICIST)*, 2014, pp. 557–560.
- [169] D. Feng, H. Xu, J. Zheng, and B. Bai, "Nonbinary LDPC-coded spatial modulation," *IEEE Trans. Wireless Commun.*, vol. 17, no. 4, pp. 2786–2799, Apr. 2018.
- [170] Y. Chen, C. Lin, and Y. Ueng, "An LDPC-coded generalized space shift keying scheme using a codebook-assisted low-complexity massive MIMO detector," *IEEE Commun. Lett.*, vol. 20, no. 3, pp. 454–457, Mar. 2016.
- [171] F. Steiner, G. Böcherer, and G. Liva, "Protograph-based LDPC code design for shaped bit-metric decoding," *IEEE J. Sel. Areas Commun.*, vol. 34, no. 2, pp. 397–407, Feb. 2016.
- [172] —, "Protograph-based LDPC code design for bit-metric decoding," in *Proc. IEEE Int. Symp. Inf. Theory (ISIT)*, 2015, pp. 1089–1093.
- [173] L. M. Zhang and F. R. Kschischang, "Multi-edge-type low-density parity-check codes for bandwidth-efficient modulation," *IEEE Trans. Commun.*, vol. 61, no. 1, pp. 43–52, 2013.
- [174] R. Knopp and P. A. Humblet, "On coding for block fading channels," *IEEE Trans. Inf. Theory*, vol. 46, no. 1, pp. 189–205, Jan. 2000.
- [175] J. Thorpe, "Low-density parity-check (LDPC) codes constructed from protographs," *IPN Progress Report*, vol. 42-154, pp. 1–7, Aug. 2003.
- [176] S. T. Brink and G. Kramer, "Design of repeat-accumulate codes for iterative detection and decoding," *IEEE Trans. Signal Process.*, vol. 51, no. 11, pp. 2764–2772, Nov. 2003.
- [177] M. F. Barsoum, B. Moision, M. P. Fitz, D. Divsalar, and J. Hamkins, "EXIT function aided design of iteratively decodable codes for the Poisson PPM channel," *IEEE Trans. Commun.*, vol. 58, no. 12, pp. 3573–3582, Dec. 2010.
- [178] L. Schmalen and S. ten Brink, "Combining spatially coupled LDPC codes with modulation and detection," in *Proc. IEEE/ITG Conf. Syst., Commun. Coding*, Jan. 2013, pp. 1–6.
- [179] Y. Fang, S. C. Liew, and T. Wang, "Design of distributed protograph LDPC codes for multi-relay coded-cooperative networks," *IEEE Trans. Wireless Commun.*, vol. 16, no. 11, pp. 7235–7251, Nov. 2017.

- [180] Z. Yang, Y. Fang, G. Han, and K. M. S. Huq, "Spatially-coupled protograph LDPC-coded hierarchical modulated BICM-ID systems: A promising transmission technique for 6G-enabled internet of things," *IEEE Internet Things J.*, vol. 8, no. 7, pp. 5149–5163, Jul. 2021.
- [181] L. Dai, Y. Fang, Z. Yang, and *et al.*, "Protograph LDPC-coded BICM-ID with irregular CSK mapping in visible light communication systems," *IEEE Trans. Veh. Technol.*, vol. 70, no. 10, pp. 11 033–11 038, Oct. 2021.
- [182] K. S. Kim, D. K. Kim, C. Chae, S. Choi, Y. Ko, J. Kim, Y. Lim, M. Yang, S. Kim, B. Lim, K. Lee, and K. L. Ryu, "Ultrareliable and low-latency communication techniques for tactile internet services," *Proc. IEEE*, vol. 107, no. 2, pp. 376–393, Feb. 2019.
- [183] G. Böcherer, F. Steiner, and P. Schulte, "Bandwidth efficient and rate-matched low-density parity-check coded modulation," *IEEE Trans. on Commun.*, vol. 63, no. 12, pp. 4651–4665, Dec. 2015.
- [184] H. Wu, A. Ashikhmin, X. Wang, and *et al.*, "Distributed error correction coding scheme for low storage blockchain systems," *IEEE Internet Things J.*, vol. 7, no. 8, pp. 7054–7071, Aug. 2020.
- [185] M. Franceschini, G. Ferrari, and R. Raheli, "Does the performance of LDPC codes depend on the channel?" *IEEE Trans. Commun.*, vol. 54, no. 12, pp. 2129–2132, Dec. 2006.
- [186] S. Aggarwal, "A survey-cum-tutorial on approximations to Gaussian Q function for symbol error probability analysis over Nakagami- m fading channels," *IEEE Commun. Survey & Tut.*, vol. 21, no. 3, pp. 2195–2223, 3rd Quart. 2019.
- [187] D. Sathwani, R. N. Yadav, and S. Aggarwal, "Tighter bounds on the Gaussian Q function and its application in Nakagami- m fading channel," *IEEE Wireless Commun. Lett.*, vol. 6, no. 5, pp. 574–577, Oct. 2017.
- [188] L. Chang, G. Y. Li, and J. Li, "Closed-form SNR estimator for MPSK signals in Nakagami fading channels," *IEEE Trans. Veh. Technol.*, vol. 65, no. 9, pp. 6878–6887, Sep. 2016.
- [189] Y. Lee and M. Tsai, "Performance of decode-and-forward cooperative communications over Nakagami- m fading channels," *IEEE Trans. Veh. Technol.*, vol. 58, no. 3, pp. 1218–1228, Mar. 2009.
- [190] Y. Fang, L. Wang, P. Chen, J. Xu, G. Chen, and W. Xu, "Design and analysis of a DCSK-ARQ/CARQ system over multipath fading channels," *IEEE Trans. Circuits Syst. I, Reg. Papers*, vol. 62, no. 6, pp. 1637–1647, Jun. 2015.
- [191] W. Lee, M. Kang, S. Hong, and S. Kim, "Interpage-based endurance-enhancing lower state encoding for MLC and TLC flash memory storages," *IEEE Trans. Very Large Scale Integr. (VLSI) Syst.*, vol. 27, no. 9, pp. 2033–2045, Sep. 2019.
- [192] Y. Liao, C. Lin, H. Chang, and S. Lin, "A (21150, 19050) GC-LDPC decoder for NAND flash applications," *IEEE Trans. Circuits Syst. I: Regul. Papers*, vol. 66, no. 3, pp. 1219–1230, Mar. 2019.
- [193] Z. Mei, K. Cai, and X. He, "Deep learning-aided dynamic read thresholds design for multi-level-cell flash memories," *IEEE Trans. Commun.*, vol. 68, no. 5, pp. 2850–2862, May 2020.
- [194] A. G. i Fabregas and G. Caire, "Coded modulation in the block-fading channel: Coding theorems and code construction," *IEEE Trans. Inf. Theory*, vol. 52, no. 1, pp. 91–114, Jan. 2006.
- [195] W. Ryan and S. Lin, *Channel Codes: Classical and Modern*. New York, NY, USA: Cambridge Univ. Press, 2009.
- [196] T. Koike-Akino, D. S. Millar, K. Kojima, K. Parsons, Y. Miyata, K. Sugihara, and W. Matsumoto, "Iteration-aware LDPC code design for low-power optical communications," *J. Lightw. Technol.*, vol. 34, no. 2, pp. 573–581, 2016.
- [197] Z. Wang, D. Yang, and L. B. Milstein, "Multi-user resource allocation for a distributed multi-carrier DS-CDMA network," *IEEE Trans. Commun.*, vol. 60, no. 1, pp. 143–152, Jan. 2012.
- [198] T. M. Cover and J. A. Thomas, *Elements of Information Theory*. New York, NY, USA: John Wiley & Sons, 1991.
- [199] E. Biglieri, *Coding for Wireless Channels*. Springer Science & Business Media, 2005.
- [200] Q. Xie, J. Song, K. Peng, F. Yang, and Z. Wang, "Coded modulation with signal space diversity," *IEEE Trans. Wireless Commun.*, vol. 10, no. 2, pp. 660–669, Feb. 2011.
- [201] C. L. Lin, T. H. Lin, and R. Y. Wei, "Bit labeling and code searches for BICM-ID using 16-DAPSK," *IEICE Trans. Commun.*, vol. 101E-8, no. 12, pp. 2380–2387, Dec. 2018.
- [202] X. Li, A. Chindapol, and J. A. Ritcey, "Bit-interleaved coded modulation with iterative decoding and 8PSK signaling," *IEEE Trans. Commun.*, vol. 50, no. 8, pp. 1250–1257, Aug. 2002.
- [203] S. Liew, L. Lu, and S. Zhang, "A primer on physical-layer network coding," *Synth. Lectures Commun. Netw.*, vol. 8, no. 1, pp. 1–218, 2015.
- [204] R. Wei, J. A. Ritcey, and B. Lu, "TCM with differential encoding: Set partitioning, trellis designs, and distance analysis," *IEEE Trans. Commun.*, vol. 63, no. 8, pp. 2776–2787, 2015.
- [205] Q. Li, J. Zhang, L. Bai, and J. Choi, "Performance analysis and system design for hierarchical modulated BICM-ID," *IEEE Trans. Wireless Commun.*, vol. 13, no. 6, pp. 3056–3069, Jun. 2014.
- [206] D. G. M. Mitchell, R. Smarandache, and D. J. Costello, "Quasi-cyclic LDPC codes based on pre-lifted protographs," *IEEE Trans. Inf. Theory*, vol. 60, no. 10, pp. 5856–5874, Oct. 2014.
- [207] N. Bonello, S. Chen, and L. Hanzo, "Construction of regular quasi-cyclic protograph LDPC codes based on Vandermonde matrices," *IEEE Trans. Veh. Technol.*, vol. 57, no. 4, pp. 2583–2588, Jul. 2008.
- [208] D. G. M. Mitchell, A. E. Pusane, and D. J. Costello, "Minimum distance and trapping set analysis of protograph-based LDPC convolutional codes," *IEEE Trans. Inf. Theory*, vol. 59, no. 1, pp. 254–281, Jan. 2013.
- [209] Y. Fang, P. Chen, L. Wang, and F. C. M. Lau, "Design of protograph LDPC codes for partial response channels," *IEEE Trans. Commun.*, vol. 60, no. 10, pp. 2809–2819, Oct. 2012.
- [210] I. Kang, H. Kim, and L. H. Hanzo, "EXIT-chart aided design of row-permutation assisted twin-interleaver BICM-ID," *IEEE Trans. Broadcast.*, vol. 64, no. 1, pp. 85–95, Mar. 2018.
- [211] P. Zhang and *et al.*, "Protograph-based LDPC Hadamard codes," *IEEE Trans. Commun.*, vol. 69, no. 8, pp. 4998–5013, Aug. 2021.
- [212] N. ul Hassan, M. Lentmaier, I. Andriyanova, and G. P. Fettweis, "Improving code diversity on block-fading channels by spatial coupling," in *Proc. IEEE Int. Symp. Inf. Theory (ISIT)*, Jun. 2014, pp. 2311–2315.
- [213] Y. Fang, G. Bi, and Y. L. Guan, "Design and analysis of root-protograph LDPC codes for non-ergodic block-fading channels," *IEEE Trans. Wireless Commun.*, vol. 14, no. 2, pp. 738–749, Feb. 2015.
- [214] L. T. N. Landau, M. Dörpinghaus, R. C. de Lamare, and G. P. Fettweis, "Achievable rate with 1-bit quantization and oversampling using continuous phase modulation-based sequences," *IEEE Trans. Wireless Commun.*, vol. 17, no. 10, pp. 7080–7095, Oct. 2018.
- [215] Z. Yang, Y. Fang, Y. Cheng, P. Chen, and D. J. Almkhles, "Protograph LDPC-coded BICM-ID with irregular mapping: An emerging transmission technique for massive internet of things," *IEEE Trans. Green Commun. Netw.*, vol. PP, no. 99, pp. 1–14, Feb. 2021.
- [216] L. Szczecinski, H. Chafnaji, and C. Hermosilla, "Modulation doping for iterative demapping of bit-interleaved coded modulation," *IEEE Commun. Lett.*, vol. 9, no. 12, pp. 1031–1033, Dec. 2005.
- [217] M. Battaglioni, A. Tasdighi, G. Cancellieri, F. Chiaraluce, and M. Baldi, "Design and analysis of time-invariant SC-LDPC convolutional codes with small constraint length," *IEEE Trans. Commun.*, vol. 66, no. 3, pp. 918–931, Mar. 2018.
- [218] M. Zhang, Z. Wang, Q. Huang, and S. Wang, "Time-invariant quasi-cyclic spatially coupled LDPC codes based on packings," *IEEE Trans. Commun.*, vol. 64, no. 12, pp. 4936–4945, Dec. 2016.
- [219] H. Huang and Y. Tsai, "Protection-level-exchanging hierarchical modulation for multiresolution services under decode-and-forward cooperative networks," *IEEE Trans. Veh. Technol.*, vol. 66, no. 8, pp. 6742–6753, Aug. 2017.
- [220] Z. Hossain and J. M. Jornet, "Hierarchical bandwidth modulation for ultrabroadband terahertz communications," in *Proc. IEEE Int. Conf. Commun. (ICC)*, May 2019, pp. 1–7.
- [221] J. J. Boutros, A. G. i Fabregas, E. Biglieri, and G. Zémor, "Low-density parity-check codes for nonergodic block-fading channels," *IEEE Trans. Inf. Theory*, vol. 56, no. 9, pp. 4286–4300, Sep. 2010.
- [222] C. T. Healy and R. C. de Lamare, "Design of LDPC codes based on multipath EMD strategies for progressive edge growth," *IEEE Trans. Commun.*, vol. 64, no. 8, pp. 3208–3219, Aug. 2016.
- [223] C. Bai, H. P. Ren, and G. Kolumbán, "Double-sub-stream M -ary differential chaos shift keying wireless communication system using chaotic shape-forming filter," *IEEE Trans. Circuits Syst. I, Reg. Papers*, vol. 67, no. 10, pp. 3574–3587, Oct. 2020.
- [224] H. Ma, G. Cai, Y. Fang, P. Chen, and G. Chen, "Design of a superposition coding PPM-DCSK system for downlink multi-user transmission," *IEEE Trans. Veh. Technol.*, vol. 69, no. 2, pp. 1666–1678, Feb. 2020.
- [225] L. Wang, G. Cai, and G. Chen, "Design and performance analysis of a new multiresolution M -ary differential chaos shift keying communication system," *IEEE Trans. Wireless Commun.*, vol. 14, no. 9, pp. 5197–5208, Sep. 2015.
- [226] M. Miao, L. Wang, and G. Chen, "Performance and capacity analysis of MD-CSK-BICM for impulsive noise of PLC," *IEEE Trans. Power Del.*, vol. PP, no. 99, pp. 1–12, Oct. 2021.
- [227] P. Chen, Z. Xie, Y. Fang, Z. Chen, S. Mumtaz, and J. J. P. C. Rodrigues, "Physical-layer network coding: An efficient technique for wireless communications," *IEEE Netw.*, vol. 34, no. 2, pp. 270–276, Mar./Apr. 2020.
- [228] T. T. Nguyen and L. Lampe, "Coded multipulse pulse-position modulation for free-space optical communications," *IEEE Trans. Commun.*, vol. 58, no. 4, pp. 1036–1041, Apr. 2010.

- [229] A. E. Morra, H. S. Khallaf, H. M. H. Shalaby, and Z. Kawasaki, "Performance analysis of both shot- and thermal-noise limited multipulse PPM receivers in Gamma-Gamma atmospheric channels," *J. Lightw. Technol.*, vol. 31, no. 19, pp. 3142–3150, Oct. 2013.
- [230] L. Dolecek and Y. Cassuto, "Channel coding for nonvolatile memory technologies: Theoretical advances and practical considerations," *Proc. IEEE*, vol. 105, no. 9, pp. 1705–1724, Sep. 2017.
- [231] S. Ouyang, G. Han, Y. Fang, and W. Liu, "LLR-distribution-based non-uniform quantization for RBI-MSD algorithm in MLC flash memory," *IEEE Commun. Lett.*, vol. 22, no. 1, pp. 45–48, Jan. 2018.
- [232] M. Zhang, F. Wu, and *et al.*, "Pair-bit errors aware LDPC decoding in MLC NAND flash memory," *IEEE Trans. Comput.-Aided Design Integr. Circuits Syst.*, vol. 38, no. 12, pp. 2312–2320, Dec. 2019.
- [233] C. A. Aslam, Y. L. Guan, and K. Cai, "Decision-directed retention-failure recovery with channel update for MLC NAND flash memory," *IEEE Trans. Circuits Syst. I*, vol. 65, no. 1, pp. 353–365, Jan. 2018.
- [234] Z. Peng, R. He, G. Han, G. Cai, and Y. Fang, "Neighbor-a-posteriori information assisted cell-state adaptive detector for NAND flash memory," *IEEE Commun. Lett.*, vol. 23, no. 11, pp. 1967–1971, Nov. 2019.
- [235] Z. Fan, G. Cai, G. Han, W. Liu, and Y. Fang, "Cell-state-distribution-assisted threshold voltage detector for NAND flash memory," *IEEE Commun. Lett.*, vol. 23, no. 4, pp. 576–579, Apr. 2019.
- [236] C. A. Aslam, Y. L. Guan, and K. Cai, "Read and write voltage signal optimization for multi-level-cell (MLC) NAND flash memory," *IEEE Trans. Commun.*, vol. 64, no. 4, pp. 1613–1623, Apr. 2016.
- [237] F. Schreckenbach and G. Bauch, "Bit-interleaved coded irregular modulation," *Eur. Trans. Telecommun.*, vol. 17, no. 2, pp. 269–282, Mar. 2006.
- [238] J. Dai, K. Tan, Z. Si, K. Niu, M. Chen, H. V. Poor, and S. Cui, "Learning to decode protograph LDPC codes," *IEEE J. Sel. Areas Commun.*, vol. 39, no. 7, pp. 1983–1999, Jun. 2021.
- [239] Q. Li, L. Shi, Y. Cui, and C. J. Xue, "Exploiting asymmetric errors for LDPC decoding optimization on 3D NAND flash memory," *IEEE Trans. Comput.*, vol. 69, no. 4, pp. 475–488, Apr. 2020.
- [240] F. Wu, M. Zhang, Y. Du, W. Liu, Z. Lu, J. Wan, Z. Tan, and C. Xie, "Using error modes aware LDPC to improve decoding performance of 3D TLC NAND flash," *IEEE Trans. Comput.-Aided Design Integr. Circuits Syst.*, vol. 39, no. 4, pp. 909–921, Apr. 2020.
- [241] Z. Chen, X. Xu, and Y. Chen, "Finite-length EXIT analyses for protograph LDPC codes over underwater acoustic channels," in *Proc. IEEE Int. Conf. Signal Process., Commun. & Comput. (ICSPCC)*, Oct. 2017, pp. 1–6.
- [242] M. Wen, B. Zheng, K. J. Kim, M. Di Renzo, T. A. Tsiftsis, K. Chen, and N. Al-Dhahir, "A survey on spatial modulation in emerging wireless systems: Research progresses and applications," *IEEE J. Sel. Areas Commun.*, vol. 37, no. 9, pp. 1949–1972, Sep. 2019.
- [243] N. Ishikawa, S. Sugiura, and L. Hanzo, "50 Years of permutation, spatial and index modulation: From classic RF to visible light communications and data storage," *IEEE Commun. Surv. Tut.*, vol. 20, no. 3, pp. 1905–1938, 3rd Quart. 2018.
- [244] V. Bioglio, C. Condo, and I. Land, "Design of polar codes in 5G new radio," *IEEE Commun. Surv. Tut.*, vol. PP, no. 99, pp. 1–12, Jan. 2020.
- [245] H. Mahdaviifar, M. El-Khomy, J. Lee, and I. Kang, "Polar coding for bit-interleaved coded modulation," *IEEE Trans. Veh. Technol.*, vol. 65, no. 5, pp. 3115–3127, May 2016.
- [246] H. Afser, N. Tirpan, H. Delic, and M. Koca, "Bit-interleaved polar-coded modulation," in *Proc. IEEE Wireless Commun. Netw. Conf. (WCNC)*, Apr. 2014, pp. 480–484.